Elasticity as an indicator of cell responses to topography and chemically modified surfaces: an atomic force microscopy approach

Gordon Malcolm McPhee

A Thesis submitted to the School of Engineering, University of Glasgow, in fulfilment of the requirements for the degree of Doctor of Philosophy.

Table of Contents

List of Figures

Acknowledgements

I would first like to thank my primary supervisor Dr Huabing Yin for encouraging me to do my best with every aspect of this project. I would like my two secondary supervisors, Dr Matt Dalby and Dr Mathis Riehle, for informative and supportive discussions when they were needed most; this is extended to the staff and students of the Centre for Cellular Engineering. I would also like to thank Prof Jon Cooper for use of the excellent facilities in the Bioelectronics group throughout the course of my PhD and the advice offered by the staff and students of this group. Thanks go to Bill Monaghan and Mary Robertson for their technical expertise during my time in the James Watt Nanofabrication Centre (JWNC), and to Margaret Mullen for tuition and help with the Transmission Electron Microscope. Special thanks go to Dr Andrew Glidle for invaluable assistance in overcoming the numerous technical problems encountered throughout the duration of the project.

Author's declaration

The work presented in this thesis was conducted by the author and has not previously been submitted for a degree or diploma at this university or any other institution.

Abstract

This thesis will describes how microfabrication techniques can be combined with Atomic Force Microscopy (AFM) to investigate the potential for cellular elasticity to be used as an indicator of cell behaviour and responses to chemical and topographical surface modifications. To this end, a robust and reliable AFM protocol has been developed to take in to account the many changeable parameters encountered when performing live cell indentation measurements. Complimented with traditional molecular biological methods, such as immunofluorescence staining and confocal microscopy, the biomechanical properties and functions of cells have been investigated to see how they respond to simple chemical and topographical cues.

Simple surface topographies have frequently been exploited to learn more about cell behaviour and subsequent function however the mechanisms by which the cells senses the surrounding cues and interprets them accordingly has remained somewhat unknown. It is the hypothesis of the work presented here that the arrangement of the internal cytoskeleton as influenced by external factors in responsible for the transmission of tensile strength to the cytoplasm and on to the nuclear membrane. This in turn has the potential to alter transcription within the nucleus ultimately affecting over all cell function.

Aims and objectives

Specific objectives targeted during this body of work are detailed here. In the beginning there were few set goals and so quickly defining a structure to work by and a set of questions to answer was essential to encourage focussed experimental design. A broader description of objectives and the outline for this thesis can be found in section 1.8 Outline of thesis.

To establish the ability to measure cellular elasticity using the NanoWizard II atomic force microscope, our first objective was to demonstrate a robust and reliable methodology for indentation; investigating parameters such as indentation speed, force and depth as well as applying the most suitable mathematical model to the data to extract the results.

Secondly, it is well known that surface coating and topographical features influence cell morphology and that this could be reflected in cell mechanics. To investigate possible difference between the two mechanisms, we aimed to quantify cellular elasticity values under the two conditions.

Our next goal was to investigate further the role of topography in cellular elasticity values. By incorporating traditional cell biology techniques we wished to show that cell behaviour could be affected by topography alone and that the atomic force microscope could provide vital early stage, label free data on how cells react.

Finally, we aimed to show the mechanisms by which topography could induce behavioural changes in cells involved the positioning and orientation of tensile filaments of the cytoskeleton; as they relate the external topographical environment of the cell to the nuclear membrane, thus resulting in transcriptional changes.

Key outcomes and findings

- Some common cell adhesion molecules can transiently affect cellular elasticity over a period of at least 24 hours. After this the cell secreted ECM will mask the initial surface coating effects and return elasticity to initial levels.
- Fibronectin can increase elasticity values as recorded by the AFM whereas Poly-L-lysine has no effect.
- Topographically induced differences in cellular elasticity can be more stable, remaining for at least 3 days.
- Specifically, cells residing in 40µm diameter pits will often be softer than those on grooves or unstructured surfaces.
- Topography can influence a cell's behaviour by impacting upon transcription of specific proteins, for example RUNX2. In this way, topography plays a role in complex processes such as differentiation.
- The mechanism by which topography influences cell behaviour is at some stage tension dependant.
- The AFM is a suitable instrument to reliably and quantitatively measure cell elasticity values as early stage indicators of behaviour and function.

Chapter one: Introduction

1.1 Abstract

This chapter will explain the background theory and experimentation upon which this work is based, beginning with an overview of the extracellular matrix (ECM) and its relevance to challenges faced by researchers today, paying particular attention to work on cell differentiation and tissue homeostasis. From this it will highlight the advantages to recreating ECM features via microfabrication techniques and the unique experiments that can be performed. Various aspects of atomic force microscopy will be detailed with particular emphasis on cell elasticity as a quantifiable marker of cell state. Lastly, the motives and outline of the thesis will be described in section 1.8 Objectives and outline of thesis.

1.2 The extracellular matrix *in vivo*

To researchers endeavouring to uncover the molecular mechanisms governing tissue differentiation and development, the extracellular matrix is as essential consideration. Evolving alongside undifferentiated cells as they gradually progress through each stage of development in to fully functioning organs and tissues, the extracellular matrix fulfils a 'cement like' role in the binding together of the various cell types that co-exist and communicate as our bodies reach functional maturity. While it may be obvious to turn to the contents of a cell to provide the missing links in the development of functioning tissues it would be foolish not to consider the extracellular matrix macromolecules when trying to understand these processes. As our knowledge of the variety of biochemical and structural cues resident in the ECM grows it has become an essential component for researchers looking to fill in the gaps in development and differentiation biology (Owen, Aronow et al. 1990; Watt, Kubler et al. 1993; Watt 1993; Geiger, Bershadsky et al. 2001).

The arrival of what could recognisably be called ECM happened very early on in evolutionary terms with the introduction of multicellularity (Karl A. Piez 1984) in sponges in particular. Then, in its most basic incarnation, it would be difficult to assign it a function other than the technical term for cell secreted proteins. Its main function as we understand it today is support (Wayne M. Becker 1996), both in plant

and animal tissue. Just as it appeared early on the evolutionary tree it appears early on in embryogenesis too – at the gastrulation stage where the first distinctions between endoderm and ectoderm are made. Its adaptability is such that in both motile and non-motile organisms the ECM has evolved to be indispensable. For plants the ECM is considered to be the cell wall – rigid and in-keeping with the stationary lifestyle of the majority of plants. In animals however, the necessity to move in order to avoid predation and in turn catch food dictates that the ECM has to be capable of flexibility, of deformability, and so although functionally similar to the cell wall of plants the ECM of animals is in stark contrast to the rigidity found in plants.

The ECM of animals can be very cell type specific, influencing the formation of basement membranes in glands and in tissues such as teeth and bone it becomes calcified to form the bulk of their mass (Yizhi Meng 2009). Collagen is the most abundant component of animal ECM, found in tendons, bone, cartilage and the dermal matrix, though other proteins such as elastin, fibronectin and proteoglycans are present in significant amounts. Combined *in vivo* they can influence aspects of development, differentiation, division and migration through a variety of secreted soluble and physical cues. Figure 1 represents the soluble and physical components of the ECM surrounding a mammalian cell.

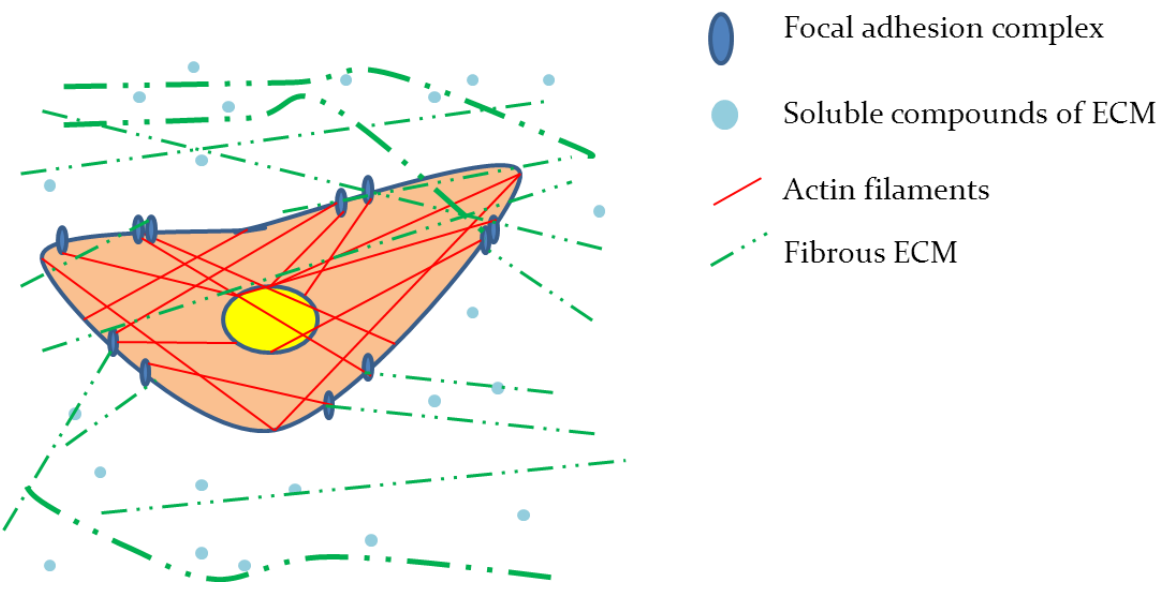

Figure 1: Simple representation of soluble and physical components of ECM surrounding and interacting with a cell.

Although the ECM can influence all these processes it is specific to the region in which it resides. This is because the cells themselves are responsible for the production of their ECM and thus the function it fulfils. The equilibrium that exists in the animal body, the homeostasis of organs and systems is in part due to the delicate balance of ECM components. Maintaining this balance is essential to the wellbeing and healthy function of the tissues and therefore the overall organism. Diseases can arise when the balance is upset and so attempts at controlling cell behaviour reported in this project can been viewed as ways of restoring homeostasis to the region or indeed preventing an imbalance in the first instance (Celeste M. Nelson 2006; Xu, Boudreau et al. 2009).

The uniqueness of an organ or tissue is the sum of its component cells, although performing different functions and secreting different proteins they all arise from the same genome. There is no mistaking a kidney for bone – the cells and cell produced ECM are completely different for each and the final products remain distinct for the duration of the life of the host. Interesting then, that tissue function remains constant throughout life yet the cells forming it are constantly changing, experiencing different stages of their life cycles, denaturing and dividing. The fact is, equilibrium at the cellular level is what keeps tissue and organ function constant (Pellettieri and Alvarado 2007).

In reality, tissue is able to maintain function by being somewhat responsive to changes in the surrounding ECM. It is important that the tissue is robust enough that every small perturbation of the cells within does not inflict significant changes to function but pliable and responsive enough that it can adapt to changing roles as time passes. For example, the external forces inflicted upon bone by physical activity serve to strengthen it resulting in beneficial changes to the tissue (French, Fulkerson et al. 2000). The effect can be increased with increased weight bearing, but under normal circumstances the bone does not break or change role, it adapts (Mueller and Maluf 2002).

For the ECM to have any influence over tissue *in vivo* it must efficiently communicate with the cells within; this can be both active and passive. While the ECM must contain the required protein components for certain cellular functions to

be possible, other processes are as a result of the passive influence of topographies present within the ECM; this behaviour is initiated by the cells themselves. For effective communication between ECM and cell the cell should be adhered and fully integrated in to the network of extracellular fibres, proteins and neighbouring cells. The ability of cells to successfully adhere themselves to the ECM is essential to processes such as wound healing and migration as mentioned earlier. Cell adhesion in the ECM requires various proteins and subcellular systems to interact in specific ways. Primary among these are the plasma membrane and cytoskeleton of the cell. The membrane acts as a semi-permeable bilayer with the job of maintaining disequilibrium amongst the hydrogen, potassium, sodium and calcium ions, tightly regulating passage in to or out of the cell. Embedded in the membrane are various receptors pertaining to a wide variety of cellular processes however it is estimated that between 25-50% play a role in adhesion (Neil Barclay 1999). The activation of a cell surface receptor by its ligand typically leads to the propagation of a biological signal through the membrane and the cytoplasm, in this way communication between the ECM and the cell is possible (Marquez, Elson et al. 2010).

Within the cytoplasm lies another essential system for effective communication between the ECM and the cell – the cytoskeleton. The cytoskeleton confers strength, shape and internal organisation to the cell. It enables the cell to migrate and supports the plasma membrane against external forces. It also rearranges the internal cell organelles during development and plays a crucial role during mitosis – first by pulling apart the chromosomes to the poles and then by dividing the cell in two. It is composed of three major classes of filaments, microfilaments (filamentous actin), microtubules (tubulin) and intermediate filaments such as vimentin. Between them they enable the internal transport of materials from place to place within the cell, particularly important for cell secretion and internalisation of vesicles. It also plays a crucial role in linking the cell membrane to the nucleus which enables changes in morphology to be communicated to the nucleus (Maniotis, Chen et al. 1997; Maniotis, Valyi-Nagy et al. 2005; Spencer, Xu et al. 2010).

Joining the cytoskeleton and plasma membrane of the cell to the ECM is a major family of cell surface receptors – the integrins. Integrins are transmembrane proteins and can function as bi-directional linkers. At the cytoplasm end the

integrin can organise filamentous components of the cytoskeleton, regulating assembly and disassembly of signalling complexes. At the ECM end it interfaces with neighbouring cells or macromolecules of the matrix (Humphries, Byron et al. 2006). In this way the integrin family are able to mediate many of the interactions between the cell and the ECM and connect the cytoskeleton to the matrix outside the cell.

One such adhesive contact formed between the cell and the ECM is a focal adhesion complex. Focal adhesions (FAs) are formed of multiple proteins including integrins, vinculin and several other cytoplasmic proteins including kinases. They form very close adhesions to the ECM or the surrounding substrate and serve as anchorage points for stress bearing filaments of the cytoskeleton such as actin, thus, they can be found widely dispersed throughout the cell (Figure 2) (Shemesh, Verkhovsky et al. 2009). By organizing filaments of the cytoskeleton on the cytoplasmic side and binding to the ECM outside the cell they are a major physical connection between the interior of the cell and the ECM. Through FAs the effects of ECM signalling are communicated to the cell. They exist in many cell types including fibroblasts, endothelial and epithelial cells and function as biochemical signalling hubs as well as mechanical anchorages (Chen, Alonso et al. 2003).

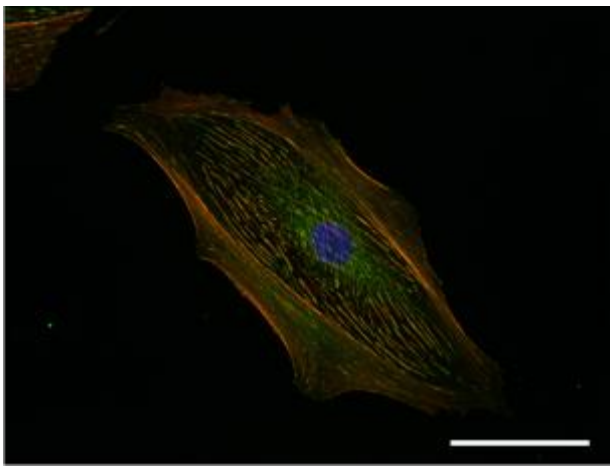

Figure 2: Mesenchymal stem cells from bone marrow stained with rhodamine-conjugated phalloidin for actin (red),mouse anti-vinculin (green) and DAPI for the nuclei (blue). This figure highlights the dispersion and positioning of focal adhesions within a cell adhered on unstructured glass coverslips. Image courtesy of Jemma Roberts, Centre for Cell Engineering, University of Glasgow. Scale = 100μm.

By acting as mechanical linkages the FAs are transmitting tensile stress from the cytoskeleton across the plasma membrane to the ECM. FAs increasingly form where free unbound integrins cluster. They can be transient complexes used as anchorage during cell migration or more permanent fixtures as seen when particularly stationary cells are cultured *in vitro* on hard substrates (Burridge, Fath et al. 1988).

FA complexes are also major determinants of cell shape. Evidence suggests that without vital FA component proteins such as vinculin and focal adhesion kinase (FAK) cells are unable to spread normally (Ezzell, Goldmann et al. 1997; Owen, Ruest et al. 1999). There is also evidence of a relationship between cell shape and the level of tension within the cytoskeleton (Chen, Alonso et al. 2003; Tan, Tien et al. 2003). It is therefore hypothesised that cell morphology can influence the position and formation of FA complexes feeding information back to the nucleus via mechanotransduction pathways (Huang, Kamm et al. 2004). During this project we have shown that topographical features can passively influence cell morphology and in some cases this leads to transcriptional changes within the cell. The molecular mechanisms by which these physical signals are transported and transformed, resulting in phenotypical change, is not discussed in this thesis. However, by inferring how the force is transmitted through the cell and observing change we are able to speculate as to the molecular mechanisms at work.

1.3 Engineering extracellular matrix *in vitro*

In order to successfully recreate extracellular matrix features through the exploitation of micro and nano fabrication technology, consideration must be given to incorporate the appropriate size scales. This can include features relevant to whole cells and subcellular components such as focal adhesions, described previously. When we consider that the average animal cell is in the region of ~10-100 μm in size, individual proteins organized in to focal adhesions are on the order 10s of nanometres in length e.g. fibronectin has been shown to be a long thin molecule of roughly 120nm (Erickson, Carrell et al. 1981) and focal adhesions themselves are only around a micron (Zhao, Li et al. 2009), it becomes clear that manipulation and visualization of these components will require specialized microscopy techniques and highly controlled fabrication processes. However, even the successful

fabrication of microenvironments incorporating such features cannot mimic the ever changing heterogeneity of the extracellular environment *in vivo*. To this end, much time and expertise has been devoted to the development of 'bionanotechnology' by researchers in fields as diverse as physics, engineering, biochemistry, genetics and molecular and cellular biology.

Such work on recreating ECM features *in vitro* appears particularly relevant when the ECM is looked at closely. What at first appears to be a mess of random fibres and features actually incorporates regular patters and structures in to the matrix. These features are present at both the micro and nano scales on components such as collagen fibres (Revenko, Sommer et al. 1994) (Figure 3) and in the general pits, troughs and pores created by the interactions within the ECM. Evidence that cells are exposed to and influenced by physical features is not new, research performed by A. Curtis, P. Clark, M. Varde, C. Wilkinson and P. Connolly beginning in the 1960's demonstrated that patterned substrates could influence much more than just cell morphology. It was demonstrated that cell movement could be both inhibited or encouraged by topography, even directed, and that topography had a role to play in the efficiency of other cues acting upon the cells as well (Curtis and Varde 1964; Clark, Connolly et al. 1990; Curtis and Wilkinson 1998). Knowing exactly which features elicit which behaviours and how to exert a greater influence over them continues to be a challenge for the researchers of today.

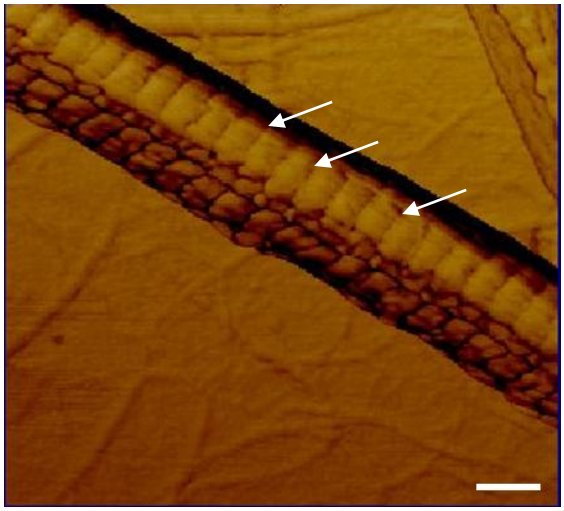

Figure 3: Phase contract image of a collagen fibre extracted from bovine tendon. Repeating structural pattern can be seen along its length (arrows). Image courtesy of Dr Shuying Cheng of the Biomedical Engineering division, University of Glasgow. Scale = 100μm.

Due to continuing advances in the micro and nano fabrication field, researchers can now routinely create precise topographies and geometries for cells to interact with. This technology necessitates a systematic approach to elucidating the complex mechanisms and behaviours observed *in vivo*, involving many other techniques at various stages of development and experimentation such as confocal microscopy, scanning electron microscopy and atomic force microscopy. What follows is a brief introduction to some common methods used to engineer extracellular matrix.

1.3.1 *Micropatterning*

Micropatterning of a surface can be achieved by photolithography, described in more details in section 2.3.1 Silicon master fabrication. When using photolithography it is advisable to commit to designs with features no smaller than 2μm as this is close to the limit of what is reliably obtainable with this method, though ultimately the main limitations on feature size achievable with photolithography are dependent on the diffraction limit and wavelength of light used to expose the substrate. Here, we have used UV exposure which theoretically limits our feature size to 1μm though feature sizes of 50nm have been achieved using deep UV light exposure (Lin 1975). Electron beam lithography should be considered for designs incorporating dimensions significantly smaller than this. The photolithography process is based on the behaviour of photoresists (light sensitive polymers) that can be spun on substrates such as silicon wafers or glass slides. When exposed to UV irradiation these photoresists can become cross-linked or break up – depending on whether the photoresist is negative or positive respectively. The patterns are produced by passing the light through pre-patterned masks thus dictating which regions of the photopolymer are exposed to the light and which are protected. Once this is complete, specialised developer solutions are used to wash away un-polymerised sections of photoresist leaving the pattern behind. In the work presented here, the remaining photoresist layer serves to protect the underlying substrate from dry etching processes used to create topographical relief on the surface.

Micropatterning is not only suitable for producing physical relief on substrates, it can also be used in a similar fashion to deposit patterns of proteins and chemicals to

mimic interactions experienced by cells *in vivo* when bound to the ECM. In a technique called 'microcontact printing', a form of soft lithography, a PDMS stamp is produced by curing the polymer against a master mould produced by the process detailed above. The stamp is then coated or 'inked' by dipping it in a solution of thiols which have the ability to soak in to the bulk PDMS. The adsorption of the thiols in to the PDMS in effect creates an ink reservoir meaning the stamp can be used multiple times. Upon the application of pressure, the stamp will transfer the pattern of thiol molecules to the surface in preparation for the application of proteins or chemicals which can bind to the thiol pattern. In this way control over the position and composition of adhesive regions is achieved. Note that the pressure required for pattern transfer can result in the lateral spreading of the solutions and in effect change the dimensions of the patterned area. This technique, originally developed by George Whiteside's group, has proved popular due to conventional photolithography techniques requiring access to expensive and highly specialised equipment; which is not easily accessible to most institutions on a regular basis. There are also substantial costs associated with microfabrication technology and so the simple but effective use of so called 'soft lithography' has help supplement conventional fabrication methods (Whitesides, Ostuni et al. 2001).

1.3.2 *Nanopatterning*

Photolithography and microcontact printing are excellent techniques for creating surface features on the micron scale however when feature sizes below ~2μm are desired another method has to be considered. This is usually electron beam lithography or e-beam for short. E-beam uses a focussed beam of electrons to write patters on to sensitive resists. Using electrons helps defeat the diffraction limit of light which governs the resolution achievable by photolithography, this means features <10nm in size can be achieved by commercial e-beam machines (Vieu, Carcenac et al. 2000). The writing process however is very slow and subject to drift. This often results in alignment errors, or stitching errors, which can cause miss matches between adjacent patterns. Small temperature variations are partly responsible for the introduction of alignment errors, other sources include the intrinsic positional drift of the beam writing tool itself and the natural limitations of the sensitive resist used (Macintyre and Thoms 2006). Even with such limitations

this method is still often preferable to alternative techniques such as lithography; especially as great efforts are undertaken by those in the field to counteract limitations such as stitching errors and writing times. Much of this type of optimisation work is carried out at the University of Glasgow's James Watt Nanofabrication Centre (JWNC), where substantial reductions in stitching errors and writing times have been reported by counteracting sample tilt (Thoms and Macintyre 2007) and increasing the efficiency with which the pattern is written (Gadegaard, Thoms et al. 2003). In particular, improvements to writing efficiency described in '*Arrays of nano-dots for cellular engineering*' by N. Gadegaard and S. Thoms *et al* have allowed larger areas to be patterned (>1cm^2) at reduced costs. This opens up E-beam technology to fields of biology such as implantation research where larger areas need to be patterned effectively if the performance of the material is to be assessed appropriately (Gadegaard, Thoms et al. 2003). However, equipment is also very expensive and requires expert technical assistance to operate and maintain. This results in the technique being available to relatively small numbers of researchers on a regular basis.

A way around some of these limiting factors has been developed recently. The technique is known as nanoimprint lithography (NIL) and is "*a parallel patterning method in which a surface pattern of a stamp is replicated into a material coated on a hard substrate by mechanical contact*" (Schift 2008). Similar in design to the micropatterning soft lithography technique described previously in that it can be high throughput and uses pressure to transfer material from a polymer stamp to the substrate. It is also based on the transfer of nanoscale features present on a mould to a layer of impressionable polymer, in this case resist spun on a hard substrate. This transfer is achieved through mechanical pressure and the result is a copy of the original pattern on the mould. It is this copy that acts as the stamp for further applications. However, because it creates patterns based on mechanical contact rather than the photons and electrons of more traditional lithographic techniques, it has the potential to achieve resolutions to beat the barriers of light diffraction and beam scattering (Guo 2007). It also greatly reduces the costs associated with e-beam, opening up access and furthering research in to cell responses to nano scale features. Using these techniques it becomes possible to write or imprint patterns of

proteins on a variety of surfaces to study not only cell behaviour on the micro scale but on nanopatterned arrays of relevant proteins.

1.4 Elasticity as characteristic marker for interrogation of living cells

Today researchers have established the link between cell function and structure. The structure of a cell contributes to its overall elasticity and is the product of more than one level of organisation. A cell's elastic quality is its ability to recover its shape following deformation due to external pressure. Cellular mechanics cannot simply be described as elastic behaviour however; other forces such as flow contribute in response to mechanical deformation. Combining the elastic and viscous behaviour of a cell is describing its viscoelastic response, influenced not only by the cytoskeleton but by the granular nature and flow-like behaviour of the cytoplasm (González-Cruz, Fonseca et al. 2012). With the appropriate mathematical models additional data can be extracted from cell deformation measurements, such as force-spectroscopy (described in section 1.6), to provide more details on cellular mechanical properties. For example, by keeping the cell under constant strain the instantaneous moduli can be identified by measuring the initial resistance to deformation; the relaxation moduli can be identified as the stiffness of the cell once the strain has reached equilibrium (Darling, Zauscher et al. 2007). Instantaneous and relaxed moduli of cells following indentation can be used as biomarkers to characterise and distinguish between various cell types (González-Cruz, Fonseca et al. 2012; Xinyu Liu 2012) however this thesis will focus on the elastic response to mechanical deformation.

Mechanical deformation of cells *in vivo* can arise from a variety of sources, it can take the form of fluid sheer in the lumen of arteries and veins or weight bearing in bone. Cell's also experience internal pressures *in vivo* which have been shown to act through the cytoskeleton and influence the mechanical properties of the cell as well; these in turn can also alter behaviour (Chan E 1997). It follows that measuring cellular elasticity is one way of probing the relationship that exists between structure and function in order to elucidate some of the intervening stages.

The elasticity of a living cell is the product of the components of the cytoskeleton and the organelles within. Little evidence exists to show that microtubules influence

elasticity directly, and intermediate filaments have been shown to wield but limited influence (Wang and Stamenović 2000); the major contributor to cellular elasticity is the actin network (Haga, Sasaki et al. 2000). Actin filaments within cells are comprised of polymerised chains of actin monomer. The process of actin polymerisation is dynamic and contributes to a variety of cellular processes, namely motility (Luca Cardamone 2011). Motility of cells involves the constant polymerisation and de-polymerisation of actin filaments to advance thin sheet-like formations known as lamellipodia and more focused finger-like projections known as filopodia (Sam Walcott 2010). In order for polymerisation to occur, the cell must have an abundance of globular actin monomers known as G-actin to form the filaments (Munter, Enninga et al. 2006), as well as an array of supporting proteins that can initiate new filaments, cap existing ones and control filament turnover (Kuhn and Pollard 2005). The polarised nature of the assembling filaments allows distinction to be made between the advancing end and the origin in the cell body, evidence suggests these are anchored to the outer nuclear membrane via specialised actin binding proteins such as nesprin (Munter, Enninga et al. 2006).

The mechanical behaviour of the nucleus has been shown to contribute to cellular elasticity also, with studies reporting that it can be between 3 and 10 times stiffer than the surrounding cytoplasm and almost twice as viscous (Guilak, Tedrow et al. 2000; Caille, Thoumine et al. 2002). Mechanically, the nucleus can be divided in to two parts – the inner core of bulk nucleoplasm consisting of chromatin and nucleoli and the outer nuclear envelope of lamins and membrane. It is possible to separate these two components of the nucleus by inducing swelling of the nuclear membranes and lamina, pulling them from the inner nucleoplasm – this enables researchers to study the contribution of the membrane independently of the inner bulk nucleoplasm. Results from this type of study by Kris Dahl *et al* using micropipette aspiration show that, swollen or un-swollen, the elastic modulus of the nucleus is unaffected by the nucleoplasm. This suggests that the overriding mechanical component of the nucleus is the envelope, which has been shown to have an average elastic modulus of 25 mN/m, much stiffer and more resilient than the plasma membrane of cells (Kris Noel Dahl 2004). Furthermore, deformation of the nucleus in response to shear flow, compression, stretching has been shown to

alter the packaging of DNA within (Maniotis, Chen et al. 1997) which in turn has an impact of gene transcription, this altering the behaviour of the cell (Gimbrone, Resnick et al. 1997).

This study, however, will deal more with the properties of the cytoskeleton. Responsible for the transport of intracellular components such as vesicles, it plays an important role in morphological changes of the cell during movement (Fletcher and Mullins 2010). In light of the fact that the cytoskeleton of a cell is constantly adapting and involved in feedback loops with the surrounding matrix and microenvironment it can be an excellent indicator of cell state (Marenzana, Wilson-Jones et al. 2006). Recording elasticity values gives us an insight in to the health of the cell, it can tell us about the suitability of the microenvironment and help us engineer more effective substrates or culture more representative cell populations (Florian Rehfeldt 2007). The homeostasis of our tissues and organs relies in part on maintaining appropriate cellular elasticity and so it can be used as a diagnostic for disease as well (van Poll, Parekkadan et al. 2008).

Researchers have been able to use elasticity as a distinguishing factor when investigating cancerous cell lines (Faria, Ma et al. 2008), ageing (Lieber, Aubry et al. 2004) and wound healing (Wagh, Roan et al. 2008). It has also helped add to the body of information available on processes such as mechanotransduction (Charras and Horton 2002; Zahn, Louban et al. 2011), migration (Schulze, Müller et al. 2009) and cell division (Houchmandzadeh and Dimitrov 1999). A variety of methods have been developed to measure cell elasticity over the years, some of which are detailed in section 1.5 Methods for measuring elasticity. Most bring the advantage of not having to stain, coat or label the cells beforehand and so elasticity can be measured with minimal pre-treatment (Dufrêne 2002; Kumar and Weaver 2009). The non-invasive aspect of elasticity measurements coupled with the ability of most methods to carry out measurements under physiologically relevant conditions has led to elasticity becoming vital to many of the areas of research listed above (A-Hassan, Heinz et al. 1998; Allison, Mortensen et al. 2010).

1.5 Methods for measuring elasticity

Several methods exist today for characterising cell elasticity of which the AFM is one. Others include micropipette aspiration, optical tweezers, magnetic bead microrheometry and most recently scanning ion-conductance microscopy (SICM). What follows is a concise but informative introduction to each method and then a more focused passage on using AFM for cell mechanical studies.

1.5.1 Micropipette Aspiration

This technique has been around since the 1950's making it one of the oldest techniques for characterising cellular mechanics. Zoologists Mitchison and Swann were using it in 1954 to elucidate the nature of the membranes of various sea urchin eggs while developing their theory of cell division, (Mitchison and Swann 1954). Their technique was modified in 1964 by Rand and Burton, (Rand and Burton 1964) and applied to erythrocytes with considerable success. It can be used on cell types ranging from the very soft to the very stiff; neutrophils (Derganc, Bo~i et al. 2000), erythrocytes (Artmann, Sung et al. 1997) and outer hair cells (Sit, Spector et al. 1997) have all been mechanically characterised this way. The micropipette aspiration technique as it is today is remarkably similar to that employed by Mitchison and Swann nearly 60 years ago however it's use is declining somewhat due to the advantages offered by more modern methods. The method is essentially simple; a small diameter glass micropipette is filled with fluid, water usually, and connected to a moveable reservoir of the same fluid. The micropipette is then carefully positioned via the use of an attached micromanipulator so that it contacts the membrane of the cell of interest and no more. Upon applying known values of negative hydrostatic pressure to the volume inside the reservoir by the use of a micrometre screw, small portions of cell membrane can be sucked up in to the lumen of the glass micropipette and the movement of the edge can be tracked manually with a cursor imposed on the video screen. In the review '*Micropipette aspiration of living cells'* by Robert M. Hochmuth it is claimed an accuracy of +/- 25 nm can be achieved using monochromatic light (Hochmuth 2000). A plot of the deformation of the cell membrane against the negative hydrostatic pressure is then taken. This 'pressure-deformation' graph essentially gives values for the elasticity of the cell membrane. The technique has been used successfully on living cells to study

their mechanical behaviour and, as will all methods of characterising cell mechanics, is subject to a variety of mathematical interpretations of the data gathered. The minimum suction force the micropipette is capable of is determined by the minimum distance the water reservoir can be moved down controllably. In theory this is around 2.5μm but in practice this is unachievable due to uncontrollable fluctuations in the system and, of course, evaporation. A more realistic minimum force is around 0.1-0.2pN/μm² and the reported maximum suction force achievable was 96nN/μm², (Hochmuth 2000), limited by the vapour pressure of water at room temperature.

1.5.2 Optical Tweezers

The first set of optical tweezers in the form we recognize them today were used in 1986 by Arthur Ashkin (A. Ashkin 1986) – the inventor and considered by many to be the father of the technique. Having previously documented optically induced gradients inflicting forces on micrometre sized particles as early as 1970 (Ashkin 1970) the method wasn't to be used successfully until the late 1980's in the field of molecular biology when *E.coli* bacterium and virions of the tobacco mosaic virus were optically trapped. While the technique has been used to great success in other fields, namely physics (Galajda 2002), in the years since it has proved valuable in the mechanical characterisation of the cell cytoskeleton and viscoelasticity measurements (Icard-Arcizet, Cardoso et al. 2008). Optical tweezers today can be used to subject biological systems, cells & motors, to precisely calibrated forces and measure the local viscoelasticity as well as the force generated by the systems themselves (Moffitt, Chemla et al. 2008). The technique is made possible by the fact that light, specifically photons carry momentum and a consequence of this is that any surface exposed to light has a force exerted on it. Of course, normally this force is too miniscule to register any effect and for this reason can be neglected, but when the light is particularly intense and impacting upon a small enough particle, forces as great as 300pN and as weak as 0.1pN can be exerted. Focusing this intense light through a good quality microscope objective lens and directing it on to small particles, ranging from <1μm to ~10μm usually, can literally trap them in a 'well' of photons with the balance of scattering and gradient forces keeping the bead stable. Trapping is made possible because of the momentum change experienced by the

photons as they are refracted by a transparent dielectric object – a bead in this example. This results in an equal but opposite momentum force which acts upon the bead; it is this force that can be divided in to 'scattering' and 'gradient' components. Scattering forces act in the direction of light propagation while gradient forces act to push the bead toward the focus point of the laser. Using this technique to investigate cellular viscoelasticity requires some modifications to the trapped beads; usually coating them in adhesive proteins such as fibronectin or specific receptors targeted toward the cell type of interest. In this way, the polystyrene or glass beads can bind to the cell and their movement observed microscopically as the optical trap is moved laterally away from the cell-bead binding site. The force exerted on the bead to pull it from binding can be calculated if certain aspects of the trapping 'well' are known and the local elasticity of the cell can be worked out using the recorded displacement of the bead i.e. the force is proportional to the distance the bead moves out of the trap.

Optical tweezers for biological applications often use high power infra-red (IR) lasers to minimize heating of the specimen while manipulating and to give high trapping stiffness. IR lasers are preferred for biological specimens because biological material is largely transparent to light of IR wavelengths and so this minimises absorption throughout the sample. However, some heat is still transmitted to the sample meaning ideal physiological conditions cannot be maintained. The manipulation is carried out through a complex series of mirrors and lenses coupled to acousto/electro-optical devices usually controlled by computer. In addition to polystyrene and glass beads, optical tweezers can also trap biological organelles themselves. Virions, whole cells, bacteria, mitochondria and chains of DNA have all been trapped using optical tweezers (Ashkin and Dziedzic 1987; Wang, Yin et al. 1997; Tang, Yao et al. 2007).

1.5.3 Magnetic Bead Microrheometry

Also known as *magnetic tweezers* this technique is often mentioned alongside optical tweezers as both involve the accurate manipulation of beads to inflict force upon the biological system of interest. As with optical tweezers, the beads used in magnetic bead microrheometry are usually coated in common bio adhesive proteins

such as fibronectin and in some cases functionalised ligands to specific cell surface receptors e.g. EGF. The beads used in this technique are typically around 5μm in diameter and need to be made of ferromagnetic materials. Once they are bound to the cell via the surface coated proteins they can be either twisted or simply displaced by the application of a magnetic field. Displacing the bead is defined as 'magnetic bead rheometry' but a magnetic field can also be used to impose a twisting motion on it; this is known as 'magnetic twisting cytometry' whereby a perpendicular 'twisting' magnetic field is momentarily applied to the beads to align then accordingly. As this field is turned off and the beads rotate back to their previous alignment; a magnetometer records the change in the magnetic field. This technique will not be discussed further in this chapter. Magnetic bead rheometry is a versatile tool which has been used in single molecule unfolding experiments and rheology studies, as well as the characterisation of force regulated processes in living cells (Kollmannsberger and Fabry 2007). Another interesting feature of the technique is the ability to map the field of strain, or deformation, inflicted upon a cell. That is, to visualize the surface area over which the movement of the paramagnetic bead is having an effect. This is done by the addition of non-magnetic probe beads coupled to the cell surface via integrins. When the magnetic field is applied to the cell they are not directly affected, however, the pull on the cell surface causes the bound probe beads to be displaced as well. Mapping the direction and distance the probe beads move in relation to the magnetic bead can effectively map the strain field sensed by the cell. This method has recently been used on umbilical vein endothelial cells resulting in data suggesting anisotropic structuring of the actin cytoskeleton (Feneberg, Aepfelbacher et al. 2004).

The forces available with magnetic bead rheometry are relatively large, in the region of 100-10,000pN (Bausch, Ziemann et al. 1998). In order to calibrate the force acting on the magnetic bead and thus reliably measure local viscoelasticity; the speed of displacement of the bead in a solution of known viscosity is measured optically in real time. Applying Stoke's law to the relationship between magnetic field and the speed of movement through the viscous solution yields force curves, able to be interpreted by the Hertz model (amongst others), and Young's modulus extracted(Bausch, Ziemann et al. 1998).

1.5.4 Scanning Ion-conductance Microscopy (SICM)

Perhaps the newest member of the Scanning Probe Microscope (SPM) family, the scanning ion-conductance microscope (SICM) sets itself apart by being designed specifically for soft biological imaging in electrolytic solutions. In existence since 1989, the microscope was initially used to image membrane filters with ion currents flowing through the pores (Hansma, Drake et al. 1989) but has since been successfully adapted for the study of living cells (Korchev, Raval et al. 2000). It involves raster scanning of a glass micropipette filled with an electrolytic solution over the surface of the sample bathed in an oppositely charged electrolytic solution. The micropipette never comes in to contact with the sample (unless directed to do so by the user) because it is kept at a constant distance perpendicularly above by careful monitoring of the ion current flowing from the pipette mouth. As the micropipette approaches the sample surface the ion current decreases as there is less space for ions to flow, this current is passed through an amplifier along with the current measured by a reference electrode placed outside the pipette in the sample solution. Differences in the current detected by the reference electrode and that passing through the tip are used to apply corresponding voltages to a Z-piezo drive controlling the scanner height. In this way, a feedback loop is created, keeping the tip a constant distance from the sample as it scans, allowing for accurate topographical information. It is conceivable that due to the techniques similarities to Scanning Electrochemical Microscopy (SECM) that the feedback mechanism would be sensitive to permeable regions of samples and thermal drift (Shigeru Amemiya 2008; Kim, Shen et al. 2012), however no literature could be identified addressing this issue yet.

SICM for cell viscoelasticity studies are at a very early stage. The technique is applicable however and perhaps the reason for the lack of published material at the moment is due to the fact that a SICM set-up has only been commercially available for a relatively short period of time. A good example of SICM for the mechanical stimulation of live cells was published in 2007 by D. Sanchez *et al* (Sánchez, Anand et al. 2007) who used the technique to indent dorsal root ganglion (DRG) cells of rats and humans and simultaneously observe calcium fluctuations. Two types of indentation are available using SICM; contact, where the glass micropipette is

directly indented into the cell with the feedback control switched off, (similar to AFM and the older 'cell poking' methods) and non-contact, when as the tip is lowered toward the sample a jet of fluid is expelled which indents the surface. Positive pressure applied via the shaft of the micropipette forces a jet of fluid out from the tip; this force appears to be controllable however no mention of controlling mechanisms were discussed in the literature. In this example the non-contact method was able to exert pressures of up to 40kPa on the DRG membrane (Sánchez, Anand et al. 2007) but similar work on the elastic modulus of cells has exerted between 0.1 – 150kPa of pressure on cells (Sanchez, Johnson et al. 2008). Using this method little or no damage to the sample is observed and no debris becomes attached to the tip, which could influence measurements. Although in this instance the SICM was not used to investigate cell viscoelasticity directly, the ability of the tool to carry out such experiments is there. As the system becomes more widely used in labs one expects to see a rise in published viscoelasticity values got from SICM.

1.6 AFM operational principle

The field of scanning probe microscopy owes a lot to the work of Gerd Binnig. In 1983 along with Heinrich Rohrer he first described the scanning tunnelling microscope (STM) (Binnig and Rohrer 1983), an instrument able to resolve surface structure to an atomic level by monitoring the current of electrons passing between a scanning conductive tip passing over a conductive sample. The STM would go on to provide some of the most detailed images of biological samples seen at the time such as DNA (Lindsay SM 1989) and viruses (A Mantovani J. G 1990) however the requirement for a conductive sample meant that the results were not always an accurate representation of the biological state. With this in mind and following along similar core principles, Binnig, Quate and Gerber invented the Atomic Force Microscope (AFM) in 1986 (Binnig, Quate et al. 1986). The AFM was primarily envisaged as a tool for measuring incredibly small forces acting upon particles but soon found a home amongst biologists excited by the ability of the microscope to

generate high resolution images of fixed and living cells (Braet, Rotsch et al. 1998; Le Grimellec, Lesniewska et al. 1998).

The key difference between the STM and the AFM is the use of a cantilever as a force sensing mechanism by which images are constructed, instead of the variations in tunnelling-current used in the STM system. The cantilever has a sharpened tip positioned at its end which is raster scanned across the sample in a similar fashion to the STM (Figure 4). As the interaction forces between the tip and the sample surface are highly distance dependant the cantilever is deflected according to the topography of the sample. These deflections are kept within a certain set margin recorded by a laser spot reflected off the back of the cantilever on to the middle of a quadrant photodetector. The voltage required to change the height of the piezo stack to keep the laser spot within the margins is used to construct an image of the surface. In this way, because the relationship between height and voltage is well defined, images of the surface can be constructed point by point and line by line. If the tip were not scanned at a constant height over the sample surface, however, then cantilever deflections would result in variations to the level of force applied between the tip and the sample. This is not advisable for most applications and so the AFM employs a feedback loop mechanism that endeavours to keep tip-sample forces equal. It works by monitoring the voltage related to the deflection of the cantilever on the surface and adjusts the z-piezo accordingly to maintain the setpoint deflection prescribed by the user. This method raises the scan height when an increase in z is detected and lowers it when the opposite is true. In this way the AFM is able to quickly react to changes in surface topography, maintaining a constant force therefore limiting sample damage and preserving tip sharpness for longer.

The first AFMs were designed to image in contact mode as described above but it soon became apparent that the lateral forces inflicted upon some of the softest biological samples were having a detrimental effect on image quality. Often fixing techniques had to be employed to maintain sample integrity and adhesion to the surface throughout the imaging process. To combat this, new imaging modes were added to the AFM's capabilities, Intermittent Contact Mode (aka Tapping Mode)

and Non-Contact mode. These techniques are described in more detail in section 1.6.1 AFM imaging.

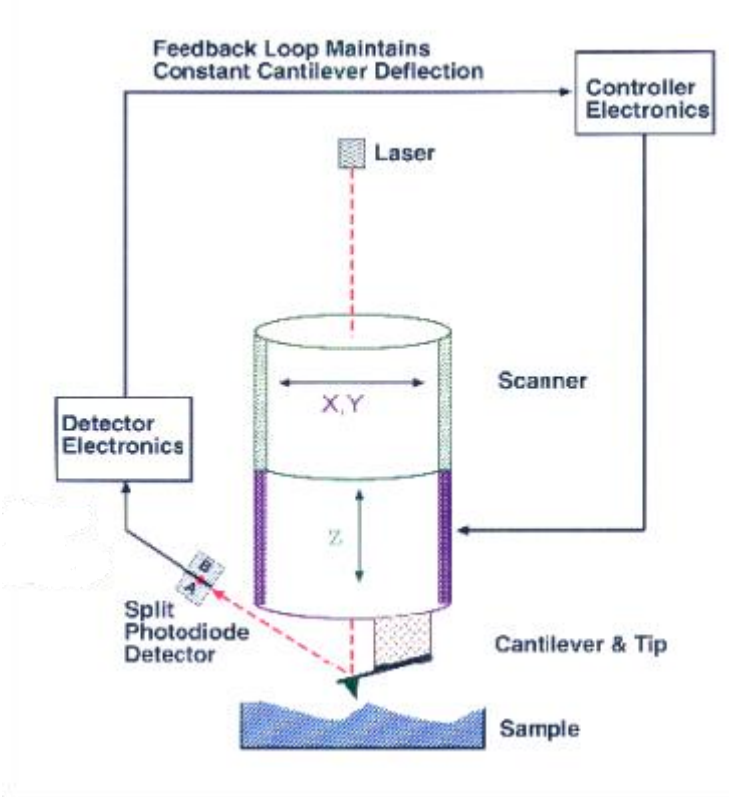

Figure 4: Basic operational principle of an atomic force microscope depicting the sharp scanning tip and laser spot reflection. Diagram from 'Atomic Force Microscopy' by Cheryl R. Blanchard (Blanchard 1996)

Using AFM to image biological samples has some advantages over conventional optical microscopy techniques. High resolution imaging of biological structures such as the F-actin cytoskeleton require no fixing, staining or labelling of any kind therefore minimal interference with the sample is an advantage. AFM images are also accurate three dimensional representations of real space and as such, height information is contained within every image. Crucially the AFM is able to work with biological samples under physiologically relevant conditions. Molecules and cells can be kept at appropriate temperatures in nutrient buffers, even at recommended CO_2 concentrations, and can be kept alive during measurements.

The imaging mechanism of an AFM does not easily lend itself to speed however. Generally speaking when image accuracy is to be increased acquisition time has to be increased correspondingly. High resolution images (1024 x 1024 pixels) can often take in the region of 15-20 minutes to complete and in that time there is every possibility that the sample has moved of its own accord, changed mechanical properties due to interaction with the tip (live cell e.g. (Charras, Lehenkari et al. 2001)) or the tip sharpness has become compromised with the accumulation of debris from the sample solution. This can have a detrimental effect on image resolution as the sharpness of the AFM tip is the primary determinant of the maximum resolution achievable. For this reason it has been difficult for the AFM to record biological phenomena in action as the process is typically faster than the AFM can competently image. However, efforts are being made in the field to increase scan speed dramatically by incorporating high-speed scanners, fast electronics, fast amplitude detectors and smaller cantilevers (Ando, Uchihashi et al. 2008). Through these enhancements fast-scanning AFM has recently been shown capable of recording molecular events such as actin-myosin walking (Kodera, Yamamoto et al. 2010) and DNA-enzyme reactions (Yokokawa, Yoshimura et al. 2006) at 25Hz. It is as yet only possible to utilize fast scanning AFM on specific samples with only slight variations in z such as artificial membranes, so for the moment live cells appear a step too far for the technique.

Another limitation of the AFM is its relatively small scan range. Normally the user is restricted to 100μm in x and y and a maximum z of around 15μm. Comparing this to the electron microscope which has a field of view in the millimetre range the limitation is apparent. Also, unlike its optical counterparts, the AFM is strictly limited to imaging the sample surface and unable to provide topographic information on what lies beneath. In spite of these limitations the AFM has a wide variety of functions at its disposal and can rightly be called the most versatile member of the scanning probe microscopy family. Its ability to provide information on several aspects of a sample simultaneously makes it an attractive tool for researchers.

Techniques that can measure more than one aspect of a sample or biological system at the same time are of great interest to biologists in particular. The ability of the

AFM to simultaneously generate high resolution images of living cells and reveal biomechanical properties make it an important addition to any biologist's toolbox. However, atomic force microscopy does not operate in a similar fashion to traditional microscopes. The sample is not imaged optically but rather 'felt' as the microscopic probe is raster scanned over the surface. Due to this, the resolution of an AFM is not limited by the wavelength of light but instead by the geometry of the probe tip and the forces acting between it and the sample surface. This brings the range of resolutions of the AFM from light microscopy territory (>200nm) in to electron microscope territory (<10nm). Naturally this appeals to biologists looking to achieve EM scale resolutions under more physiologically relevant conditions common to light microscopy, but the AFM is best able to achieve 'atomic' resolution under highly controlled circumstances. On flat mica substrates at low temperatures and under high vacuum conditions the AFM can achieve its full potential in terms of resolution (Seo and Jhe 2008), however these conditions do not lend themselves to living biological samples. While it is possible to resolve most biopolymers to sub-molecular resolution under *in vivo*-like conditions (Victor J. Morris 2010), it remains a challenge to achieve similar results with live cells.

It is the range of available operational modes that set it apart from other microscopy techniques, presenting not only the capability to image at high resolution under biologically relevant conditions but also the ability to directly measure protein-protein interactions mechanically and investigate the locations and distribution of binding sites as well as measuring stiffness (Dufrene, Evans et al. 2011). Today, the AFM has come a long way from simple contact mode imaging and now the range of samples that can be measured and the types of data that can be generated is such that the AFM has found a home in many fields of research. So versatile in fact, that a paper by Friedbacher *et al* in 1999 attempted to list all the known terms used to describe operational AFM modes and identified over 20 (Gernot Friedbacher 1999). In this chapter we will focus on one of those techniques, force spectroscopy, and in particular its application to live cell elasticity measurements, but first an introduction to imaging using AFM.

1.6.1 AFM imaging

Fundamentally the AFM depicts the surface topography of a sample when it images, accurately representing heights and distances but not penetrating through the sample as one would expect when using light microscopy. This means colours and shadings are artificially added to give a more user friendly interpretation of the sample. As mentioned previously, the resolution of an AFM image has a lot to do with the geometry of the cantilever tip, generally the sharper the tip the higher the resolution achievable as it will be able to resolve smaller and smaller topographical variations in the sample as it is raster scanned across. Early AFMs adopted a static probe, scanning stage approach to imaging which lead to complications when the AFM was mounted on an optical microscope; most notably that it is not possible to focus on something that is continually strafing the field of view. Modern AFMs have gotten around this early technical problem by employing a scanning AFM head atop a static microscope stage, meaning the user can maintain focus on the sample whilst imaging and watch for any changes. This enables the simultaneous recording of optical images, including fluorescence, together with topographical information (Shaw, Epand et al. 2006). Imaging with AFM can be divided in to two main sub-types; those in which the static deflection of the cantilever is measured and those which measure changes in the oscillation of the cantilever. Standard contact mode AFM is an example of the former and was the original method of imaging offered by early AFMs.

1.6.1.1 Contact Mode

Contact mode operates in the repulsive contact region of tip-sample interactions (Figure 7) here, the tip remains in constant contact with the sample surface as it is scanned back and forth across it, typically exerting forces on the order of 10-30nN on the sample (Allison, Mortensen et al. 2010). Forces of this magnitude are not thought to damage the cell however they are sufficient to 'feel' the underlying tensile structures of the cell as the plasma membrane is folded around these due to the force of the tip. In Figure 5 it is possible to see the actin stress fibres of a 3T3 cell. Here, the deflection of the cantilever acts as a feedback signal for the AFM to adjust its scanning level and results in the tip closely following the topography of the surface. Contact mode cantilevers are often made of silicon nitride (Figure 6). This

makes them extremely flexible and soft enough to image live cells. Although this mode stabilises the vertical force exhibited by the cantilever over the sample, it also subjects it to high lateral forces which are capable of displacing or even tearing delicate biological samples such as cells and biopolymers. It can also suffer from the effects of capillary forces when carried out in air. Capillary forces come about due to the presence of a thin layer of liquid found coating all surfaces in air; this layer is referred to as the 'fluid layer' and consists of condensed water vapour and other atmospheric contaminants, usually several nanometers thick (though this will vary with atmospheric conditions)(Putman 1994; C.B. Prater 2004). Under ambient conditions the absorbed water molecules form a thin layer on the sample surface and when a tip is brought close to this fluid layer it forms a meniscus – this meniscus causes an attractive force between the tip and the sample known as the capillary force. For these reasons some prefer to image biological material in tapping mode (aka intermittent contact mode) where the tip is intermittently in contact with the surface as it oscillates near its resonance frequency. The amplitude of the oscillations on the cantilever are typically greater than 20nm and commonly between 100-200nm in free air and are able to pull the cantilever out of contact and out of the influence of the fluid layer with each oscillation if the restorative force of the oscillation is greater than that of the fluid layer (Constant A. J. Putman 1994). Another way of negating the effects of the fluid layer is to image in liquid.

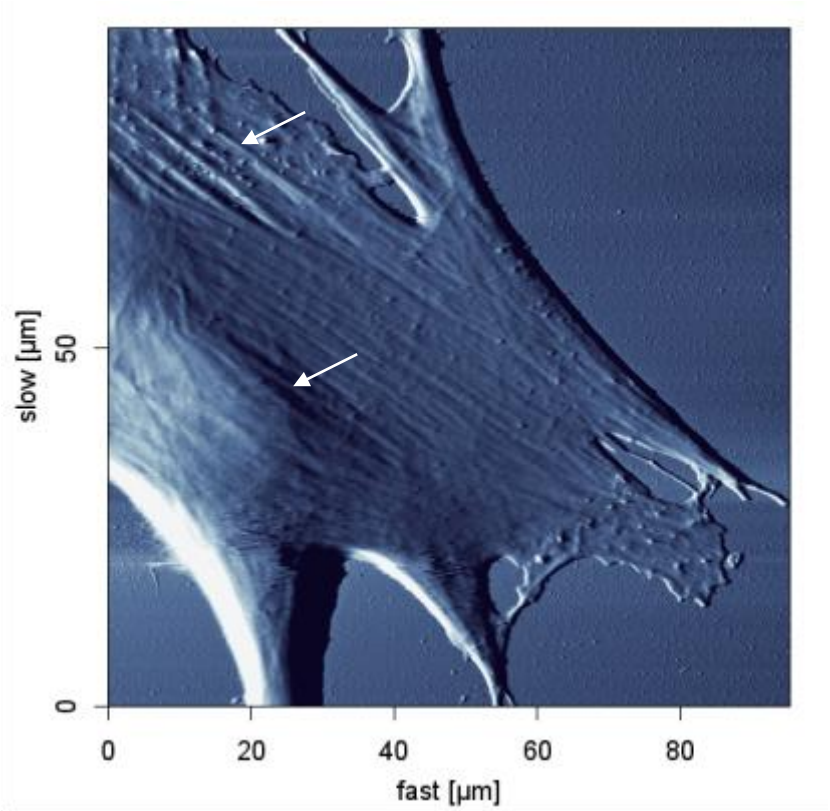

Figure 5: Contact mode 'vertical deflection' AFM image of a 3T3 cell body. The vertical deflection channel highlights edges within a sample because it uses the correction signal used by the feedback mechanism to adjust the height. Actin stress fibres (arrows) can be seen stretching across the cell.

As shown in Figure 5 the scan range of the AFM (100µm x 100µm max) is large enough to encompass the majority of a cell body and so can be used to gain an overview of the whole cell before the deciding upon the locations for further investigation.

1.6.1.2 Tapping mode

This operational gets round the problems associated with contact mode by greatly reducing the time the tip is in contact with the sample and the force of the tip-sample interaction. This is achieved by oscillating the cantilever at or near its resonant frequency using a piezoelectric drive located inside tip mount (or head). The oscillating cantilever is then lowered near to the sample and surface is detected by the subsequent dampening of the oscillation amplitude as the tip 'taps' into the repulsive region close to the sample surface with each oscillation cycle (usually between 50,000 and 500,000 cycles per second). In this way, the tip is only in

contact with the sample for a fraction of a microsecond in each cycle and therefore lateral dragging forces are greatly reduced. Tapping mode also prolongs the lifetime of the tip as blunting can be reduced and is kinder to loosely adhered or fragile samples, imparting a typical tip-sample force of around 2nN with each 'tap' (Constant A. J. Putman 1994). Due to the nature of the technique, tapping mode cantilevers must be significantly stiffer than contact mode cantilevers to allow such high frequency oscillations with the power to overcome the adhesive fluid layer mentioned previously (Figure 6); they are usually in the range of 2N/m to 50N/m. Like contact mode, tapping mode takes place in the repulsive contact region of the force potential curve (Figure 7) and therefore although lateral forces acting upon the sample are greatly reduced, the sample is still subject to compression forces which can impact upon the behaviour of the specimen.

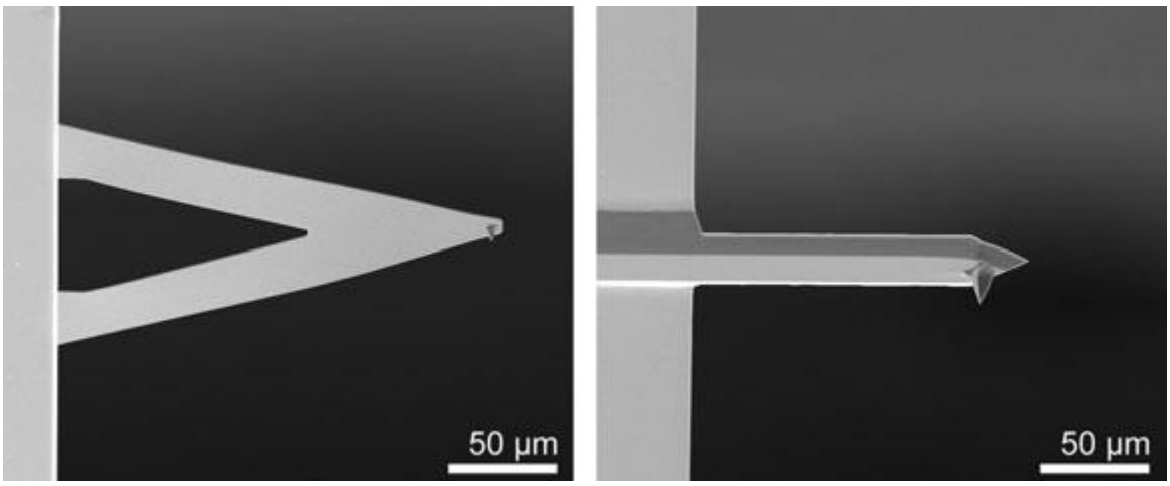

Figure 6: Typical contact mode and tapping mode cantilevers. Left image shows a v-shaped contact mode cantilever made of silicon nitride (Si_3N_4). Right image shows a rectangular tapping mode cantilever made of silicon. Note; tapping mode can be performed with v-shaped cantilevers so long as the resonance frequency is sufficiently high, likewise many contact mode cantilevers can be rectangular in shape. Traditionally, v-shaped cantilevers are thought to have better lateral stability than rectangular cantilevers; however this has been shown not to be the case for certain geometries as explained in this paper by Sader in 2003: (Sader 2003). Image from 'Atomic Force Microscopy' by Peter Eaton and Paul West (Peter Eaton 2010).

1.6.1.3 Non-contact mode

Non-contact mode imaging also uses changes in the oscillation of the cantilever to produce an image, however rather than detecting reduced oscillation amplitudes due to contact with the sample it uses the changes in the attractive van der Waals forces that pull on the tip during approach to the surface to determine surface topography. It has many of the benefits of tapping mode in that it greatly reduces tip-sample forces while maintaining high resolution and does so without coming in to repulsive contact with the sample thus theoretically eliminating the possibility of sample damage and preserving tip sharpness. As with other imaging modes that rely on monitoring oscillatory changes to detect surface topography, scanning speeds are often lower than with contact mode and high frequency cantilevers are needed (resonance frequency in the range of 300-400 kHz). This is because non-contact mode operates in the attractive region of the tip-sample potential curve (Figure 7) and stiff cantilevers enable better control over the influence of the van der Waals forces. To achieve optimal image resolution and minimum 'wear' on the tip it is essential that this type of imaging be performed in air under ambient conditions. In this way, the fluid layer can be used to dampen the oscillations of the cantilever without the tip ever contacting the surface. These conditions should mean the tip will not pick up debris from the sample surface or blunt itself upon contact with the surface, both of which will result in alteration of the tip geometry and a reduction in image resolution (Ho and West 1996).

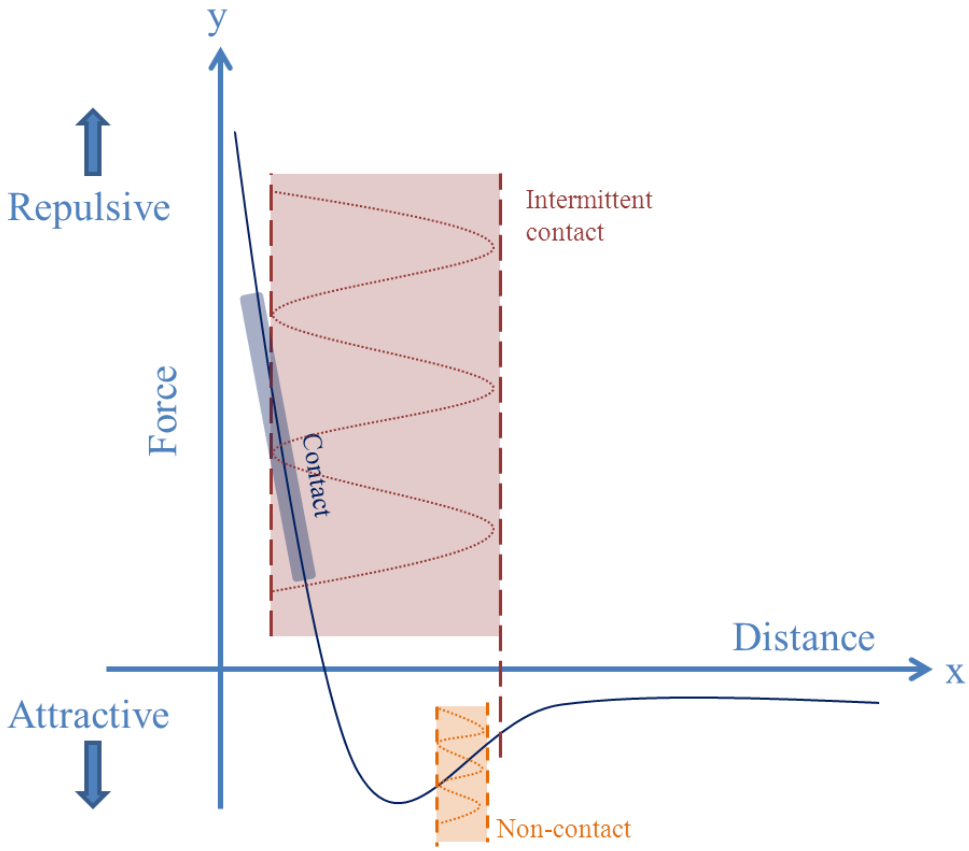

Figure 7: Force potential diagram showing the operational regions of each of the three main imaging modes. Figure inspired by JPK User Manual (2008).

1.6.2 AFM force spectroscopy

AFM force spectroscopy complements the micro and nanoscale topographical detail offered by imaging with the ability to simultaneously measure the elastic properties of biological samples also under physiological conditions. In particular, force spectroscopy on living cells allows the user to gain vital mechanical information from any given location on a cell with high spatial resolution. In the fields of cancer and developmental biology today, information on cell mechanical properties is proving vital to the greater understanding of mechanisms of metastasis and differentiation (Guck, Schinkinger et al. 2005; Kumar and Weaver 2009). Fundamental cellular behaviours such as locomotion, division and ageing can also manifest themselves as changes in the elasticity of the cytoskeleton and so with the aid of the AFM these changes have the potential to become early stage markers for important behavioural abnormalities. Biologists now accept that cell many cell

functions and behaviours are largely influenced by structure and so force spectroscopy has become the primary function of the AFM for many groups.

Since the cantilever of an AFM is effectively a spring it only seems natural to utilize it as a nanoscale indenter. Force spectroscopy mode is just this, the x and y position of the cantilever remain static while in the z direction the tip is pushed in to repulsive contact with the sample and retracted. Each time one of these extend-retract cycles is completed a force-distance curve is produced (Figure 9). Although there are various types of force spectroscopy, including single-molecule force spectroscopy (SMFS), molecular recognition mapping (MRM) and single-cell force spectroscopy (SCFS) (Gernot Friedbacher 1999), this chapter will focus only on force spectroscopy in perhaps its simplest form. Here we are pushing the cantilever in to the samples and extracting the Young's modulus from the resulting force distance curves through application of a mathematical model of fit for each curve. Knowing the applied force, tip geometry and spring constant of the cantilever is essential for this. Stiffness mapping, or force mapping as it is sometimes referred to, is a technique which takes advantage of the high spatial resolution offered by force spectroscopy; it involves performing multiple identical force indentation curves covering the surface of the sample, in the process building a map based on the recorded stiffness values. When performed on living cells this type of force spectroscopy can identify stiff regions of the cell corresponding to large actin filaments or the nucleus (Figure 8). In this way, alterations in cytoskeletal arrangement and strength can be observed over time as changes are induced (Rotsch and Radmacher 2000). The resulting stiffness map is a 2D representation of stiffness gathered independently of any AFM topographical image; to combine the two techniques it is possible to utilise pulsed-force mode (PFM) AFM.

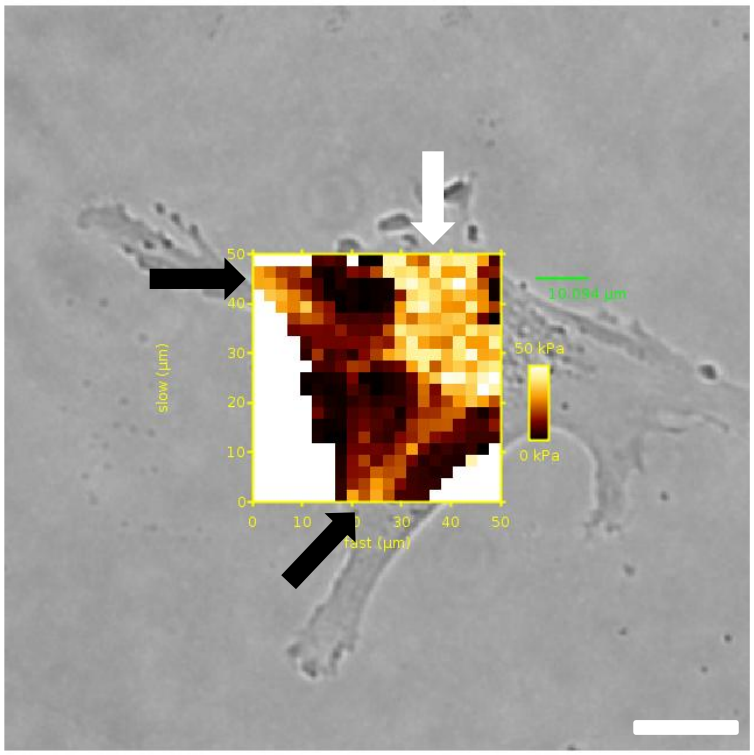

Figure 8: The gridded square in the centre of the image is an example of a force map. It is a visual representation of the Young's modulus values obtained from each point measured on the cell in the optical image on which it is overlayed. By overlaying the two images this way it is possible to observe the regions of varying stiffness across a cell. Resolution depends on how many points are included in the force map grid – this example shows a grid of 50 x 50µm containing 441 force indentation measurements, one in the centre of each square. It is possible to increase this to 1000 measurements; giving increased spatial resolution to the force map. However, in the image above it is still possible to identify a relatively stiff area near the top right hand corner of the force map, represented by the lighter colour squares, (white arrow) which in this case corresponds to the nuclear region. At least two lines of increased stiffness are also apparent, we hypothesise these correlate to underlying filamentous actin structures (black arrows). In this example the cell measured was a mature mouse osteoblast courtesy of You-Ying Chau of the MRC Human Genetics Unit, University of Edinburgh, Western General Hospital. Scale bar represents 20µm.

Pulsed-force mode AFM has been designed to combine the advantages of tapping mode and force spectroscopy into one measurement process (Peter Eaton 2010). In this operational mode the AFM is able to gather information on topography, elasticity, electrostatic forces and adhesion simultaneously while maintaining the relatively high scan speeds and low lateral forces of tapping mode. This is achieved by performing full force-distance curve cycles while imaging in tapping mode and usually requires additional high speed electronics to be integrated in to the traditional AFM setup to deal with the huge amount of data generated at high speed – the system works at up to several thousand pixels per second (A Rosa-Zeiser 1997). This technique has proved useful when the distribution of elastic or adhesive regions on surfaces is of interest, such as on the development of racing car tyres (Innovations 2001) and on microcontact printed patterns (Okabe, Furugori et al. 2000).

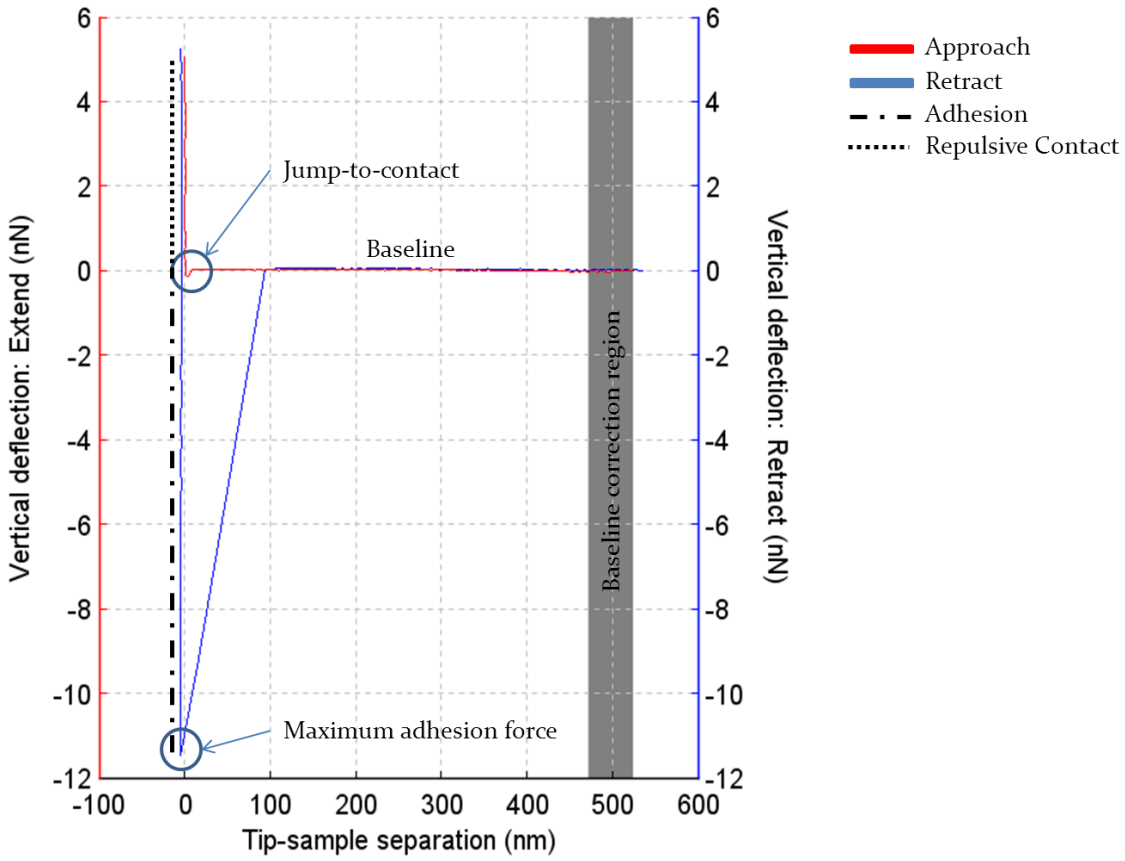

Figure 9: Example of a force-indentation curve performed with a sharp MLCT tip on glass in air. Note, this curve has been corrected for cantilever bending; this means the actual indentation depth has been calculated by taking the difference between the vertical piezo movement and the vertical deflection of the cantilever in units of length (Neumann 2011). Following this calculation the x-axis is renamed 'tip-sample separation' to highlight this change. The figure highlights characteristic features of measurements in air on glass such as the 'jump-to-contact' region where the tip is overpowered by the capillary force of the fluid layer and the vertical repulsive contact region caused by the inability of the tip to indent the glass substrate. Also of note is the overlapping of the approach and retract baseline traces. Measurements in liquid tend to result in a gap between the baseline traces due to the viscosity of the liquid. Hysteresis is less prevalent with measurements in air also. The vertical grey bar represents the portion of the approach baseline that has been used to determine zero force and level the curve.

The resulting force-distance (f-d) curve from a force spectroscopy measurement can tell the user several vital pieces of information pertaining to the nature of the sample being indented and the measurement environment. There are essentially 4 parts to a f-d curve highlighted in Figure 10:

1. The approach portion of the measurement before the tip has contacted the surface. Here, the cantilever is moving toward the surface experiencing only thermal fluctuations and viscous forces (if the measurement is taking place in liquid). No significant deflections are observed at this stage.

2. As the tip contacts the surface the cantilever begins to deflect. The cantilever is now in repulsive contact with the surface and – in the case of living cells – pushing in to them.

3. Once the deflection is such that the pre-defined force setpoint is reached, the AFM stops indenting and begins to reverse the path of the cantilever, retracting it from the surface.

4. Upon retracting from the sample surface it is common to observe adhesion between the tip and the sample surface as it tries to pull free. In air this can be caused by capillary forces, with live cells this can be specific and non-specific binding of proteins to the tip.

The thermal fluctuations alluded to at stage 1 are a fundamental source of noise in AFM measurements. These environmental fluctuations constantly provide small pulses of force either in air of in liquid – though they are more prevalent in liquid. This type of movement can be seen observing the diffusion of small particles in liquid, known as Brownian motion. The severity of effect of the fluctuations depends on the spring constant of the cantilever and the temperature at which the measurement is being performed – softer cantilevers are more susceptible (Jaschke 1995).

Some of the characteristics of measurements in air on glass are described in Figure 9 such as capillary force and the linear nature of the repulsive contact potion. Measurements in a liquid environment have several unique characteristics of their own; these are detailed in Figure 10 and include hysteresis influenced by thermal

fluctuations and mismatching of the approach and retract baselines due to viscous forces of the liquid.

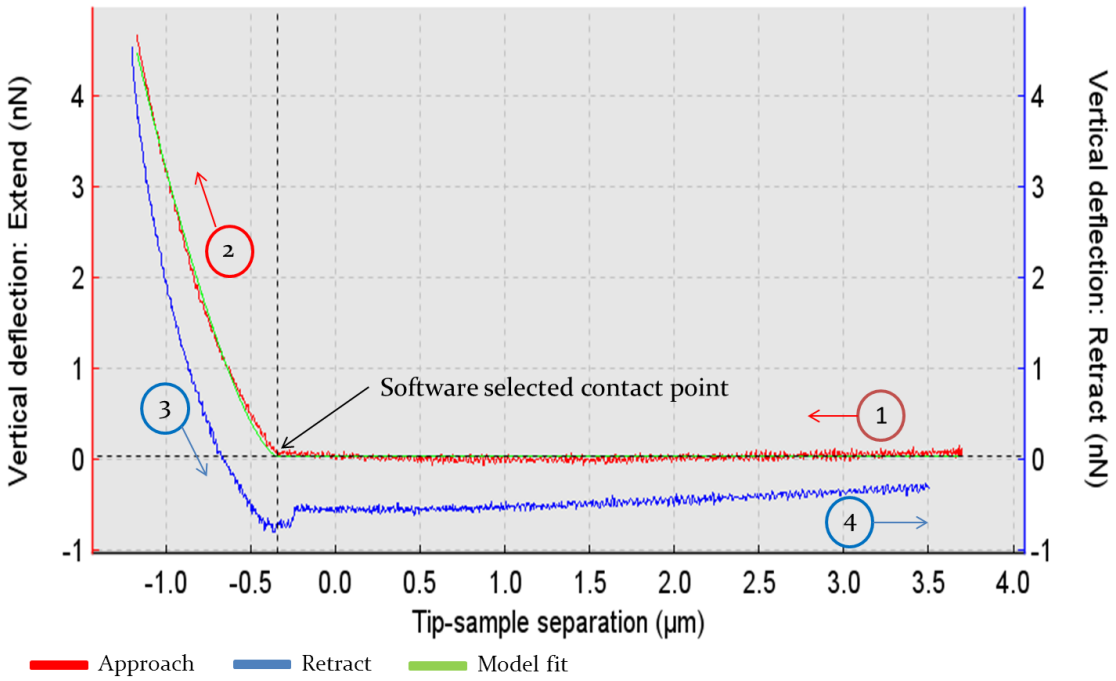

Figure 10: Shows an example of a force-indentation curve performed on a live MG63 cell nucleus in a liquid environment at 37°C. Evidence that this curve was performed in liquid can be seen by the increased levels of hysteresis in the baseline portions; the primary cause is thermal fluctuations in the measurement medium which are more prevalent in liquid than in air. Note also that the approach and retract traces do not return to the same 'o force' deflection point, this is due to the viscosity of the liquid inducing hydrodynamic drag on the cantilever hence why it is not seen in Figure 9. Note the repulsive contact portion of the curve is sloping rather than vertical pertaining to the fact that the tip is able to indent the sample in this instance, also not seen in Figure 8.

1.7 Cell elasticity quantification by AFM

The Young's modulus of living cells varies considerably throughout the range of cell types and techniques available to measure it. One reason for this is that elasticity measurements performed by the AFM are based on Hooke's law of elasticity (Vinckier and Semenza 1998) (Eqn 1). This states that the extension of a spring (in this case the cantilever) is directly proportional to the strain applied to it. This is appropriate for linearly elastic or 'Hookean' materials only and as cells cannot be considered linearly elastic, the correct application of the mathematical model of fit is essential. For this reason it is important that we standardise the method by which we derive the Young's modulus from the initial force distance curve.

$$F = -kx$$

Equation 1: Hooke's law of elasticity, where 'F' is the restorative force exerted by the spring, 'x' is the size of the displacement and 'k' is the spring constant specific to each spring.1.7.1 Evaluation of elasticity from indentation measurement

To evaluate cellular Young's modulus, a force-indentation curve has to be derived from the general force-distance curves, where the deflection of the cantilever is plotted as function of Z-stage displacement (z). In an indentation measurement, the cantilever movement toward the cell (z) consists of both the indentation of the sample (δ) and a cantilever deflection (d, d=F/k) (Figure 11). The indentation distance into the sample (δ) can be corrected by subtracting the cantilever deflection (d) from the pizeo-displacement, resulting in the force indentation curve (also called force-tip-sample separation in the software used).

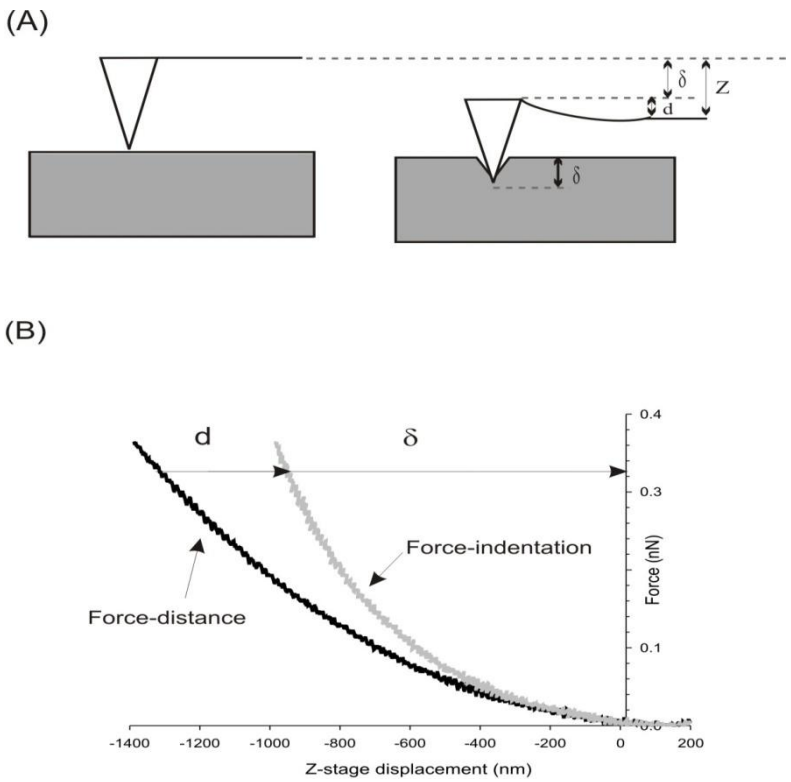

Figure 11: (A) Schematic diagram showing indentation of a soft substrate by an AFM tip and cantilever. (B) The indentation distance into the sample (δ) can be corrected by subtracting the cantilever deflection (d) from the pizeo-displacement; discussed in Figure 8, (W. Richard Bowen 2009).

To calculate Young's modulus of cells the Hertz model was applied to interpret the force-indentation curve throughout this project. This model is discussed in greater detail in the following section 1.7.1 Models for deriving elasticity from force distance curves.

1.7.1 Models for deriving elasticity from indentation measurements

To extract a value of elasticity from a force distance curve the data must be fitted with a mathematical model designed to calculate the particular parameter of interest, which in this case is elasticity or 'Young's modulus'. Many such models exist but in reality most are modifications on the Hertz model (Eqn 2), which has become the most commonly used model of fit for biologists in particular.

$$F = \frac{4}{3}\frac{E}{1-\nu^2}\delta^{3/2}\sqrt{R}$$

Equation 2: Where R is the radius of the sphere, F is the indentation force, E is the Young's modulus, ν is the Poisson's ratio, and δ is indentation depth. The cell was assumed to be incompressible and a Poisson's ratio of 0.5 was used.

In its basic form, the Hertz model describes contact between two smooth elastic glass spheres and demonstrates that the size and shape of the region of contact varies with the deformation of the contacting bodies (K. L. Johnson 1971). In this original version of the theory, two main assumptions are made: 1) that the indenter geometry is parabolic and 2) that the total indentation depth comprises an insignificant proportion of the total thickness of the sample. Assumption one is able to be met if the maximum depth of the indentation is less than 1/3 the radius of the spherical indenter (Mahaffy 2000). Assumption two requires that the maximum thickness of the sample be known in order to judge the indentation depth accordingly.

Variations on the model arise when experimental parameters or sample conditions do not meet the requirements of the model and call for an extra factor to be taken in to consideration, for example; sample thickness, sample-surface adhesion or alternative indenter geometry. This is important because the fundamental assumptions made by the Hertz model cannot be true for most biological samples and certainly not for living cells, however alterations to the model have been incorporated to account for various indenter geometries such as cones and four-sided pyramids (Lin, Dmitriadis et al. 2007). In addition to the assumptions listed above, the model also approximates the sample as a homoelastic solid and treats the

indenter as non-deformable with no additional interactions with the sample – such as adhesion. Should all these parameter be met, the Young's modulus (or elasticity E) can be calculated accurately using the Hertz model. However when working with living cells this is simply not possible therefore it is unavoidable that some degree of error be present in each calculation.

As mentioned above, the Hertz model is the most commonly implemented model today and contains the basic principles upon which most other models of elasticity are based. Being essentially an elastic model designed for use on soft materials (Mahaffy, Park et al. 2004), it can also incorporate viscoelastic contributions also and is particularly suited to thicker samples or indeed thicker areas of cells such as the nuclear and perinuclear regions, so long as relatively shallow indentations are performed (<10% of total sample thickness). However, AFM measurements by their very nature become susceptible to the substrate effect as they penetrate deeper in to the cell. The substrate effect becomes a pertinent problem when the indentation location falls on a particularly thin sample region such as the leading edge (lamellipodia) of living cells or especially thin polymer gel samples mounted on stiff glass or plastic substrates. It is characterised by the tip of the AFM 'feeling' the increased stiffness of the substrate through the comparatively soft material of the sample and registering the impact in the resulting force indentation curve. Typically it leads to artificially increased values of elasticity when the curve is fitted with the model. By making indentation depth a negligible proportion of total sample thickness it helps to negate the impact of the endogenous error incorporated by the model on the elasticity result. The model is therefore not suited to indenting thin regions of cells such as lamellipodia (<1000nm) on account of the strong influence the underlying stiff substrate can have on the recorded elasticity. For regions such as this, the Tu or Chen models (Eqn3; Eqn 4) are more appropriate.

Chen model for adhered thin regions of cells

$$\frac{K_{Hertz}}{K_{Chen}} = \frac{3\pi}{4}\ 1-\vartheta\ \ \frac{\alpha_{Chen}}{\alpha_{Hertz}}\ \sum_{i=1}^{N} \frac{\rho_i^c\ \vartheta}{1+2i}$$

with

$$\alpha_{Chen} \equiv \alpha, \qquad \alpha_{Hertz} \equiv\ \ R\delta^{\ 1\ 2}$$

Equation 3: An expression of the equation used to convert values obtained by the Hertz model in to those of the Chen model. With the Chen model, unlike the Tu model, the values ρ_i^c are dependent on the Poisson's ratio; therefore the ratio of $\frac{K_{Hertz}}{K_{Chen}}$ is dependent on the Poisson's ratio (Mahaffy, Park et al. 2004).

Tu model for non-adhered thin regions of cells

$$\frac{K_{Hertz}}{K_{Tu}} = \frac{3\pi}{4}\frac{\alpha_{Tu}}{\alpha_{Hertz}}\ \sum_{i=1}^{N} \frac{\rho_i^T}{1+2i}$$

with

$$\alpha_{Tu} \equiv \alpha, \qquad \alpha_{Hertz} \equiv\ \ R\delta^{\ 1\ 2}$$

Equation 4: This equation shows the relationship between the elastic values obtained by the Hertz model and those obtained by the Tu model. Unlike the Chen model, the ratio of $\frac{K_{Hertz}}{K_{Tu}}$ is independent of the Poisson's ratio. The Tu model can account for a spherical body (AFM colloidal probe) impacting on a non-adhered layer (thin region of cell) and was first solved in 1964 by Tu *et al* (Tu 1964).

The Tu (Eqn 4) and Chen (Eqn 3) modifications of the Hertz model are suited to indentation experiments where the sample is particularly thin, because these models take the boundary effect imposed by stiff substrates in to account and so are better able to handle the influence this has on the force indentation curves (Park, Koch et al. 2005). Additionally, the height of the sample at the point of indentation is of particular importance for proper use of these models, which can also be applied to thin polymer films (Dimitriadis, Horkay et al. 2002). Although both modes are

better equipped to deal with thin regions each has a particular speciality pertaining to sample adhesion. Note that for very thick samples or regions of cells; the Tu and Chen models behave similarly to the Hertz model (Mahaffy, Park et al. 2004), it is only when significant contributions are made by the hard underlying substrate that the values of the Tu and Chen models will deviate from those of the Hertz. Both are also able to be extended in order to calculate viscoelastic behaviour of thin regions of cells.

The Chen model is designed to handle measurements performed on well adhered samples – or well adhered regions of samples, therefore it assumes a rigid sample-substrate bond. A well adhered region is described as one which is unable to move at the sample-substrate interface, conversely, a region is considered non-adhered if the sample is able to slip freely over the substrate. This can be described simply as a sphere contacting a layer of known thickness which is being supported by a hard, adherent substrate (Mahaffy, Park et al. 2004). The Chen model also has the advantage of being able to determine both the elastic constant and the Poisson ratio; which in previous measurements was just assumed in order to deduce the Young's modulus.

The Tu model originated from a problem described in 1962 by Popov which set out to address the problem of a spherical indenter contacting a non-adhered layer on a stiff substrate (Popov 1962). This problem was solved by Tu *et al* for substrates within a limited thickness range (Tu 1964). Because the Tu model assumes the sample is not adhered to the underlying substrate it allows for lateral slip and considers it unconstrained. Precisely how much lateral slip can be tolerated by the model is not presented in the literature. It assumes boundary conditions analogous to two identical spheres indenting a layer double its actual thickness (Margetson 1970).

However in the paper '*Quantitative Analysis of the Viscoelastic Properties of Thin Regions of Fibroblasts Using Atomic Force Microscopy*' by R. E. Mahaffy *et al* (Mahaffy, Park et al. 2004) they explain that by utilizing both models it is possible to correlate the adhesion of the cell in each specific location with the Young's modulus. This information can prove useful when relating it to cell motility at the

leading edge. For a full explanation and complete solution to both models please consult the methods papers '*Impact and contact stress analysis in multilayer media'* and *' Computation of stresses and displacements in a layered elastic medium'* by Chen *et al (Chen 1971; Chen and Engel 1972)*. Throughout this project the Hertz model as modified for indenter geometry was used to extract all Young's modulus values. It is the most commonly used and best characterised model meaning the limitations are well documented and understood; this makes reducing their influence possible by careful consideration of experimental protocol. For more detailed discussion of experimental protocol see Chapter Three. Also, due to the location of measurements performed in this thesis being on the nuclear region, the cell is thick enough here for the Hertz model to adequately describe the experimental data (Kuznetsova, Starodubtseva et al. 2007; Lee YJ 2011).

1.8 Outline of thesis

This thesis aims to investigate the elasticity of living cells as a potential label free indicator of cellular responses to their microenvironment. To enable systematic investigation in to this, microfabrication technology has been used to design model substrates that mimic defined aspects of the extracellular matrix *in vivo*. I have exploited atomic force microscopy as a promising tool to enable the reliable quantification of cellular elasticity. In addition to cell elasticity studies, more traditional molecular biological methods were employed to complement the investigation in to cell responses.

Throughout this thesis the results of elasticity studies have been used to guide further investigations in to the mechanisms by which cells respond to their surrounding environment. Elasticity data is not being advocated as a definitive diagnosis of cell phenotype, fate or function, rather as an additional piece to elucidate the puzzle.

Chapter one: Introduction, explores the background and basics of the extracellular matrix as observed *in vivo* and goes on to highlight the advantages on offer to researchers attempting to recreate aspects of it using microfabrication technology. Fundamental features of cell adhesion are described and the basics of atomic force

microscopy are explained with particular emphasis on force spectroscopy measurements.

Chapter two: Materials and methods, is restricted to aspects of the project than can be generally applied throughout the work. This includes basic cell culture and statistical analysis techniques as well as fabrication protocols and immunofluorescence detection techniques.

Chapter three: Optimisation of cellular elasticity measurements will highlight the methods used to create a robust protocol for using AFM to quantify cellular elasticity. Important issues to consider before commencing any experiment such as probe selection and measurement environment will be discussed in detail. The aim of this is to best limit variation in the end result thus improving reliability and confidence in the measurement.

Chapter four: Can common cell adhesion molecules affect elasticity? An AFM approach looks at the initial work done to demonstrate the effectiveness of the protocol developed in chapter three. The effect of simple chemical modification of substrates is the focus of this chapter and the longer term influences of topography are demonstrated.

Chapter five: The topographical influence on cellular elasticity, takes the findings from chapter four – specifically that topography can have a lasting influence on cellular elasticity – and investigates the possibility that elasticity changes are precursors to more fundamental transcriptional changes. The aim here is to demonstrate that elasticity values as recorded by the AFM can provide additional information to help unravel the mechanisms of mechanotransduction and that topography alone can induce transcriptional changes in cells.

Chapter six: Conclusions and future work, draws from the conclusions of the previous three experimental chapters in order to summarise the main points of the project and evaluate them against the aims originally stated in section 1.8. Also included are sections on the limitations of the AFM technique and possible routes for improvement, as well as ideas for future work continuing on from the findings presented here.

Chapter two: Materials and Methods

This chapter details only those materials and methods which have been generally applied to all experiments. Those which are specific to a particular chapter are detailed within the materials and methods section of that chapter.

2.1 General reagents

Unless otherwise stated general reagents used during the course of this work were purchased from Sigma Aldrich.

2.2 Cell Culture

NIH/3T3 fibroblasts & MG63 osteoblast-like cells (ATCC) were cultured at 37 °C and 5% CO_2 in Dulbecco's modified Eagle medium containing nutrient mixture F-12 (DMEM/F12, GIBCO) supplemented with 10% foetal bovine serum (FBS), 2 mM L-glutamine and 100 U/ml of penicillin and streptomycin. Confluent cultures were detached from tissue culture flasks using Trypsin/EDTA solution to generate cell suspensions for subsequent passage or cell culture on substrates.

Cell seeding concentration on a glass / PDMS substrates was chosen to be 2 x 10^4 cells/ml to produce well developed single cells for AFM measurements. Prior to AFM measurements, an overnight cell culture on the prepared glass / PDMS substrates was carried out at 37°C, 5%CO_2. The substrate with cells was then quickly mounted on a heated 'BioCell' stage (JPK instruments) which maintains cells and medium at 37°C for the 2 hour duration of the AFM experiments. Similar cell seeding densities were used when culturing cells for immunofluorescence microscopy and transmission electron microscopy.

2.3 Fabrication of topographic substrates

Described here is the process by which structured PDMS substrates were produced from etched silicon wafers to be used in cell studies.

2.3.1 Silicon master fabrication

Photolithography and dry etch procedures were used to create silicon master moulds for topographically structured PDMS substrates. The basic photolithographic procedure is shown in Figure 12. The process begins with cleaning

the silicon wafer: 3 x 5 minute washes in an ultrasonic bath in methanol, acetone and isopropyl-alcohol respectively. Next, the photoresist was spun on to the wafer at 4000rpm for 30 seconds. In this work we used AZ4562 and Shipley S1818 positive photoresists therefore any areas exposed to UV light were developed away. To evaporate solvents from the resist the wafer is placed on a hot-plate for 3 minutes at 90-95°C. The sample was then ready to be exposed to UV light (360nm) through a patterned photomask in the MA6 mask aligner (SUSS Micro Tec, Garching Germany). The MA6 exposure conditions are set to 'hard contact, 50μm gap' for 3-4 seconds for S1818 resist and 10 seconds for AZ4562. S1818 resist samples are developed in a 1:1 solution of distilled water and 'Microposit developer' for ~30 seconds and AZ4562 sample are developed in a 1:4 solution of 'AZ400k developing solution' and distilled water for 2-3 minutes. Results are checked under optical microscope to ensure complete removal of exposed photoresist. Sample is then dried using a nitrogen gun and subject to a post-bake at 120°C for 30 minutes. The sample is now ready to be dry etched.

Samples were etched using a custom gas mixture (UDO1) at a rate of 1μm/min in the STS dry etch apparatus. After etching the remaining photoresist is removed by sonication in acetone. The etch depth was checked using the atomic force microscope.

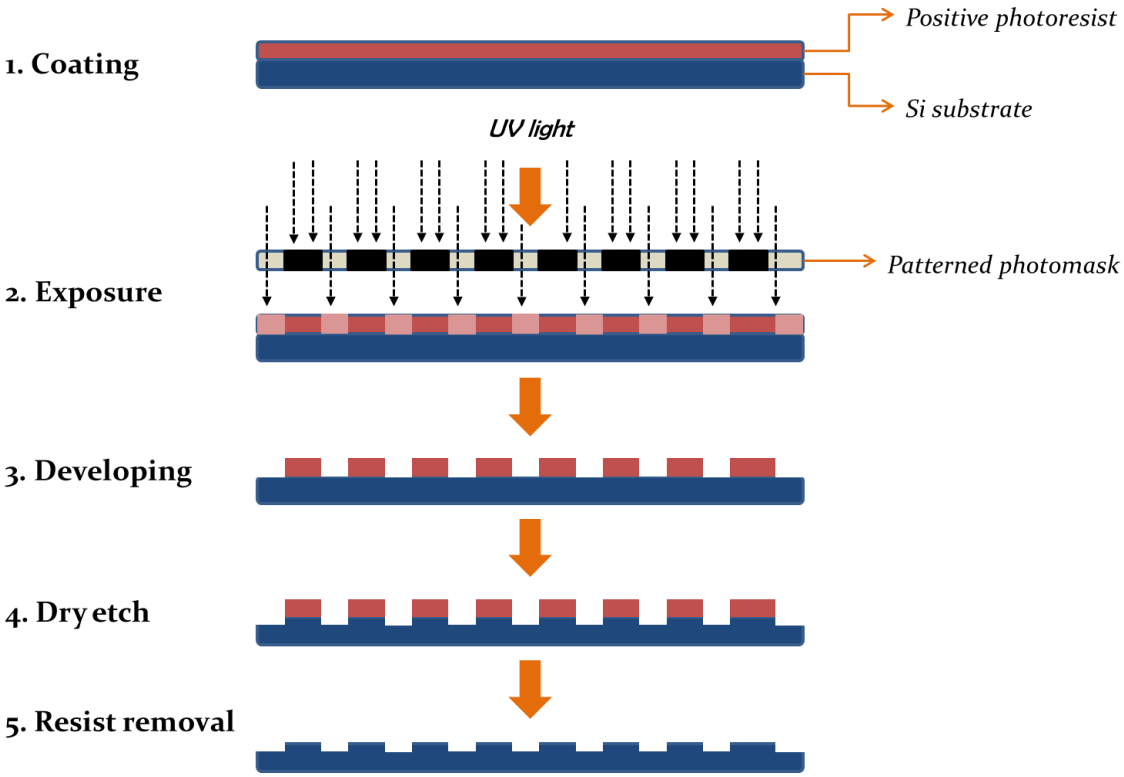

Figure 12: Basic stages of photolithography and etching to produce silicon master moulds for use in soft lithography techniques. Photoresist used was S1800 series® (Shipley). Silicon wafers from.

2.3.2 PDMS replica preparation

Microstructured Poly(dimethylsiloxane) (PDMS) substrates were prepared using soft lithography as follows: pre-polymer (a mixture of 10:1 silicon elastomer and curing agent) was degassed inside a desiccator under vacuum conditions achieved using an external motorised pump, then cast against silicon masters and cured at 70 °C overnight. The solidified PDMS substrates were then washed with ethanol and plasma treated in an oxygen barrel asher (Gala Instruments Plasmaprep 5) for 30 seconds before cell seeding.

2.4 Optical and fluorescent detection

Both transmission and fluorescent images of stained cellular structures were recorded using a Zeiss Axiovert inverted fluorescence microscope coupled to a cooled monochrome CCD digital camera (Andor iXon, Andor Technology). A filter set, containing an exciter D475/40, a dichroic 495LP, and an emitter E510LP were used for the FITC fluorescence imaging. A filter set, containing an exciter EX630/50, a dichroic 650, and an emitter E695 were used for the Cy5 fluorescence imaging. A filter set containing an exciter 500±25, a dichroic 525nm and an emitter 545nm were used for rhodamine fluorescence detection. All the samples were imaged using the same acquisition conditions.

2.5 AFM

All AFM work was carried out using the NanoWizard II Bio AFM (JPK Systems, Berlin), mounted on a Zeiss Observer A1 inverted optical microscope placed on top of a Halcyonics Micro 40 anti-vibration table. The complete set-up was acoustically isolated in an in-house manufactured chamber in order to reduce the interference of ambient noise during the measurement. More details of AFM measurements are described in Chapter three: optimisation of cellular elasticity measurements. Unless otherwise stated, all the elasticity results detailed here were got from the application of the Hertz model –modified only for spherical indenter geometry- to force distance curves. The probe used was an Arrow TL1 tipless cantilever with 4.8µm silica microsphere attached (see section 3.3.3 AFM colloidal probe preparation for details).

2.6 Transmission Electron Microscopy

Transmission Electron Microscope (TEM) images were taken using a LEO 912AB TEM at 4000 x magnification. The accelerating voltage was 100kV. Cells for imaging under the transmission electron microscope were seeded on PDMS substrates as per the standard protocol detailed above and cultured overnight. Preparation for TEM imaging was as follows:

1. Fix cells in solution of 2.5% gluteraldehyde 0.1M sodium cacodylate for one hour at room temperature.
2. Rinse cells in 0.1M Sodium cacodylate and store at 4°C until able to commence next stages.
3. Wash 3 x 5 minutes in 0.1M Sodium cacodylate solution.
4. Submerge in 1% osmium tetroxide for one hour at room temperature.
5. Wash 3 x 10 minutes in distilled water.
6. Submerge in 0.5% Uranyl acetate for one hour in the dark.
7. Quickly submerge in distilled water.
8. Wash 2 x 5 minutes in a series of increasingly concentrated ethanol solutions;
    a. 30%
    b. 50%
    c. 70%
    d. 90%
    e. Absolute – 4 x 5 minute wash.
    f. Dried absolute – 4 x 5 minute wash.
9. Submerge in 1:1 solution of dried absolute ethanol : Epon resin overnight.
10. Submerge in pure Epon resin (minus accelerator), perform 3 solution changes over the next day.
11. Samples embedded and polymerised in Epon resin (including accelerator) at 60°C for 16-24 hours.
12. Ultrathin (~70nm) transverse sections cut using Leica Ultracut UTC (Ultratome).
13. Sample sections contrast stained for 5 minutes in 2% Methanolic Uranyl Acetate then 5 minutes in Reynolds Lead Citrate prior to imaging with TEM.

2.7 Statistical analysis

A two-sample Student's t-test was employed to test the null hypothesis that the means of two populations of cells were equal with no significant difference. This test was used when a direct comparison of only two population means with varying cell numbers was required. The test expresses the actual difference in sample means in relation to the variation in the data, which must be expressed as the standard deviation of the difference between the means.

Data presented in chapters 3, 4 and 5 (sections 3.3.4, 3.7.2, 4.3.1, 4.3.2, 5.3, & 5.3.3) and throughout the thesis on cell elasticity values are expressed as mean ± 1StDev. Standard deviations were used to demonstrate the variation from the mean within the populations measured. If the standard deviation is large (relative to the mean) then the sample values are spread over a large range of values whereas a smaller standard deviation will indicate that sample values lie closer to the mean. Standard deviations were calculated with n-1 as the denominator, this is consistent with only a sample of the population being measured i.e. not every cell in every population could be indented with the AFM.

Sample precision was calculated using the formula below (Eqn 5). The precision of the results gives the maximum difference between the sample mean and the true mean of the whole population.

$$E = \frac{1.96 \times SD}{\overline{n}}$$

Equation 5: Used to calculate the precision (E) of the results. SD is standard deviation and *n* is sample number.

Using the standard deviation from the results of section 3.4.4 we aimed to achieve a precision of 0.4 kPa or better throughout the project. This required a sample size of at least 22 cells however no fewer than 25 cells were used for any quantitative analysis of cell heterogeneity. Meeting the minimum sample number meant that 95% of the time we could be sure that our observed sample mean fell within 0.4 kPa of the true population mean.

Chapter three: Optimisation of cellular elasticity measurement

3.1 Abstract

Indenting live biological samples with the AFM is a difficult task with many parameters to control. A comprehensive understanding of these parameters is essential if AFM results are to be considered reliable. In this chapter, all aspects of live cell indentation measurements will be investigated with the aim of producing a robust and reliable protocol that can be adapted to various specific experimental requirements.

3.2 Introduction

Cell heterogeneity is endemic amongst populations of cells. Perhaps not always obvious from the outset; it can take high resolution techniques to discover. The behaviour of the population or tissue as observed could in some cases mask individual differences (Wong, Tsai et al. 2007), however this does not negate their influence. When indenting single cells with the AFM these differences become altogether more influential due to the relatively small sample size (~30 cells) typically dealt with in AFM studies. Cell heterogeneity has the power to influence the overall view of a population's elasticity and cast doubt over findings. Conversely, the behaviour of the population may not always accurately represent the behaviours of the individual cells within. Differences will always exist if you look with a fine enough resolution (Altschuler and Wu 2010). The challenge for researchers is to differentiate between endemic differences and those which yield important information relevant to the study at hand. In our case, measuring differences in cellular elasticity has, over the years, been the focus of many an instrument and many an experimental procedure. All these sources of variation mean that special consideration has to be given to new data sets generated.

Upon searching the literature for a range of elasticity values as measured by AFM for various cell types it immediately becomes apparent that for each cell type the values reported for their elasticity vary widely. For example, osteoblasts have

recorded elasticity values of between 0.3 and 20 kPa (Simon, Cohen-Bouhacina et al. 2003), red blood cells of between 19 and 33 kPa (Dulinska, Targosz et al. 2006) and 3T3 fibroblasts of between 3 and 12 kPa (Rotsch, Jacobson et al. 1999). This is partly due to the natural heterogeneity found in living biological samples but could also be attributed to various imperfections or misunderstandings in the AFM method employed and indeed the methods used for analysis of the force-indentation curves. In this chapter we look at what can be done to limit the level of variation introduced by the AFM indentation method while reliably uncovering variation found naturally in cell populations through careful consideration and optimisation of the method. Here the aim was to develop a robust and reliable protocol for cellular elasticity measurements by optimising parameters such as indentation force, indentation speed and indentation depth as well as investigating the merits of varying tip geometry between sharp and spherical probes. Sample specific preparations are also taken in to consideration, for example, whether a cell is adherent or in suspension, whether microtopography is used and if cells are present as part of a monolayer or on their own.

Optimisation has, to some degree, been considered by all who have published AFM results. This includes images, adhesion maps and force spectroscopy data; at some point parameters such as scan speed (Sulchek, Yaralioglu et al. 2002), force (Dimitriadis, Horkay et al. 2002) and depth (McPhee, Dalby et al. 2010) have all been considered and optimised by the operator. This is because optimisation is an inherent aspect of working with AFM and indeed most other complex scientific instruments. Instructions for optimisation are present in every handbook issued with equipment such that a novice would be able to guide themselves through the first initial steps on the road to becoming a competent user. However, optimisation is often very sample specific. What works for imaging microfabricated silicon wafers in air is not applicable to live cells. Indeed, working with biological samples requires many more factors to be considered and therefore optimisation becomes all the more important to achieving reliable results.

3.3 Materials and methods

Since living cells are not a simple homogenous elastic material and as they actively respond to external stimuli, reliable determination of their elastic properties is dependent on both optimised experimental acquisition and suitable modelling to fit the data. Previous studies have shown that when using AFM to measure a cell's mechanical properties, tip geometry, indentation depth and loading frequencies are all factors that can contribute to differences in the elastic modulus measured (Kuznetsova, Starodubtseva et al. 2007). In addition, the elastic modulus is also cell type dependent. Here, materials and methods specific to the optimisation and operation of the AFM are detailed.

3.3.1 AFM probe selection

It is important to select an appropriate probe for force spectroscopy experiments, taking in to account cantilever geometry, tip geometry, coating and spring constant. Taking each factor in turn, this section will detail considerations to be addressed when selecting a probe for elasticity measurements on living cells.

3.3.2 Spring constant and cantilever coating

Cantilevers with a soft enough spring constant to be considered suitable for force spectroscopy on biological samples are often fabricated from silicon nitride (Si_3N_4) as it is extremely flexible and unlikely to break during even the deepest of indentations; however pure silicon (Si) cantilevers are also capable of extremely soft indentations. It is important to select a probe with a spring constant similar to that which you expect the sample to have for the most reliable results. If indenting live cells this would typically be around 0.02 N/m. Stiff cantilevers (> 0.1 N/m) do not have the sensitivity suitable for indentations on live cells. Suitable chips include the MLCT series (Bruker AFM Probes) which have a pyramidal shaped tip and the Arrow TL series which are tipless and require the addition of a colloid tip to be suitable for force spectroscopy on cells.

Often, chips are coated with a reflective metal in order to increase the proportion of the laser light reflected off the back of the cantilever. When selecting a cantilever for use with live cells, be it for imaging or force spectroscopy measurements, it is important to select one with a coating that is not prone to dissolving in to the

culture medium possibly harming cells. For this reason, silver or aluminium coated cantilevers should not be used on live cells but gold coated cantilevers are appropriate. Gold coated cantilevers are prone to thermal drift however; this is due to the expansion of the metal coating caused by the heat of the laser spot and surrounding cell culture media (if incubated). They also suffer from molecules adhering to their surface from the sample media which can cause image artefacts and interfere with force-spectroscopy measurements. Some cantilevers, such as the Arrow TL1 series, are not coated at all and so the material retains a slight transparency under the microscope. While this reduces the amount of light reflected, it has the advantage of allowing accurate positioning of microspheres when preparing spherical probe indenters (3.3.3 AFM colloidal probe preparation) as the sphere can be seen through the cantilever itself. Cantilevers also vary in geometry in relation to their intended purpose. For example, triangular shaped cantilevers are typically best suited to contact mode applications (1.6.1.1 Contact Mode) as their spring constant tends to be a lot softer than the rectangular shaped cantilevers which, although sometimes capable of contact mode applications, tend to be the shape of choice for tapping mode (1.6.1.2 Tapping mode).

3.3.3 AFM colloidal probe preparation

To minimize the influence of the above variables on elastic modulus determination, conditions for indentation measurements were first evaluated. Carefully prepared and characterized spherical colloid AFM probes were used in this study to eliminate the possibility of penetrating cell membranes with a sharp tip. The spheres also provided a well-defined geometry for evaluating elastic modulus by fitting the data to specifically formulated indentation models (Costa and Yin 1999). The choice of indentation force is always dependent on the AFM tip and the cell type, as evident from a range of published values (e.g. from 0.2 (Li, Lee et al. 2008) to 20 nN (Wozniak, Kawazoe et al. 2009)).

In-house prepared AFM colloidal probes were used for indentation measurements (Figure 13). The colloidal probes were prepared by attaching a 4.8µm silica microsphere (Microparticles GmbH, Berlin) to a tipless silicon nitride cantilever (Arrow-TL1, NanoWorld). This was done by first locating a suitable microsphere,

one which was isolated from surrounding microspheres, and gently nudging it using the AFM's fine positioning screws to ensure it was not strongly adhered to the Petri dish surface. Next, the cantilever was carefully lowered on to UV curable glue (Loctite® 349) and pulled out laterally to remove any excess before being raised up off the surface (microspheres and glue on same 30mm Petri dish lid). Upon relocating the original microsphere the cantilever was brought in to repulsive contact manually using the AFM's stepper motor controls and held there while the microsphere was positioned correctly in the centre. The positioning was monitored by the inverted optical microscope onto which the AFM was mounted. Once satisfied with the positioning the cantilever was raised once more and moved laterally to ensure the microsphere had not remained adhered to the surface. The cantilever was the exposed to UV light for ~10 minutes to cure the glue and secure the bead to the tip. The end result is shown in figure 13B. Before commencing cell indentations, the sensitivity and spring constant of each individual cantilever was determined (JPK manual). Cantilever sensitivity is the conversion factor for cantilever deflection from volts to nanometers; this is dependent on the kind of cantilever and the mounting therefore it must be repeated each time before measurements are recorded although values will be similar for identical cantilevers mounted in a similar way. This value was typically around 80-100 nm/V. Spring constant values were usually ~0.02N/m.

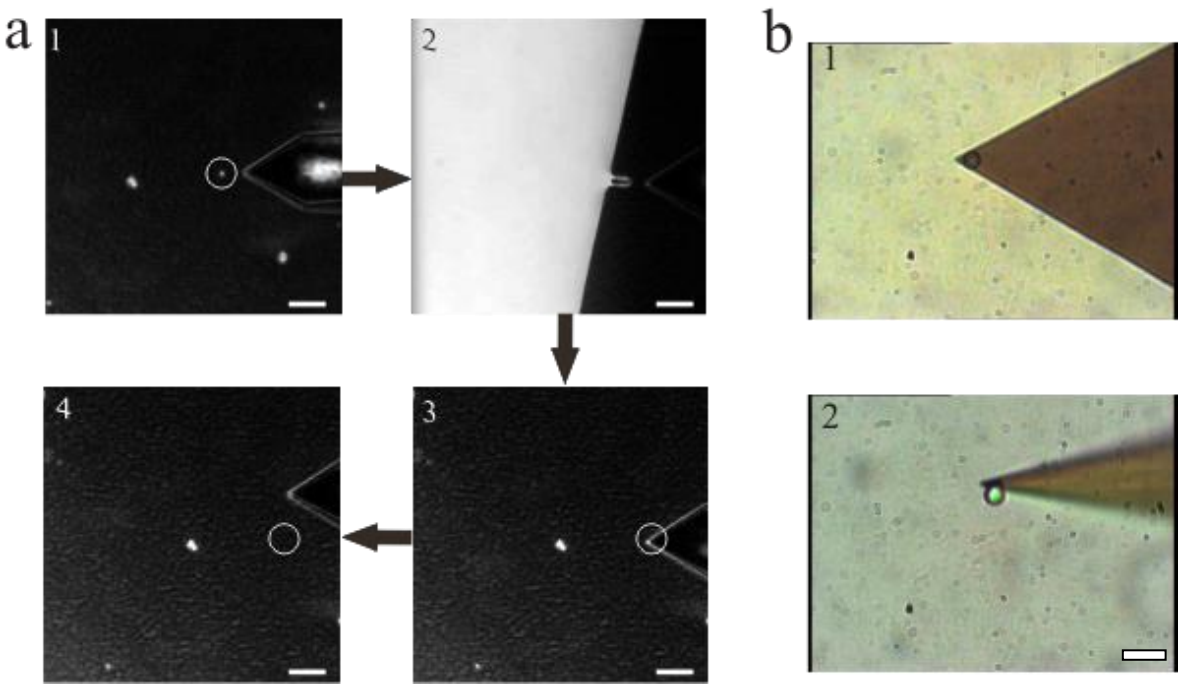

Figure 13: **A**; Illustrates the process of attaching a microsphere to a tipless AFM cantilever. 1) A suitable microsphere is selected. 2) The cantilever is carefully lowered on to the glue. 3) Returning to the selected microsphere, the cantilever is brought in to repulsive. 4) The cantilever is moved to confirm attachment. Dotted white circle indicates original microsphere position in each image. **B**; Finished spherical 4.8µm diameter probe seen from below (1) and from side (2). Scale = 50µm in 'a' and 10µm in 'b'.

3.3.4 Measurement environment

The first factor to be taken in to consideration is the environment in which the cells are measured. It is well known that external factors such as temperature and carbon dioxide levels can quickly and significantly affect cell behaviour. Studies have shown that it is possible to induce changes in elasticity without any observable morphological change, and that external conditions such as temperature can have a much stronger influence on cell elasticity than on morphology (Kuznetsova, Starodubtseva et al. 2007); therefore, observing through the optical microscope will not always alert the user to the changing mechanical properties of the cell. Therefore it is important when working with live cells to take every precaution to maintain an *in vivo*-like environment during experiments. To this end, all live cell imaging and force spectroscopy on the AFM were carried out using the JPK BioCell™ (Figure 14) stage, which maintained a constant 37°C throughout in full serum culture medium.

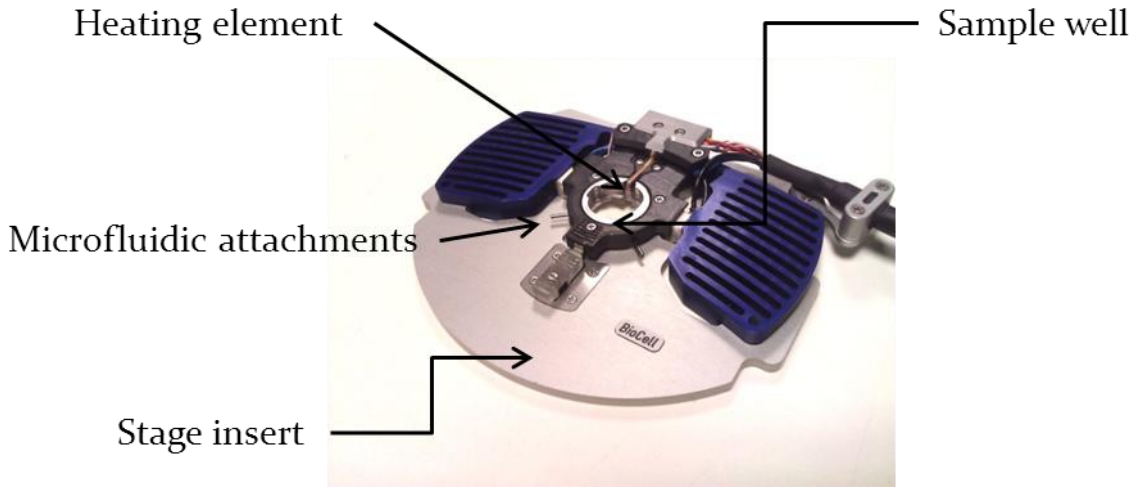

Figure 14: JPK BioCell™ temperature controlled stage for live cell measurements.

Due to the AFM being an inherently 'open' system, that is open to the wider environment of the lab, maintaining the recommended 5%CO_2 95% air mixture as used in incubators was not practicable. CO2 acts to make sure the buffer in the media performs as intended but is not actually used by the cells themselves. The media used for incubator cultures and AFM measurements here includes phenol red, a pH indicator, which enables us to see a colour change as the acidity of the media changes. This colour change – from red at pH7 to purple – happens within the time the cells are outwith the incubator and so during the measurements alkalinity is increasing. To ascertain how much the pH of the cell culture media was changing over the ~90 minutes the cells were under the AFM; measurements were recorded every 10 minutes with a pH meter at 37°C and 22°C room temperature of the DMEM/F12 media used in all experiments. Although temperature was kept constant by use of a water bath, no attempt was made to influence CO_2 levels. Results showed that at both temperatures pH remained remarkably constant, beginning at 7.2 in both cases and rising to 7.4 at 37°C and 7.3 at 22°C room temperature. This shows the capacity of the media to maintain its pH when CO_2 levels are that of air, however as no cells were present in the media tested these results do not represent a fair example of the conditions experienced during AFM measurements. For this to be accurate the experiment would need to be repeated with a culture of respiring cells present in the media. Although no morphological changes are observed during the time cells are under the AFM; it is possible that

unseen and unmeasured characteristics such as viability and cell growth speed are being affected by the conditions (Vistica, Scudiero et al. 1990). It must, therefore, be possible that these could manifest themselves discretely in the elasticity results. Attempts were made to carry out AFM experiments in a home-made CO2 independent media to further limit variables within the experiment however the cells reacted adversely to this solution and so a return to DMEM was necessary. In order to limit the impact of reduced $CO_{2,}$ all AFM measurements were carried out within 90 minutes of the cells being removed from the incubator when no noticeable morphological changes had been observed.

3.3.5 Optical overlay

In order to accurately position the AFM tip over the areas of interest during force spectroscopy measurements the operator has to either a) image the cell in question then use the software to position the cantilever over the required area b) observe down the microscope eye-piece the exact location of the cantilever and use the fine positioning screws on the AFM head to manually position the probe, or c) overlay the optical image displayed on the CCD camera on to the scan region of the AFM.

The preferred option is to overlay the optical image displayed on the CCD camera to the scan region of the AFM, in this way the locations are superimposed on the optical image instead of the AFM image (Figure 15). Direct overlay of the optical image takes into account aberrations in the optical image introduced by the effects of the mirrors and lenses of the microscope. The software is able to use recognized positions of the cantilever to calibrate the optical image accurately before mapping it on to the AFM scan region. The advantage of this is the time saved – overlaying the optical image takes ~1 minute compared to the ~15 minutes to scan a cell therefore locations are more accurately selected. Although the optical image cannot give the nanoscale detail of the AFM image it is more than sufficient for locating areas of interest such as the nucleus and can also display fluorescence information.

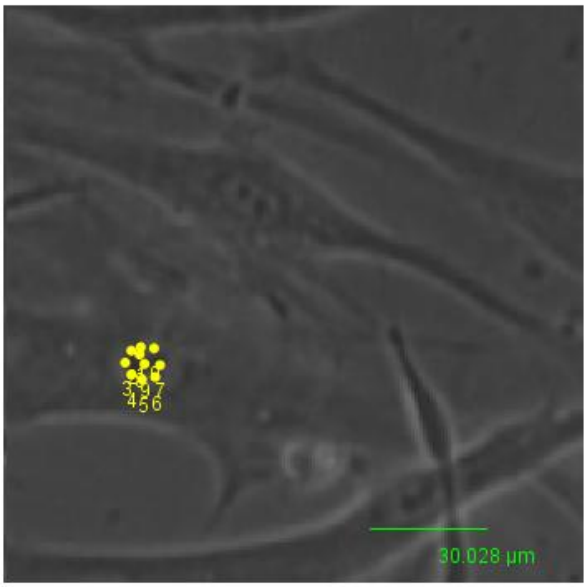

Figure 15: Brightfield image overlayed on to AFM scan region with locations of force-indentation curves represented by yellow dots, shown here situated on the nucleus of a 3T3 cell.

However, the optical overlay technique cannot always be applied. As the software relies on good contrast of the cantilever against the background to automatically recognise its position and thus calibrate the image – focusing on the sample itself can lead to mistakes. The chances of accurate overlay can be increased by focusing on the cantilever instead of the sample and changing to brightfield mode instead of phase. As the data generated for overlay is completely independent of the AFM experiment the optical settings can be re-set once overlay is completed. Some biological samples can be particularly difficult to observe with many bright spots caused by rounded dead cells or floating debris. This appears to confuse the overlay algorithm and therefore results in unsatisfactory mapping of the optical image. In order to avoid any unreliable positioning of the AFM probe, optical overlay is only employed when the resulting overlay has a low standard deviation error of less than 1 pixel, this corresponds to ~0.2µm under normal 512 x 512 AFM resolution. Successful overlays typically have an error of between 0.4 and 0.6 pixels however. It is also important to note that because the x and y scanners on the JPK NanoWizard II are open loop it is best to allow the piezo electric crystals time to adjust if large changes in area dimensions are made; as no feedback mechanism exists to monitor

piezo movement in these directions. This is to allow tip position on the scan area selected for overlay to be accurately mapped by the AFM.

3.4 Results and discussion.

Presented here are the results of various experiments performed to characterise and optimise the indentation parameters used during AFM experiments. Focussing particularly on the identification of a suitable indentation force and how this can influence elasticity values recorded. Factors such as measurement speed and tip geometry are also explored.

3.4.1 Effect of loading force on cell integrity

To identify a range of indentation forces that didn't breach the plasma membrane, we carried out a series of force-indentation curves on live MG63 cells in the presence of trypan blue. Trypan blue is a stain used frequently to identify dead cells and tissue; it does so by passing through the membrane and colouring the damaged areas blue. Cells and tissues with undamaged membranes can successfully block entry of the stain and remain unaffected. Should any of the measurements cause damage to the membrane these would subsequently be detected as the stain would be permitted access to the cytoplasm – colouring it blue. Figure 16 shows the results of indentations with both sharp pyramidal tips and spherical bead indenters. Forces used ranged from 3.5nN - used in force indentation measurements throughout this project, to 20nN - the highest force achievable with the Arrow TL1 cantilever on which the beads were attached.

When comparing spherical and pyramidal indenters it is important to realise that indenter geometry has considerable influence on the distribution of pressure within the cell during indentation. It is pressure, not loading force, which deforms the cell as pressure is the *effect* of loading force. For spherical indenters, the area over which this pressure is distributed is considerably larger than that for pyramidal or conical indenters. Pressure distribution also differs with increasing indentation depth for different geometries. For example, the radius of contact between the tip and the cell increases faster than the depth of the indentation as load is applied for spherical

indenters. For conical indenters, the relationship between the radius of contact with the cell and depth is a constant ratio, independent of applied load (McCann 2004)- note that pyramidal geometry is often approximated by equations for conical geometry in the literature (VanLandingham 2003). Thus, when indenting with a conical indenter the cell should experience a constant strain with increased loading force. Note, indentation strain describes the ratio of the radius of contact over the radius of the indenter. For a spherical indenter, increasing loading force is analogous to decreasing the half-angle to face of a conical indenter i.e. making it sharper (McCann 2004). In order to compare the distribution of pressure inflicted by spherical and sharp probes, one would calculate the area over which the pressure is applied. This can be done using equation 6 below:

$$p = \frac{F}{A}$$

Equation 6: Used to calculate pressure: 'p' is pressure, 'F' is the loading force and 'A' is the area of contact with the surface.

For this experiment, indentation approach and retract speeds were kept at a constant 10μm/sec to ensure comparability with indentation measurements throughout the project. All the cells tested (n=6) remained intact and no blue colouring was observed after 10 minutes, indicating that the membranes were not being penetrated. N.B. to illustrate the appropriateness of the experiment, with each tip a cell was deliberately scraped off the surface and observed for until it turned blue, this occurred after approximately 5 minutes. These positive results are shown in the bottom row of Figure 16 however the CCD camera was unable to clearly represent the colour change in the damaged cells (indicated by the white arrows).

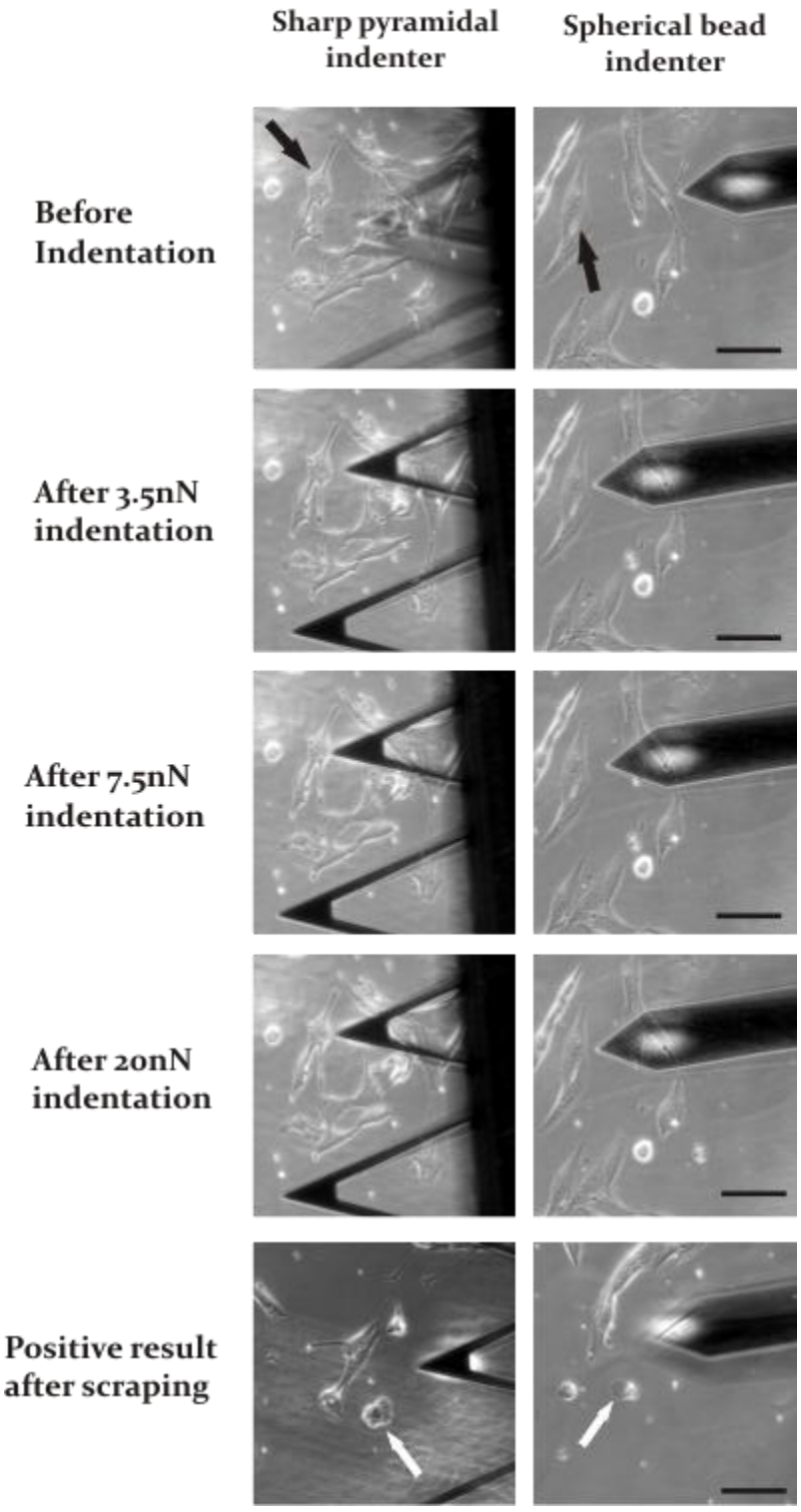

Figure 16: Indentation measurements performed with sharp pyramidal indenters (left column) and spherical 4.8µm silica bead indenters (right column) in the presence of trypan blue. Performing this type of dye exclusion assay with trypan blue will allow the identification of cells with compromised membranes as these will allow the dye to pass into them. Cells with intact functioning membranes will not permit the dye to enter. Should the AFM indenter breach the cell membrane the cell would appear blue when observing with a microscope – as can be seen in the bottom row of images this colour change is not obvious

when captured with a ccd camera. In this experiment the cells were indented using forces far beyond what is typically used during normal elasticity measurements, even so it was not possible to puncture the membranes with either indenter and cells had to be scraped from the surface in order to achieve a positive result (white arrows). The black arrows point to the cell which was indented at each force. Scale bars are 100 μm.

3.4.2 Determination of loading force (nN)

To determine a suitable indentation force for live cell force spectroscopy, 3T3 fibroblasts were used as a model cell line. A series of deeply penetrating (≥ 1 μm) force-distance curves were obtained from cells seeded onto untreated glass coverslips and cultured overnight. Using Hertz's model for data fitting graphs of indentation depth versus elastic modulus (Figure 17 & Figure 18) were produced, from which we could identify a plateau region where elasticity values remained relatively constant. Shallow indentations <50 nm often resulted in massively underestimated values possibly due to the insufficient indentation depth. An increase in elasticity was seen in all examples as the tip penetrated deeper in to the cell; indicating a contribution from the nucleus itself and possibly the substrate. To minimise this influence, only the portion of the indentation curve up to 500 nm was used for the analysis (N.B. this also ensures the validity of Hertz's model: indentation depth < 10% of sample height). Considering that cells are inherently heterogeneous, an indentation force of 3.5 nN was chosen to provide enough indentation depth. No alterations in cell morphology or cell integrity were observed at the applied force. Note; only one graph of indentation versus elasticity was produced per cell however a value for whole cell elasticity was recorded with each indentation. The repeated measurements (5x/cell over 5min) did not show any directional change in the elastic modulus measured other than random fluctuation.

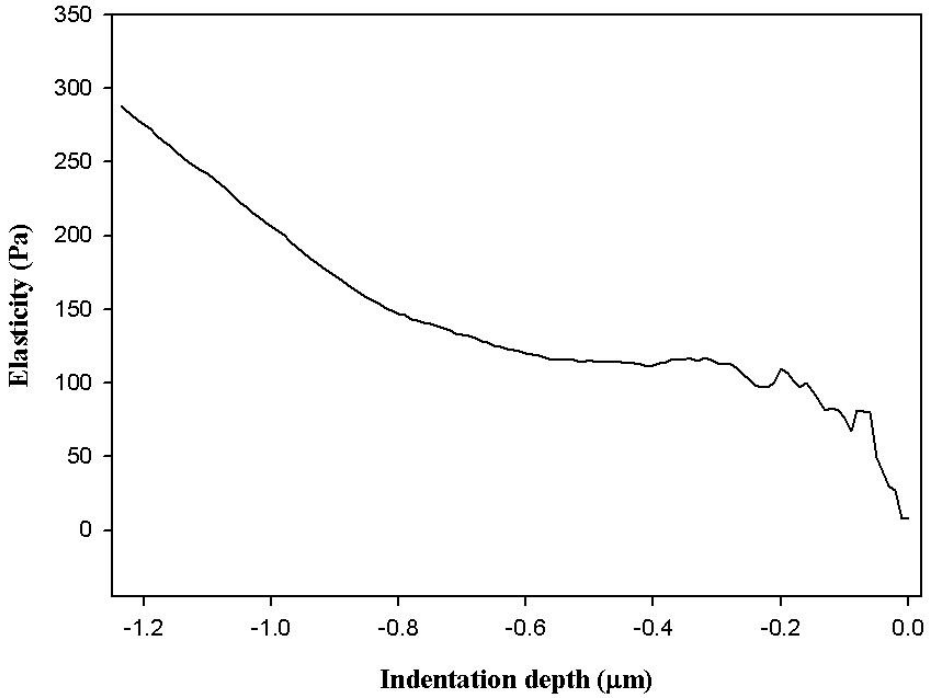

Figure 17: Effect of indentation depth on cell elasticity calculation. Values of elasticity were recorded at 20nm increments starting with initial contact between the tip and the sample (0.0 on x-axis). Figure shows the tendency of the values to increase as the curve penetrates deeper. Very shallow curves (<50nm) tend to underestimate elasticity. In this example, the plateau region of reliable elasticity values is present between ~300nm and 600nm deep and the final indentation depth is 1.2μm.

Plotting the elasticity against indentation depth revealed a region of reliable results in each case however it varied in size between cells, as can be seen in Figure 18. Values before the constant region tend to be variable and underestimate elasticity possibly as a result of insufficient stress being exerted on the cytoskeleton beneath the plasma membrane, an exception being Figure 18C where values are constant from initial tip-sample contact until ~500nm deep. With deeper indentations elasticity values began to rise constantly, this was observed in all cases. This could be due to the influence of the underlying substrate which starts to couple in mechanically or the tip could be detecting the nucleus and pushing it through the cell. For these reasons all curves were analysed up until a 500nm depth limit as this was an appropriate depth for most cells, even if the total curve depth often reached ~1.2μm, approximately 24% of typical cell height.

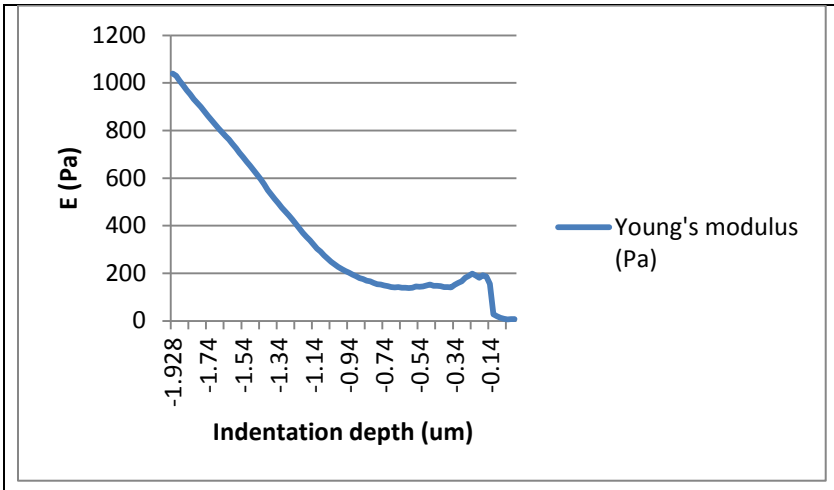

A: Plateau region present between ~200n and 800nm. Shows similar trend of increasing elasticity values as indentation penetrates deeper and unreliable values for very shallow depths of <50nm. Total depth of indentation is 1.928µm, significantly deeper than the other curves recorded.

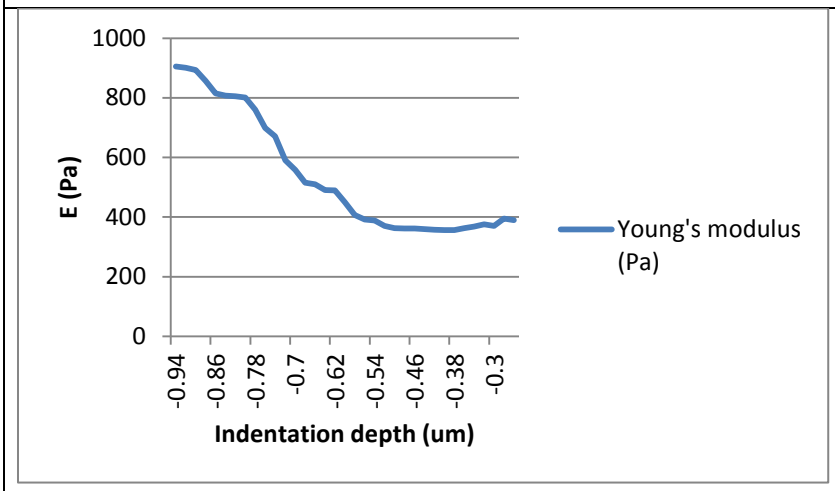

B: Plateau region present from beginning of recorded values (~200nm) until ~500nm deep, then elasticity values increase in a similar fashion as indentation deepens.

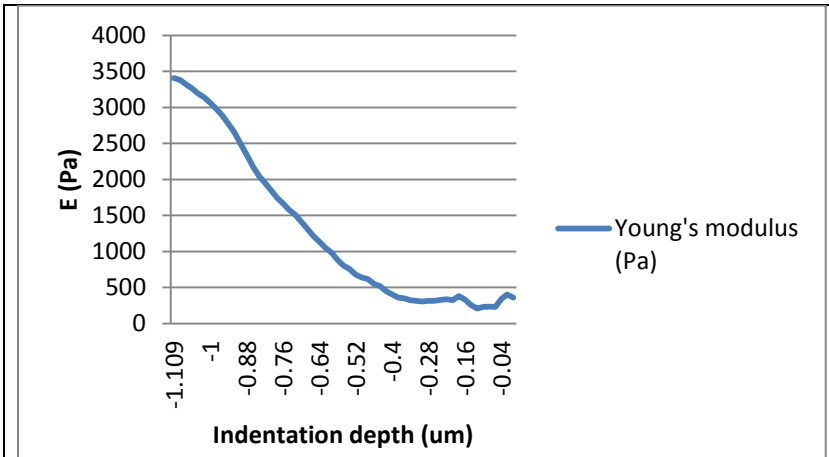

C: This graph again shows relatively constant elasticity values present from the initial stages of indentation (~4nm) until approximately 500nm deep where the values begin to increase as seen in graphs A, B and Figure 16.

Figure 18: Indentation depth versus elasticity graphs for three other 3T3 cells. These graphs were constructed in a similar way to that shown in Figure 16 and show indentations on three different cells, A, B and C, of the same population. Observed are differences in final indentation depth, plateau region and elasticity value.

Figures 17 and 18 highlight the variation possible within cells of the same population. Under identical indentations each cell behaved differently, showing the difficulties present when attempting to construct a reliable method for force spectroscopy on live cells. The plateau region of elasticity values varied in depth and size with each cell, as did the final indentation height and value of elasticity. Certain constants emerged however – the tendency to exaggerate elasticity with deeper penetrating indentations and the presence of a plateau region – if not its size and depth. This experiment has gone some way to explaining levels of variation observed in published AFM results and informing new users of the need to devise protocols to cater for the majority of cells in a population as there is little chance of accurately predicting the behaviour of every one.

3.4.3 Indentation depth.

Using an indentation force of 3.5nN ensures a sufficient depth of curve will be available for analysis. This value was chosen because the total depth of a force-distance curve for any given force is very variable and can often result in shallow indentations (<500nm). However, the possible effect of the nucleus on the elasticity results remained a concern. Inclusion of the nucleus in elasticity measurements by indenting deep enough to contact it could have an effect on elasticity values because the nucleus of mammalian cells is reported to be significantly stiffer than the surrounding cytoplasm (Guilak, Tedrow et al. 2000; Caille, Thoumine et al. 2002). If this is true, then a probe encountering the nucleus during the approach period of a force distance curve would effectively be pushing the nucleus through the cytoplasm. This could have knock-on effects on the resulting stiffness values, which are extracted using the Hertz model modified for the specific geometry of the indenter. Should the probe push the nucleus through the cell this would be akin to changing the indenter geometry for a portion of the indentation. In an attempt to investigate the distance available under the plasma membrane before the nucleus would be contacted, transmission electron microscopy (TEM) was utilised to image transverse sections of MG63 cells situated in PDMS grooves and pits. This technique enabled us to visualise the cytoplasm above and below the nucleus and determine if it was likely that the nucleus could be mechanically affected during force distance measurements. Five cells were imaged in total, three on pits and two on grooved PDMS surfaces. Unfortunately, due to the low seeding density of the samples and difficulties adapting the TEM preparation procedure with the PDMS discs, a full set of images was not possible as several samples were destroyed. Of the five cells that were imaged, measurements were taken at three points above and below the nucleus 1µm apart so as to average the thickness of cytoplasm in each region. As can be seen in Figure 19, there was ca. 820nm between the upper membrane of the nucleus and the outer membrane of the cell, and ca. 530nm between the lower membrane of the nucleus and the base cell membrane. These values were typical of the 5 cells measured, showing cytoplasm thickness varying between ~600nm and ~900nm above the nucleus and ~300nm – 600nm below.

It is important to note that the sample preparation steps necessary to image using a TEM are often associated with shrinkage, which can sometimes introduce artefacts in to the image. It has been demonstrated using high resolution scanning electron microscopy that shrinkage during preparation is uniform across all organelles within the cell and structural components are preserved in their previous arrangements; however sample to sample levels of shrinkage are variable (Gusnard and Kirschner 1977). Because of this it was not possible to know by exactly what volume our samples would shrink as no study in the literature could be identified as recreating the conditions and cell type used here, though studies report that ethanol dehydration / fixation and critical point drying techniques employed during sample preparation can cause up to a 25-30% reduction in sample size (Gusnard and Kirschner 1977; M. Loferer-KroBbacher 1998). Due to the excellent preservative qualities of the resins, their ability to be easily sectioned, their stability under the electron beam and the fact that no alternative preparation method was available, it was necessary to proceed with the method.

Although only 500nm of indentation was analysed after the initial contact point with the membrane it is impossible to rule out contributions from the nucleus in the resulting Young's modulus values. As discussed, the Hertz model is accurate for indentations <10% of the total sample thickness; total sample thickness in these conditions includes the nucleus of the cell in each case. To rule out nuclear contributions we would need to be indenting <10% of the cytoplasm thickness above the nucleus, which would result in an indentation depth of around ~800nm maximum. As shown in Figures 17 and 18, indentations of this depth are too variable to ascertain a reliable value of elasticity therefore it must be conceded that nuclear position and movement is in some way influencing the force-indentation curve and as a result the extracted value of elasticity with each measurement.

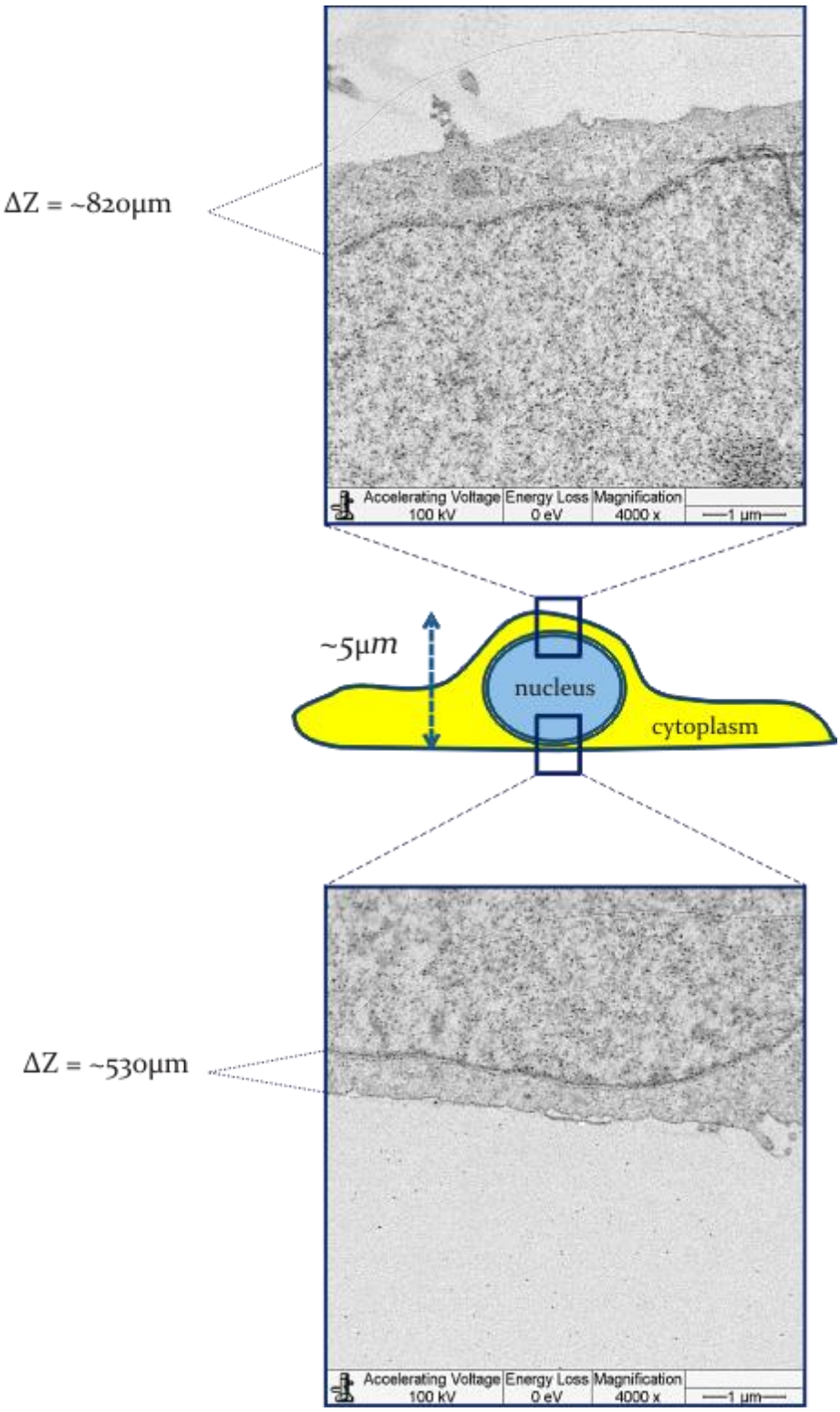

Figure 19: Schematic highlighting areas of cell depicted by TEM images. Shows approximate distance between nuclear membrane and plasma membrane above and below cell. Note it was not possible to determine the exact lateral position of the transverse section imaged. Cell shown is an MG63 cell situated within a 40μm PDMS pit. Scale = 1μm.

3.4.4 Determining indentation speed (μm/sec)

Previous studies showed that both elastic and viscous properties of cells can contribute to the information gained through AFM indentation (A-Hassan, Heinz et al. 1998; Mahaffy, Park et al. 2004; Smith, Tolloczko et al. 2005; Rosenbluth, Lam et al. 2006). The viscous property is associated with time-dependent relaxation of cells upon indentation and thus its contribution to indentation measurements was frequency dependent. Since the viscous relaxation time is dependent on cell type and associated with the subcellular structure where testing takes place, as well as the state of the cells adhering to the substrate, indentation speeds varying from 1μm/s to 25μm/s (i.e. from 0.1 to 1.5 Hz) were investigated. Ideally, this would allow us to identify an appropriate "operating window" that minimized the viscous response of the fibroblasts.

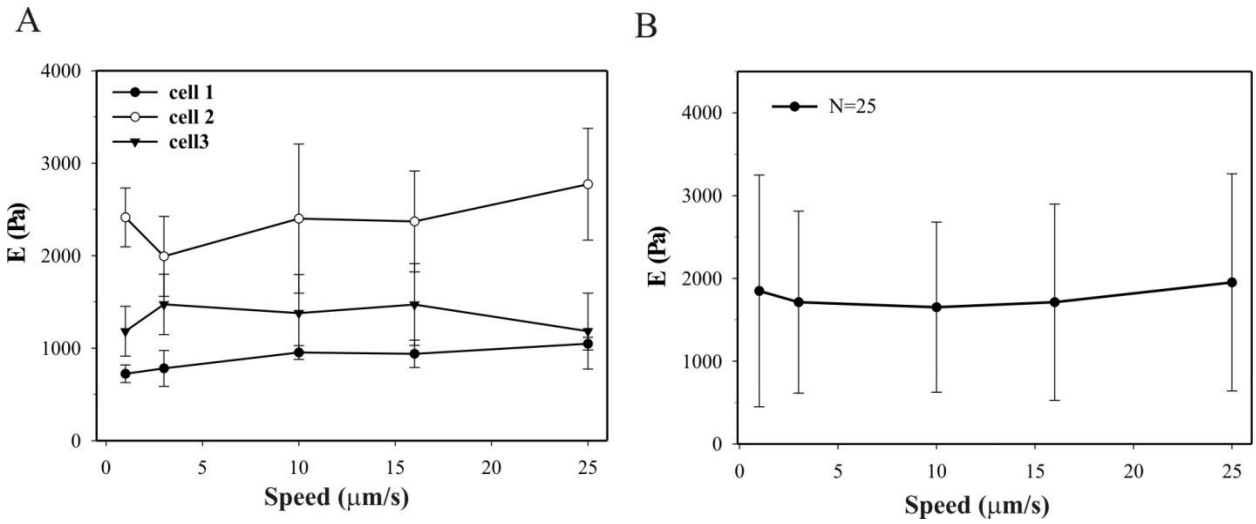

Figure 20: Influence of indentation speed on cell elastic modulus. A) The elastic modulus of three single cells measured at difference speeds. The three cells are randomly chosen to illustrate cell heterogeneity. The data were fitted with Hertz's model adapted for a spherical indenter. B) Average elastic modules of 25 cells measured at different speeds. The speeds range 1μm/sec to 25μm/sec. Error bars show 1 standard deviation from the mean value.

Figure 20A shows the representative elastic response of individual cells to a systematic change in the indentation speed. All the 3T3 cells were plated on uncoated glass coverslips for 12 hours prior to the indentation test and Hertz's model was applied to derive the elastic modulus of the cell from the force-distance curves. The data obtained highlight the high levels of variation at the single cell

level showing no significant change in elasticity over the range of speeds tested. The average elasticity of 25 single cells at different indentation speeds (i.e. 125 force-distance curves for each speed) is shown in Figure 20B. Results show an average elasticity of 1.31 ± 0.95 kPa for cells indented at 1µm/sec, 1.06 kPa ± 0.66 kPa for cells indented at 3m/sec, 1.07 ± 0.650 kPa for cells indented at 10um/sec, 1.12 ± 0.76 kPa for cells indented at 16µm/sec and 1.17 ± 0.88 kPa for cells indented at 25µm/sec. Again it is not possible to identify a significant trend as the variation is too large. From these results we concluded that indentation speed did not affect the resulting values of elasticity over the range tested, however as the smallest standard deviation value observed was for 10µm/sec and so this was selected as the indentation speed for the rest of the project. To limit any pre-conditioning effect on the cells caused by the repeated order of measurements carried out on each cell, we alternated the order in which each speed was tested. This meant that some cells experienced increasing indentation speeds, some decreasing and some an alternating pattern.

Using the largest standard deviation value (0.95 kPa) obtained for the range of speeds tested here we aimed to calculate the sample size required for a precision of 0.4 kPa. Using the Equation 5 detailed in section 2.7 Statistical analysis, we calculated that for a sample precision of 0.4 kPa the minimum sample size required was 22 cells, therefore for the remainder of the project the minimum sample size measured for quantitative assessment of cell heterogeneity was 25.

3.4.5 Cell Plasticity

The elastic response of a cell is its ability to recover morphology following mechanical deformation. Plasticity describes any non-recoverable aspect, the tendency to be 'moulded' by the mechanical deformation. In this case, indentation with a spherical probe is the method of deformation. In order to test for the cells ability to recover following indentation, cell height was measured as the first point of contact between the probe and the cell with each indentation performed using the software tools described in section 4.3.3 AFM Measurements. Five indentations were performed in total, each one second apart with a loading force of 3.5nN on the centre of the nuclear region. The cells used were MG63 cells cultured on uncoated

glass coverslips overnight in DMEM/F12 media under 5% CO_2 conditions. The results are shown in Figure 21.

It is of interest to know if cell height at the point of indentation is recoverable, if not then with each subsequent indentation the probe will penetrate deeper in to the cell and the influence of the nucleus and underlying substrate will become more influential. This could manifest itself as a time dependant increase in apparent elasticity over the course of the measurements on each cell.

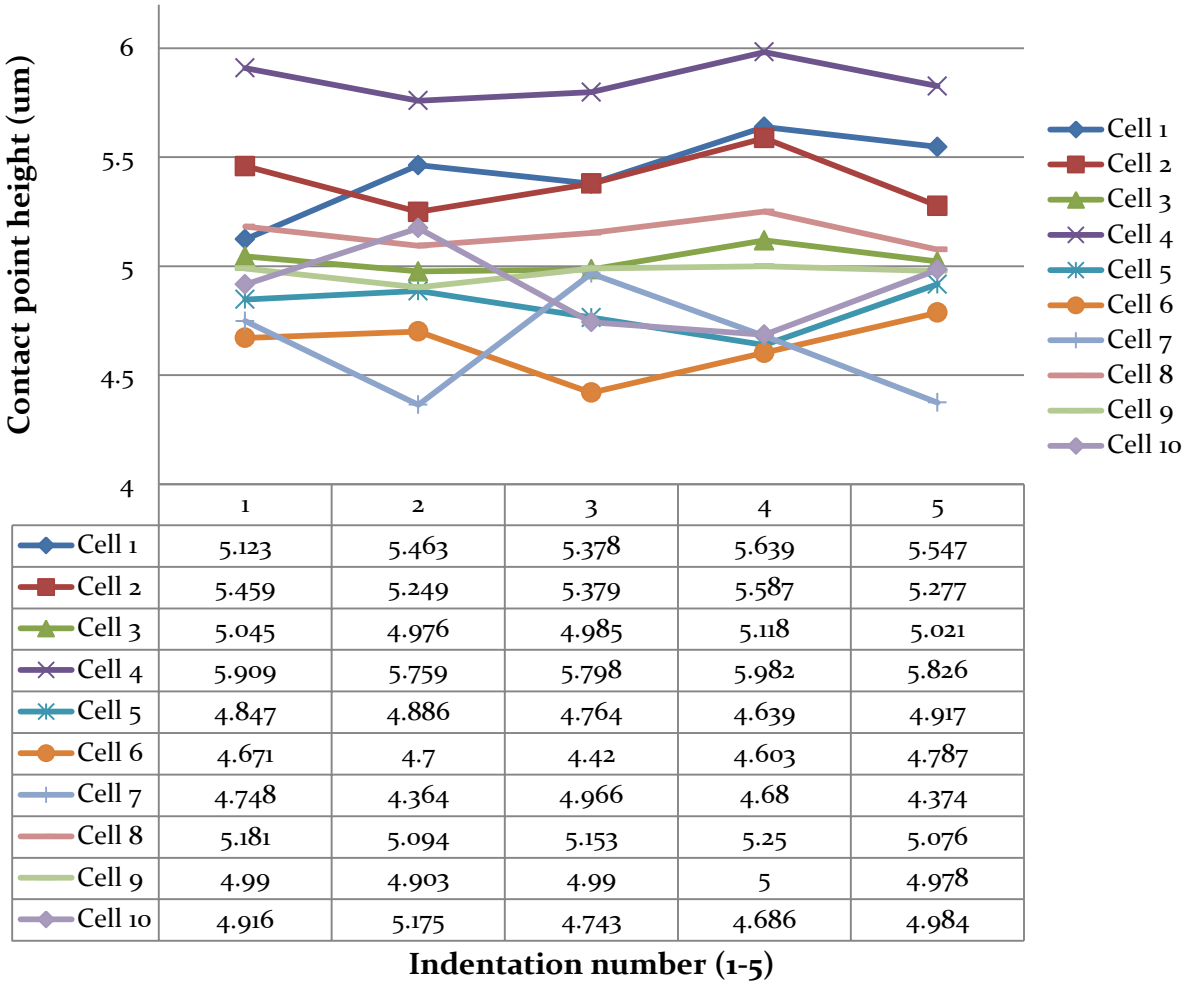

	1	2	3	4	5
Cell 1	5.123	5.463	5.378	5.639	5.547
Cell 2	5.459	5.249	5.379	5.587	5.277
Cell 3	5.045	4.976	4.985	5.118	5.021
Cell 4	5.909	5.759	5.798	5.982	5.826
Cell 5	4.847	4.886	4.764	4.639	4.917
Cell 6	4.671	4.7	4.42	4.603	4.787
Cell 7	4.748	4.364	4.966	4.68	4.374
Cell 8	5.181	5.094	5.153	5.25	5.076
Cell 9	4.99	4.903	4.99	5	4.978
Cell 10	4.916	5.175	4.743	4.686	4.984

Figure 21: Line plot of recorded cell height over the course of 5 sequential indentation measurements on 10 MG63 cells. The table lists the height at which the probe first contacts the cell. Values shown in µm. The line plot shows the relationship between indentation number and contact point height.

As can be seen in Figure 21, there is no clear trend of cell deformation over the course of the measurements; 4 cells show a higher contact point on the final indentation compared to the first (cells 1, 4, 5 & 10) and the remaining 6 show a lower contact point on the final indentation compared to the first (cells 2, 3, 6, 7, 8 & 9). Although the contact point does fluctuate by ~130nm for each cell the variations are not significant enough to suggest that cell height is affected by indentation; it is likely that this is a manifestation of the limitations of the experiment. As a result of this experiment we can conclude that the indentation protocol used throughout this thesis does not result in non-recoverable cell deformation at the point of contact.

3.4.6 Application of Hertz model

Referring back to section 1.7.1 Models for deriving elasticity from indentation measurements, it was discussed that the Hertz model is most reliable for indentations between 5-10% of total sample depth. For a cell this is approximately 300-500 nm. Identifying the force needed to arrive at this depth and analysis of elasticity results versus depth can be seen in sections 3.4.2 and 3.4.3. However, identifying an optimum indentation force range for generating reproducible curves is just part of the correct application of the Hertz model – the model itself has to be applied correctly to the measurements at the analysis stage of the experiment.

Because of the variation in final indentation depth it is not suitable to automatically apply the Hertz fit to the entire curve using the JPK Data Processing software, manual interpretation of the correct depth for analysis is required. This involves discarding sections of the curve that go beyond the limit of reliable Hertz fitting, Figure 22 and 23. To do this, the entire force indentation curve is selected and the point of first contact between the tip and the sample is highlighted by the software. If the selected contact point is appropriate, the fit is applied to the entire non-contact portion of the curve and up to ~500 nm past the contact point. If the automatically selected contact point is not suitable the curve is either discarded or a more suitable point chosen manually. In this way it is possible to analyse the same curve for different indentation depths and check the repeatability of the results, as shown in Figure 17. Note that different methods exist for identifying an appropriate

first contact point on a force indentation curve, these include; the first instance the approach curve crosses the baseline in to positive forces and does not cross back, a significant dampening in hysteresis caused by contact between the tip and the sample or the first time the approach curve reaches a predefined force. The method used by the JPK analysis software shown here could not be identified unfortunately as this information could not be made available to us.

As mentioned in section 1.7 Cell elasticity quantification by AFM, the Hertz model has been adapted for various geometries of indenter including cone, paraboloid, quadratic pyramid, flat cylinder and sphere and so it is important that the correct version is chosen at this stage. For more details of the model used see section 1.7.1 Evaluation of elasticity from indentation measurements.

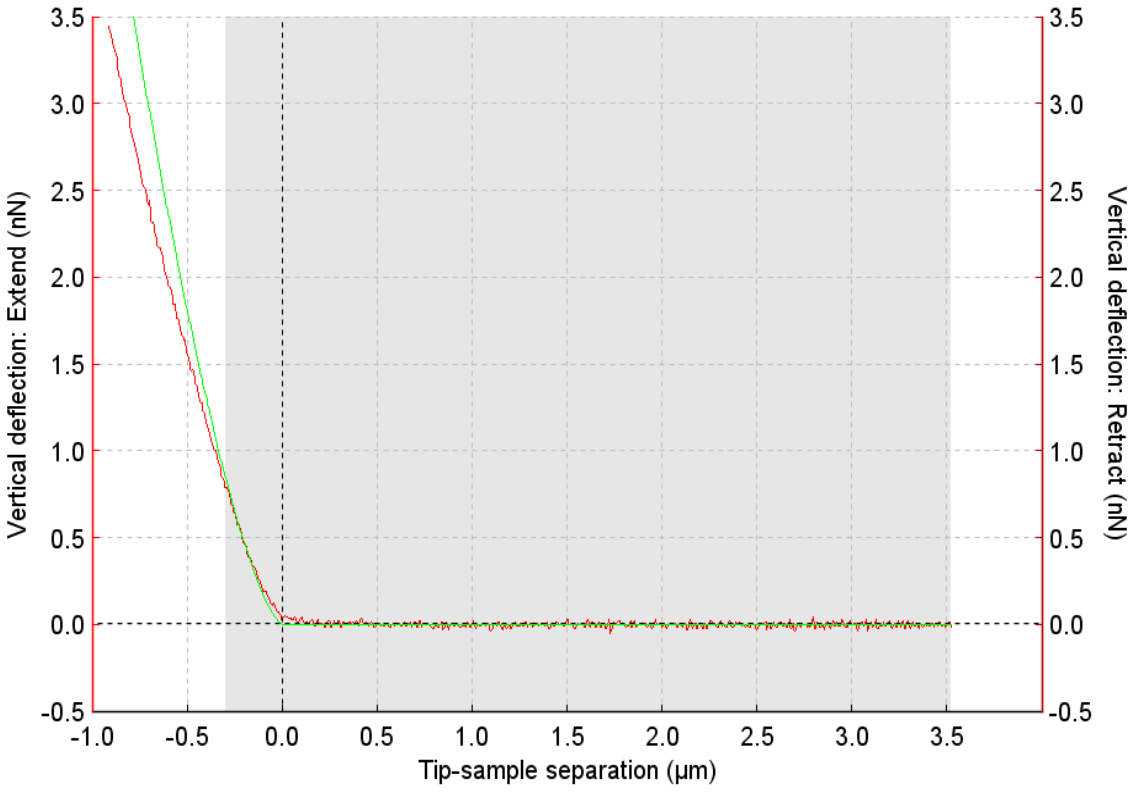

Figure 22: Identification of a fit range from a force – indentation curve (processed to show tip-sample separation as discussed in Figure 9). The red line is the approach curve, the vertical dashed line denotes the contact point of the approach curve and the green line indicates the fit of Hertz's model. The blue shaded region highlights the area selected by the user to be considered for the elasticity calculation – in this instance the first ~300nm has

been chosen for analysis. Shown is an example of a good fit of the Hertz model to the tip-sample separation curve as selected by eye, with an RMS value of ~30pN.

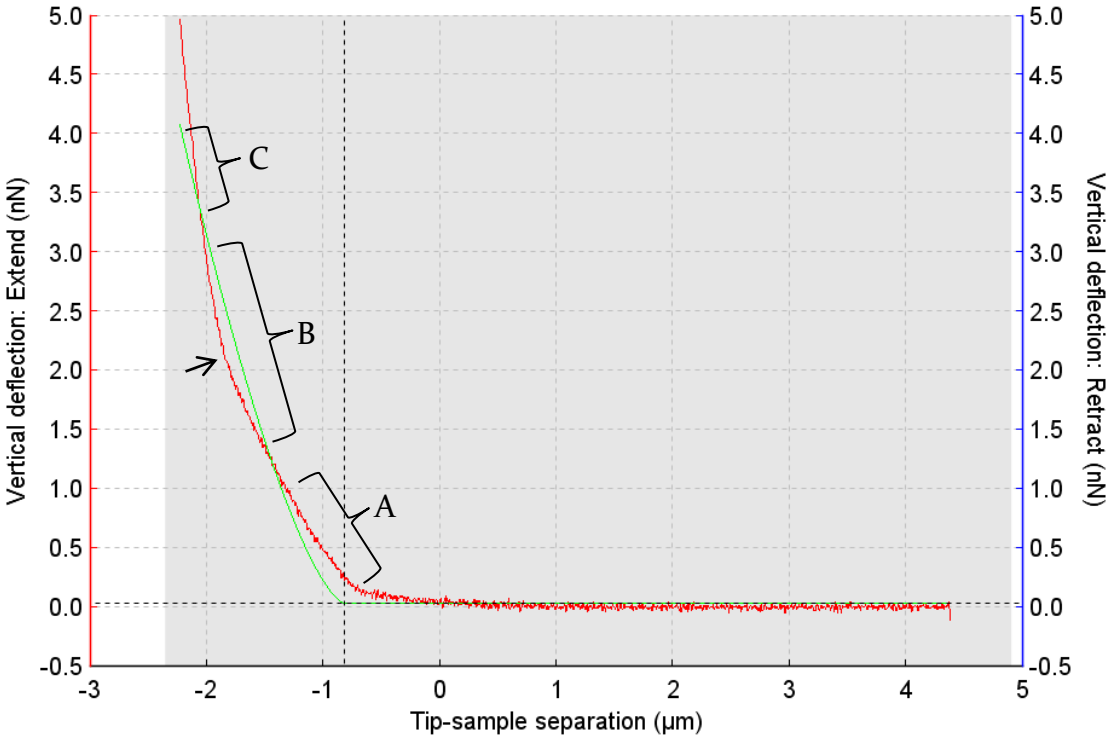

Figure 23: Shown is a typical example of when the Hertz model fails to accurately fit the indentation curve. Areas identified by eye as being too ill-fitting to analyse are highlighted A, B and C. Section 'A' shows an obviously inaccurate contact point location and little correlation between the initial ~500nm of the red indentation curve and the green fit of the model. This is not acceptable as the first 500nm of each indentation are used to extract the Young's modulus value for that measurement. Sections 'B' and 'C' fail to fit the measurement due to the change in angle of the indentation curve, highlighted by the arrow. This type of angle change, or 'two-stage' shape, seen in the repulsive contact portion of the curve resulted in a poor fit and the measurement was discarded. Here, the RMS value was 148pN.

As shown in Figure 23, the software was not always able to accurately fit the model to the data. This occurred most commonly on force indentation curves with a 'two-stage' repulsive contact region and a difficult to identify contact point. A 'two-stage' approach curve is when the angle of the repulsive contact portion of the curve

appears to change abruptly during indentation, resulting in large differences between the approach curve and the model fit. It is hypothesised that this phenomenon could occur because the tip has encountered two or more layers of elasticity within the cell, perhaps contacting the nucleus or pushing the nucleus out of the path of the tip. Difficult to identify contact points are often very shallow increases in force found on the approach curve where it is not clear exactly when the tip has begun to push upon the cytoskeleton of the cell instead of the ECM and membrane protrusions found on the surface. Often there would be no amount of curve selectable that would result in an accurate fit of the like seen in Figure 22 and so these curves would be discarded outright. If there were not at least three accurately fitted curves for a cell then that cell would be excluded from the final results. It was estimated that between 5 – 15% of cells were discarded per experiment for this reason. The decision to emit or include a curve was left to the discretion of the user as no RMS range was identified. Each measurement was judged by eye meaning that any curve fit that did not appear to follow the approach curve closely was instantly discarded. The most important region of the curve fit judged was the initial ~500nm of repulsive contact, if this was observed to be accurate with no deviations from the measurement then the result was recorded. Variations in contact point were tolerated to within ~100nm if the repulsive contact portion was deemed accurately fitted. This is because of the intrinsic difficulty in selecting contact points when the indenter must first contact secreted cellular proteins and other membrane protrusions which may register on the measurement but not indicate the elasticity of the cell. The subjective nature of this technique is a weakness in the analysis process as it allows room for user interpretation, therefore when carrying out analysis we erred on the side of caution and when in any doubt, the curve was discarded. A retrospective look at the RMS values of several included and excluded curves highlighted significant variation, perhaps influenced by the conditions of the measurement. It appears as though the limitations of applying the Hertz model to indentations can be influenced by cell type, cell position (within surface grooves / pits) and perhaps even the surface material on which cells are seeded. This observation could not be explored further due to time constraints however it seems to indicate that an RMS range for the exclusion of ill-fitting curves

would have to be specifically catered to each cell type and experimental condition and could not be applied retrospectively across the board.

To investigate the comparability of the JPK analysis software two other software programs were utilised to analyse the same set of measurements. It was hoped that by comparing the analysis software used throughout this project to similar programs some measure of reliability could be invested in the results. These additional programs were gifted to us by Dr Kristian Franze of the University of Cambridge Departments of Physiology and Neuroscience and Dr Robert Kiss formerly of Heriot-Watt University Department of Chemical Engineering and used with their permission; the programs will be referred to as 'Cam' and 'Rob' respectively. Both software tools were constructed individually with the aim of fitting the Hertz model to AFM indentation data and extracting the Young's modulus. Neither software was 'open' to us and so no code could be scrutinised however full functionality was available and each program was applied according to instructions specific to it. In the case of the Cam software; the program attempted to fit the Tu and Chen models in addition to the Hertz in order to select a winning fit for each measurement. For the data set tested in this example the Cam software returned the Hertz model as the winner 62% of the time, the Chen model 28% of the time and lastly the Tu model won 10% of the time. This is evidence that the Hertz model, although limited, is an appropriate choice for indentations on the nuclear regions of cells for reasons detailed in section 1.7.2 Models for deriving elasticity from indentation measurements.

The sample data set tested was a culture of 3T3 cells seeded on uncoated glass coverslips for 24 hours previous to the measurements. 25 cells were measured. A similar protocol for indentation was followed to that described earlier in the chapter, briefly; 5 indentations on the nuclear region with a maximum force of 3.5nN and a constant speed of 10µm/sec were performed. A spherical 4.8µm silica microsphere mounted on an Arrow TL1 tipless cantilever was used as the probe. The elasticity of each cell was got by averaging the values of the 5 indentations performed.

Figure 24 shows comparable values of elasticity returned by both the JPK and the CAM software programs of 2.07 kPa ± 1.37 and 2.03 kPa ± 0.86 respectively; however a significant difference was observed in the results returned by the ROB software, showing average cellular elasticity to be 5.79 kPa ± 2.24. This highlights one possible source of variation in published AFM elasticity data.

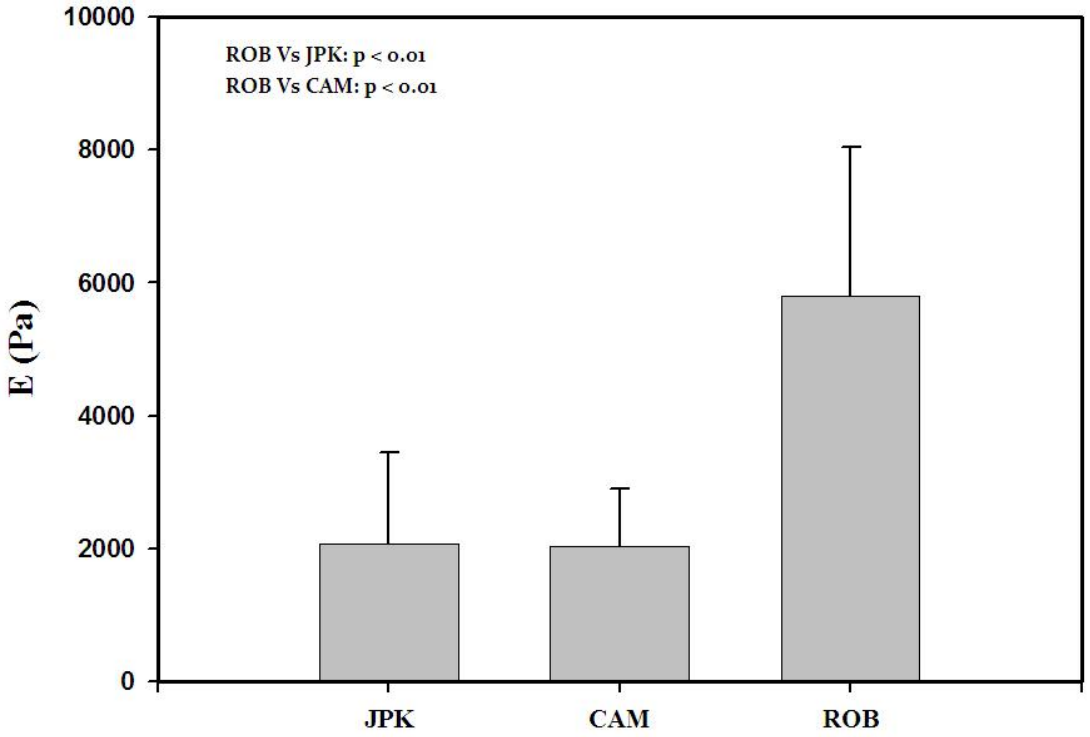

Figure 24: Analysis software comparison. This figure shows the returned values of elasticity for a population of 3T3 cells given by each of the three programs tested. The ROB software returned significantly different values ($p < 0.01$) to those of the JPK or CAM programs, showing the average elasticity of the population to be 5.79 kPa ± 2.24. The JPK and CAM programs returned average elasticity values of 2.07 kPa ± 1.37 and 2.03 kPa ± 0.86 respectively; there was no significant difference between these values. Error bars show 1 standard deviation from the mean.

Possible reasons for the disparity in the results are hard to identify as they likely lie within the code of each program. They could pertain to how the software deals with indentations over the recommended 10% of total sample thickness; for example, the JPK software allows the user to manually discard regions of an indentation curve should they penetrate too deep within a cell however the CAM and ROB programs

have no such feature. Perhaps, where the indentation is too deep, the CAM software is able to select a more appropriate model to fit thus limiting the influence of the substrate effect, whereas the ROB software has no such feature. Ultimately, the success of these home-made programs depends on the background experience of the creator, both in the physics of AFM indentation theory and in computational modelling. The take home message from this comparison must be that if the user is not confident in either of the afore mentioned fields then care must be taken to ensure that the most repeatable, reliable method for analysis has been adopted and applied throughout. In this way, the potential of the AFM as a biological toolbox is unlocked and the resulting data can be incorporated in to and important for progressive stages of investigation.

3.4.7 Tip geometry: sharp vs. sphere

To investigate the effect tip geometry can have on elasticity values we compared elasticity results from 3T3 cells indented both with a sharp MLCT pyramidal tip (Bruker AFM Probes) and a spherical silica microsphere mounted on a tipless cantilever (3.3.3 AFM colloidal probe preparation). In each case the cells were indented five times directly over the nuclear region in a square formation with a central point, the average elasticity value from the 5 force measurements was averaged again to identify the population average. Four populations were measured, those cultured on uncoated glass, N_3, RGD and mannose coated glass. The Hertz model was used to extract Young's modulus values. The effect of surface coating on cellular elasticity will be discussed in detail in Chapter 4 however to improve sample numbers these conditions have been included here. Each population was cultured overnight on their respective substrate before force measurements were carried out the following day. Separate populations were used to test the two different probe geometries. The aim was two-fold; to investigate whether these molecules could affect cellular elasticity and to what extent the tip geometry could affect the resulting elasticity values. As can be seen from Figure 25 there are significant differences between the results returned from each probe. Elasticity values got from using the sharp pyramidal indenter are at least three-fold stiffer that those got from using the spherical indenter, returning values of 9.3kPa, 6.1kPa, 6.2kPa and 7.2kPa

for N_3, RGD, mannose and uncoated glass respectively. Elasticity values reported by the spherical indenter are 1.2kPa, 2.0kPa, 2.2kPa and 2.2kPa for the same conditions.

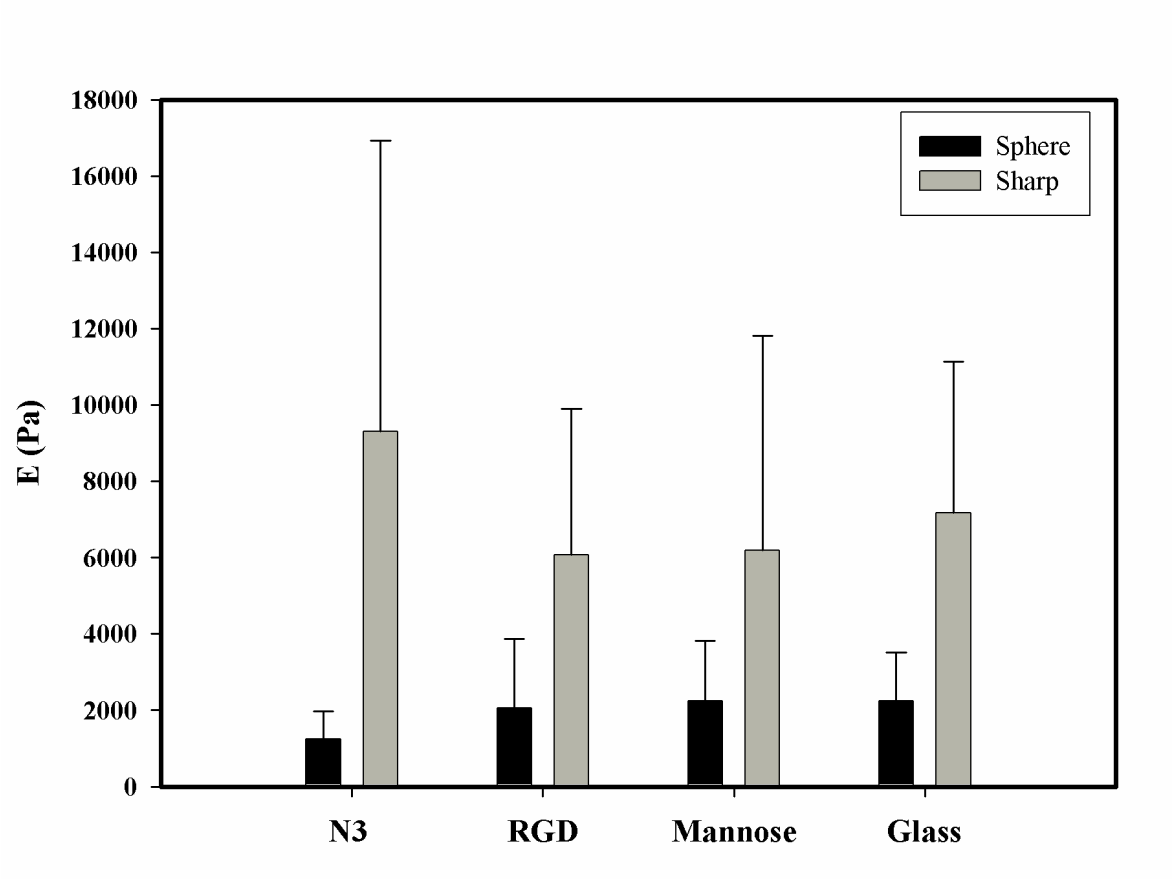

Figure 25: Graph compares elasticity results from 3T3 cells cultured on N_3, RGD, Mannose and uncoated glass surfaces after indentation with either a sharp pyramidal MLCT tip (grey bars) or a spherical silica microsphere (black bars). Ten cells were measured on each substrate (5 x sharp and 5 x sphere). Errors bars show 1 standard deviation from the mean value.

It seems obvious that indenter geometry will change the indented footprint on the sample during the repulsive contact portion of the curve, resulting in a different elasticity value being returned. The theory behind using spherical indenters for live cell measurements is to indent a larger surface area of the sample, providing a more representative value. It is plausible that sharp indenters could penetrate the fragile plasma membrane of the cell during indentation because all the pressure of the indentation is focused on a relatively small area on the cell surface. This would presumably increase the chance of the tip contacting directly individual cytoskeletal elements underneath the membrane during the measurement and effectively push

these through the cell. Due to the relatively increased stiffness of e.g. F-actin in comparison to the surrounding cytoplasm this could have the effect of artificially increasing the measured elasticity and explain the difference in values observed in Figure 25. However as shown in Figure 16 this was unlikely to be the case in this instance as it proved not possible to breach the membrane using the forces described here.

Sharp indenters could conceivably indent between the filamentous fibres of the cytoskeleton, without penetrating the cell membrane, which could result in the elasticity of the cell being misrepresented. The larger imprint of the spherical indenter is more likely to push upon the structural filaments and therefore return a more representative value of elasticity. Since the filamentous actin of the cell is the main contributor to cellular elasticity (Kuznetsova, Starodubtseva et al. 2007) it is important that its influence is taken in to account when indentation measurements are performed. For this reason we opted to employ spherical indenters for all live cell measurements unless otherwise stated. For more details on how pressure can be related to indenter geometry for a given loading force, see section 3.4.1.

3.5 Conclusions

By systematic evaluation and optimization of operational parameters in AFM indentation measurements, as well as by selecting the appropriate models for data fitting, we have demonstrated that AFM can be a robust method for monitoring living cell mechanical properties.

By first evaluating indentation force and the possible effects on the cell membrane we arrived at the conclusion that the range of forces that could conceivably be applied to a living cell (~3.5-5 nN) were not likely to damage the plasma membrane, Figure 16. Once the non-lethality of the measurements had been established it was important to identify a level of force that could comply with the limitations of the chosen Hertz model and return repeatable values of elasticity. In section 3.4.2 Determination of loading force (nN), it was shown that depth of indentation could significantly affect elasticity results and so it was important to find a depth range at which the returned values of elasticity were as repeatable as possible. This range was

identified as between ~300 – 600 nm (Figure 17) which is in agreement with the conditions of applying the Hertz model to cells as reported in the literature, which state that between 5-10% of total sample thickness is an appropriate depth range.

At this range we are in a good position to get repeatable elasticity results which suit the application of the Hertz model, however it remained unknown whether the indentations were compressing purely cytoplasmic material or if the effect of the nucleus was also being measured. In order to investigate this, TEM images of sample cells were examined and found to have sufficient distance between the plasma membrane and nuclear membrane to accommodate indentations of the range selected, however it was clear that the influence of the nucleus could not be ruled out just because the indenter does not physically contact it. This is due to the indentation depth being greater than 10% of the cytoplasm thickness above the nucleus, implying that nuclear contributions are unavoidable unless indentation depth is reduced to ~80nm – a depth that has been shown to result in unreliable values for elasticity. To what extent and in what manor the results are affected by enhanced cell spreading on flat surfaces as opposed to structured ones – and how this in turn affects nuclear mechanics was not investigated as part of this thesis although it does propose interesting questions, such as how much can the thickness of the cytoplasm above the nucleus influence the elasticity results? Could cell height indicate the thickness of this layer and therefore be proportional to elasticity and is this cell type dependent?

A statistically significant relationship between indentation speed and resulting values of elasticity could not be established as large cell-cell and intra cell variations were present in the calculated results, particularly for speeds at the extreme ends of the measured range (1μm/sec and 25μm/sec). Caution should be taken when interpreting the absolute values obtained since these are dependent on both the cell type and subcellular units being probed. Importantly, we have found that the mechanical properties recorded on cell nuclear area give a reliable comparison between cells under the same measurement conditions.

Chapter four: Can common cell adhesion molecules affect cell elasticity? An AFM approach

4.1 Abstract

The phenomenon that cells respond to chemical and topographic cues in their surroundings has been widely examined and exploited in many fields ranging from basic life science research to biomedical therapeutics. Adhesion promoting molecules such as Poly-L-lysine (PLL) and fibronectin (Fn) are commonly used for *in vitro* cell assays to promote cell spreading/proliferation on tissue culture plastic and to enhance the biocompatibility of biomedical devices. Likewise, engineered topography is often used to guide cell growth and differentiation. Little is known about how these cues affect the biomechanical properties of cells and subsequent cell function.

4.2 Introduction

In this study, we have applied atomic force microscopy (AFM) to investigate these biomechanical properties. Operational factors, including indentation depth and speed, and mathematical models for data fitting have been systematically evaluated (see Chapter 3 section 3.3). We then quantified how PLL, Fn and microtopography affected cellular elasticity and the organisation of the cytoskeleton. Cellular elasticity after 1 day in culture was greater on Fn coated surface as compared to PLL or glass. These statistically significant differences disappeared after two more days in culture. In contrast, the significantly higher elasticity associated with cells grown on micrometric grooves remained for at least three days. This work sheds light on the apparently simple but debatable questions: *Are engineered chemical cues eventually masked by a cell's own matrix proteins and so only exert short-term influence? Does engineered topography as well as engineered chemistry affect cell elasticity?*

Most soft tissues such as skin and muscle appear to be pliable and elastic – this is evident in their deformability and their ability to recover shape after deformation (such as after pinching) - however they are in fact viscoelastic materials. Tissue cells

are engaged in a constant equilibrium, assembling and disassembling their cytoskeleton in response to surrounding environments. The continued reorganisation of cytoskeletal components (i.e. actin filaments, intermediate filaments and microtubules), contributes to the complicated and dynamic viscoelasticity displayed by cells (Ingber, Dike et al. 1994; Janmey and McCulloch 2007). In recent years it has become increasingly evident that the cytoskeleton plays an essential role in detection, transduction and regulation of the interaction forces between a cell and its extracellular matrix (Burridge and ChrzanowskaWodnicka 1996; Janmey 1998). These processes are associated with fundamental cellular functions and other important events (Chen, Mrksich et al. 1997; Kramer, Shen et al. 2005; Paszek, Zahir et al. 2005; Engler, Sen et al. 2006).

Naturally occurring extracellular matrix consists of proteins and glycosaminoglycans which act as chemical and physical cues to the cells. Mimicking the natural habitat *in vitro* is a necessary approach for unravelling the mechanisms underlying basic cell functions and for developing effective therapeutic medicines. Benefiting from advancements in micro-/nano-technology, significant developments have been achieved in a few decades. A large body of literature has detailed cellular responses to ECM protein patterns (Folch and Toner 2000), physical topography (Guilak, Cohen et al. 2009) and substrate stiffness (Engler, Sen et al. 2006; Engler, Carag-Krieger et al. 2008). For example, adhesive ECM micropatterns regulate initial adhesion of cells on substrates and determine cell fates (i.e. apoptosis or proliferation) (Chen, Mrksich et al. 1997), and have also been valuable for studying spatial regulation of cell-cell interaction (Folch and Toner 2000). Similarly, micro- and nano-topography has been shown to modulate the structure of the cellular cytoskeleton, cell-phenotype and gene expression (Curtis and Wilkinson 1997; Dalby 2005). Despite these cues being in different formats, it is well recognized that the resultant alterations in cell behaviour might be interlinked with the mechanical behaviour of cells being influenced by the many regulatory pathways associated with focal adhesions (Chen, Alonso et al. 2003).

However, little is known about the mechanisms involved in these pathways. This is partly because of the highly variable, heterogeneous and dynamic nature of living

cells that impose formidable challenges to retrieve reliable information. For a long time, mechanical properties of living cells have been examined as a whole, using methods such as micropipette aspiration (Hochmuth 2000), optical stretching (Guck, Schinkinger et al. 2005) and optical (and magnetic) tweezers (Moffitt, Chemla et al. 2008). However, these methods provide average information and are more suitable for cells in suspension. More recently, techniques such as magnetic twisting cytometry (Fabry, Maksym et al. 2001), traction force microscopy (Parker, Brock et al. 2002; Wang, Tolic-Norrelykke et al. 2002) and AFM (Tao, Lindsay et al. 1992) have been developed to probe the mechanical properties of heterogeneous subcellular structures. Among these, AFM is perhaps the most flexible tool as it allows both the imaging of cells and the quantification of cell mechanical properties with nanoscale spatial resolution (Butt, Cappella et al. 2005).

The last few years have witnessed a significant growth in the use of AFM for quantifying local elastic and viscoelastic properties of living cells (Tao, Lindsay et al. 1992). A number of studies have shown that cellular mechanical properties are linked with cellular phenotype (Mathur, Collinsworth et al. 2001; Darling, Topel et al. 2008), pathological states of cells (Paszek, Zahir et al. 2005; Dulinska, Targosz et al. 2006; Cross, Jin et al. 2007), aging (Lieber, Aubry et al. 2004; Berdyyeva, Woodworth et al. 2005) and cellular differentiation stages (Pajerowski, Dahl et al. 2007). For example, using AFM it has been observed that aging increases cardiac myocyte stiffness which contributes to the occurrence of left ventricular (LV) diastolic dysfunction (Lieber, Aubry et al. 2004). In addition, it has been demonstrated that the mechanical properties of cells can be a promising marker for cancer diagnostics (Discher, Dong et al. 2009). Despite these developments the investigation of cellular mechanics is still in its early stages but has the promise to make significant contributions to many fields. One such field is tissue engineering, where cellular mechanical properties can be quantitative markers, monitoring the regulation of cell differentiation towards a targeted function (for example, regenerated bone tissues, fat tissue) using engineered microenvironments.

In this study we investigated the potential of local cellular mechanical properties, as determined by AFM, to quantitatively evaluate the influence of an engineered

microenvironment on cellular structure and function. We have established a robust measurement regime that has been applied to study the effect of two commonly engineered aspects of the cellular microenvironment, namely (A) the chemical properties of the substrate (i.e. the presence of ECM proteins) and (B) surface topography. In addition, by incubating the cells for one or three days on different types of substrate we wished to shed light on the apparently simple but debatable questions: *For how long does a particular substrate property influence cell behaviour? Is physical topography a permanent cue that constantly affects cells? Are engineered chemical cues masked by a cell's own matrix proteins and so only exert short-term influence?* The results of our studies demonstrate that the local elasticity of the nuclear area can serve as a reliable marker for the overall mechanical properties of a cell and permits intercellular comparison. This presents the opportunity to connect cellular mechanics with overall and sub-cellular morphology.

4.3 Materials and methods

Only materials and methods unique to this chapter are detailed in this section. For more general materials and methods, see Chapter 2.

4.3.1 Substrate preparation.

Common adhesion promoting molecules, namely Poly-L-lysine (MW 70-150,000 kDa, Sigma) and Fibronectin (Bovine plasma, Sigma) were used to coat glass coverslips (diameter of 24mm) according to manufacturer's guidelines. Glass coverslips were first cleaned by 5 minutes of sonication in 70% ethanol then dried using nitrogen gun. For PLL coating, glass coverslips were incubated for 10 minutes at 37°C in a 0.01% PLL (w/v) aqueous solution and left to dry at room temperature. For Fibronectin (Fn) coating, the coverslips were soaked overnight at 4°C in a sterilised Fn solution at a concentration of 5µg/ml. Wherever necessary, substrates were sterilised under UV light for 15 minutes prior to cell culture. All the substrates were washed in PBS followed by incubation at 37°C with 1% BSA/PBS solution to block non-specific binding of the proteins. This was to negate any possible influence from the proteins in the supplemented culture media.

4.3.2 Cytoskeleton & fibronectin detection

To stain the F-actin cytoskeleton cells were cultured on the various substrates using the same conditions as those for AFM measurements. Briefly, cells were first fixed in 4% formaldehyde/PBS, with 1% sucrose at 37 °C for 15 min and then stained for F-actin filaments using phalloidin-fluorescein in PBS/Tween (1:50; Sigma) at 37 °C for 1 hour (Faulstich, Trischmann et al. 1983). The slides were stored in PBS/Tween solution until imaged.

Immunofluorescence labelling was applied to differentiate between the fibronectins secreted from the 3T3 mouse fibroblasts or that derived from bovine serum that was present in the culture medium and on the Fn-coated substrates. Cells were first fixed and permeabilized with BD Cytofix/Cytoperm solution (BD Biosciences, San Diego) for 15 minutes at 37°C. They were then washed with PBS and left to soak in 1% PBS/BSA blocking solution for 5 minutes at 37°C. After this, cells were stained with primary antibodies specific to each type of fibronectin following the protocol provided by the suppliers. For this, ab23750 (Abcam Ltd.) from rabbit was used for mouse specific fibronectin, and ab26245 (Abcam Ltd) from mouse for bovine specific fibronectin. Having the primary antibodies raised in different species is necessary to avoid cross reactivity when the secondary antibodies are added. This was followed by thorough washing of cells with 0.5% PBS/Tween20 and the addition of the secondary antibody solution, namely Cy5 conjugated goat anti-rabbit or FITC conjugated anti-mouse IgG in 1% PBS/BSA solution at concentrations of 20 µg/ml. Finally, the cells were washed again in PBS/Tween20 and stored in the dark at 4°C until imaged.

4.3.3 AFM measurements

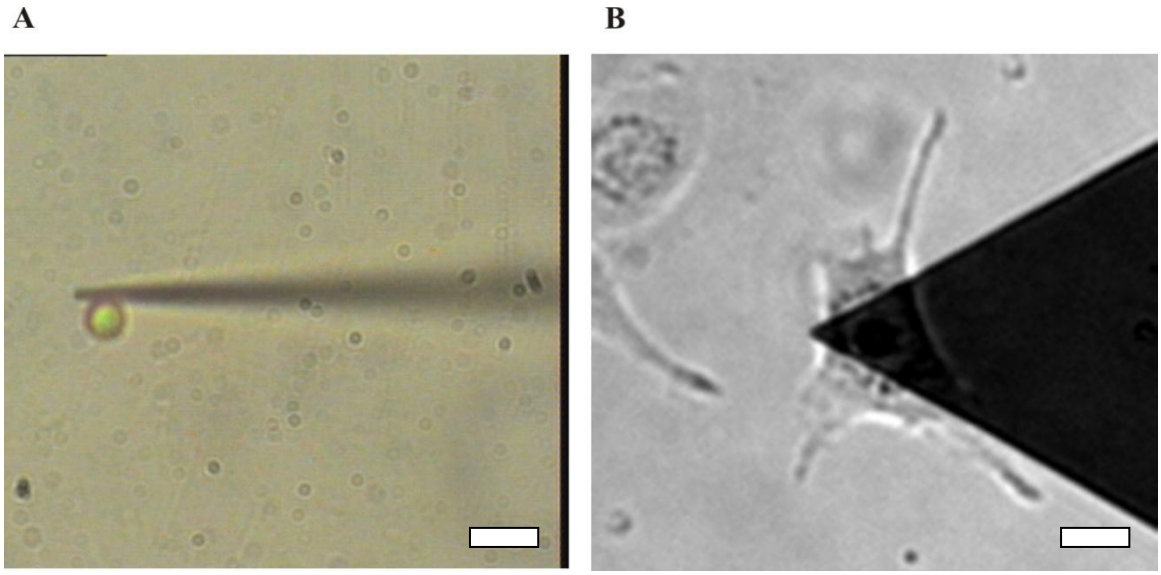

Figure 26: a) An optical image of a silica microsphere (diameter 5µm) glued to the end of a tipless cantilever using UV curable glue. b) An optical image of the cantilever (with microsphere attached) positioned over a 3T3 cell nucleus attached to an uncoated glass coverslip. Scale = 10µm.

Spherical indenter probes of the type shown in Figure 26A were prepared for the experiment according to the protocol detailed in Figure 13. The location of elasticity measurements was the nucleus of each cell (Figure 26B) and the pattern of indentations is shown in Figure 27.

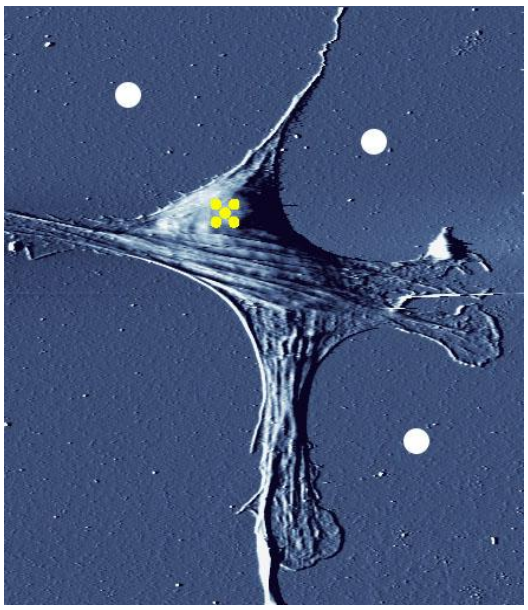

Figure 27: A contact mode AFM image of a live 3T3 cell showing the indentation area. Superimposed on the image are three white dots representing the locations of the glass force-distance curves used to calculate cell height by the custom built software and five yellow dots representing the pattern of indentations performed on the cell nucleus. The dots are not to scale. The centre indentation is always carried out first as it is selected first on the AFM software, no correlation between indentation order and elasticity results observed.

After 1 or 3 days culture, cells had developed a spread morphology (Figure 26B), resulting in different elasticities within each cell (Ingber, Dike et al. 1994; A-Hassan, Heinz et al. 1998). With the aid of the optical microscope the AFM probe could easily be located on a particular cell and its subunits of interest with μm scale positional accuracy (Figure 26B). To enable comparable elasticity measurements of individual cells while eliminating the local variations within a cell, only the nuclear area was selected for indentation measurements. This permits the evaluation of the overall mechanical properties of the cytoplasm using optimised conditions. For each cell, five indentation measurements were carried out on the nuclear area: The first indentation was carried out on the centre of the nucleus and the remaining 4 in a 3μm x 3μm square around it (Figure 27). Prior to indenting the nuclei, three indentations on the glass surrounding the cell of interest were performed (indicated in Figure 27). The contact points of these three measurements were used to define the average z-position of the underlying substrate (i.e. a z-position reference). Subtraction of this z-reference from the cantilever's z-position at the moment it

comes into contact with the cell returns the height of the cell at each individual position. For cells on a microgrooved substrate reference curves were performed on troughs to ensure the cell body was on the same plane as the contact point of the curve.

The apparent elastic modulus of the nuclear area of a cell was then derived by analysing the obtained force-distance curves with the JPK software using Hertz's model (see chapter 1 section1.7.1 Models for deriving elasticity from indentation measurements) A range of indentation speeds were tested and the optimal one used for subsequent systematic investigation of the influence of different substrates, see section 3.4.4. The range of indentation speed parameters explored included 1µm/s and 3µm/s with a ramp size of 5 µm, and 10µm/s, 16µm/s and 25µm/s with a ramp size of 8 µm, see section 3.4.4.

The elasticity of a given cell was determined from the average of the values obtained by the 5 indentations made. At least 25 cells on 4 replicate substrates were measured for each experimental condition unless otherwise stated.

4.4 Results and Discussion

4.4.1 Chemical cues affect cellular elasticity significantly in the short term only

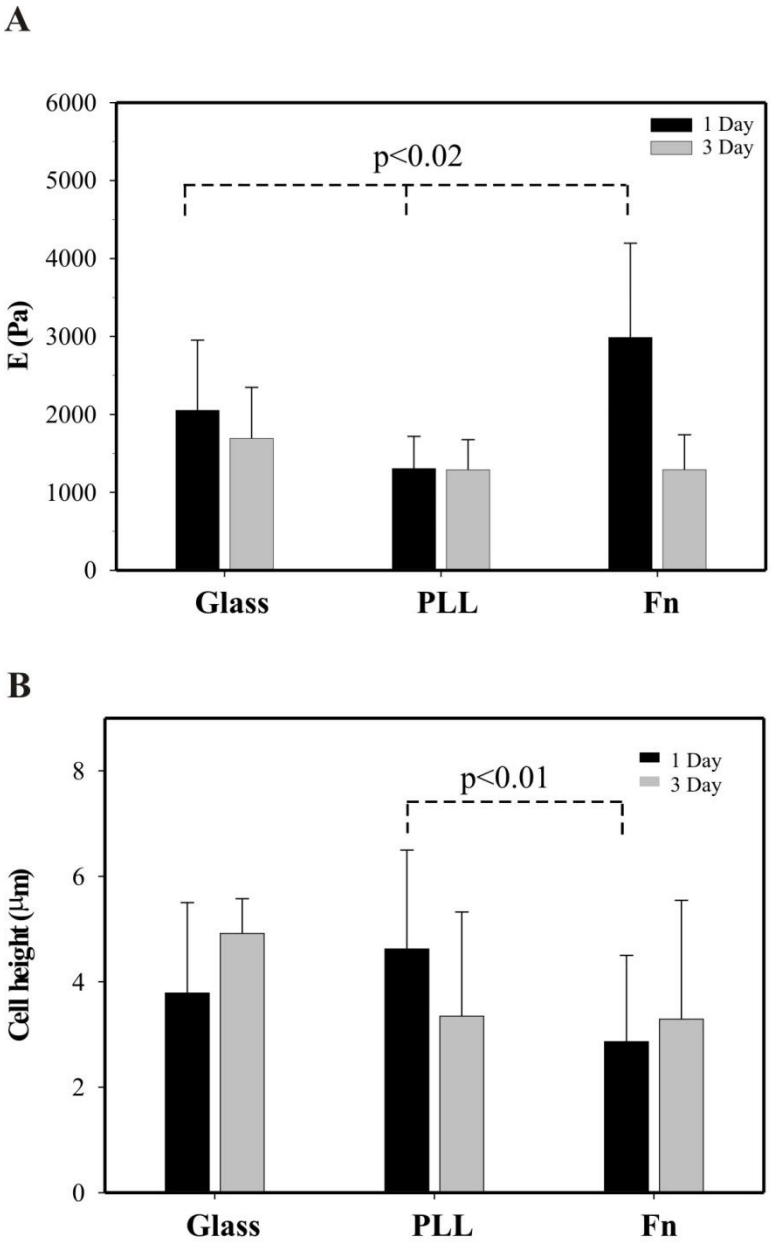

Figure 28: Influence of common adhesive molecules, Fn and PLL, on cell elastic properties. A) Elastic modulus and B) cell height of 3T3 cells cultured on Fn, PLL and uncoated glass overnight and after 3 days. Note cells were isolated after overnight culture and were still sub-confluent after 3 days culture. For elastic modulus, significant differences were found for any pair of the three populations ($p<0.02$) after overnight culture; however, there is no significant difference between them after 3 days culture. In the case of cell height,

significant difference was observed only between cells cultured overnight on Fn coated and those on PLL coated substrates. Error bars show 1 standard deviation from the mean value.

ECM proteins (e.g. Fn and collagen) and adhesion enhancing molecules (e.g. PLL and 3-aminopropyl-triethoxysilane) are often used to promote initial cell attachment on surfaces (Folch and Toner 2000). In this short term, one day study, 3T3 fibroblasts were seeded at low density and cultured overnight on Fn coated, PLL coated and uncoated (control) glass coverslips giving rise to single cells with a spread morphology. The average elastic modulus of cells (n=25) for each set of substrates was determined using the standardized protocol derived in Chapter 3. As shown in Figure 28A (black bars), cells cultured on Fn coated glass coverslips had a higher elastic modulus of 3.0 ±1.2 kPa in comparison to those cultured either on PLL coated (1.3±0.4 kPa) or on uncoated glass coverslips (2.0 ± 0.9 kPa). Student t-test showed that the differences observed between each pair of these three populations were statistically significant (p<0.02).

It is well known that the interaction between a cell and its surrounding environment influences the focal adhesion formation (Geiger, Spatz et al. 2009). As a consequence, the cell adapts its shape (i.e. becomes more spread, flattened when the material is more adhesive), leading to variations in cell height. Since both cell height and elastic modulus were derived from the same force-distance curve, a correlation between these could be identified. The average cell heights of cells cultured on Fn coated, uncoated glass and PLL coated glass were 2.9±1.6 µm, 3.8±1.7 µm and 4.6±1.8 µm respectively (Figure 28B, black bars). This represented a statistical difference in height, cells cultured on Fn coated glass were flatter in comparison to those on PLL coated glass (p<0.01) and those on uncoated (control) glass substrates (p=0.06). However, the height difference was not significant when the cells cultured on uncoated and PLL coated glass (p=0.1) were compared. Interestingly, a lower cell height correlated well with a higher elastic modulus, suggesting that more flattened, isolated cells might be stiffer in general. A spread cell indicates that a cell has developed a well organised contractile cytoskeletal network which contributes to the cell's stiffness. This finding is in line with a previous study which showed that the elastic moduli of osteoblasts plated on Fn or collagen coated surfaces were higher than of those cells plated on either plain or

PLL coated glass, during the first hour after seeding (Takai, Costa et al. 2005). It is also a possibility that lower cell height results in a larger percentage of the total cell height being indented, thereby increasing the contributions of the stiffer nucleus or enhancing the substrate effect, giving rise to increased Young's modulus values.

On all of the tested substrates cells became sub-confluent after 3 days growth. Interestingly, the coating dependant difference in cellular stiffness observed at 1 day of culture disappeared (Figure 28, gray bars). Similar elastic moduli were found for cells cultured on PLL (1.3±0.4 kPa) and Fn (1.3±0.5 kPa) coated substrates. Although cells cultured on uncoated glass appeared stiffer (1.7 ± 0.7 kPa) than those on either of the other two substrates, the difference was not significant ($p>0.2$ for both cases). Similarly, there was no significant difference in cell height after 3 days culture (Figure 28B, grey bars).

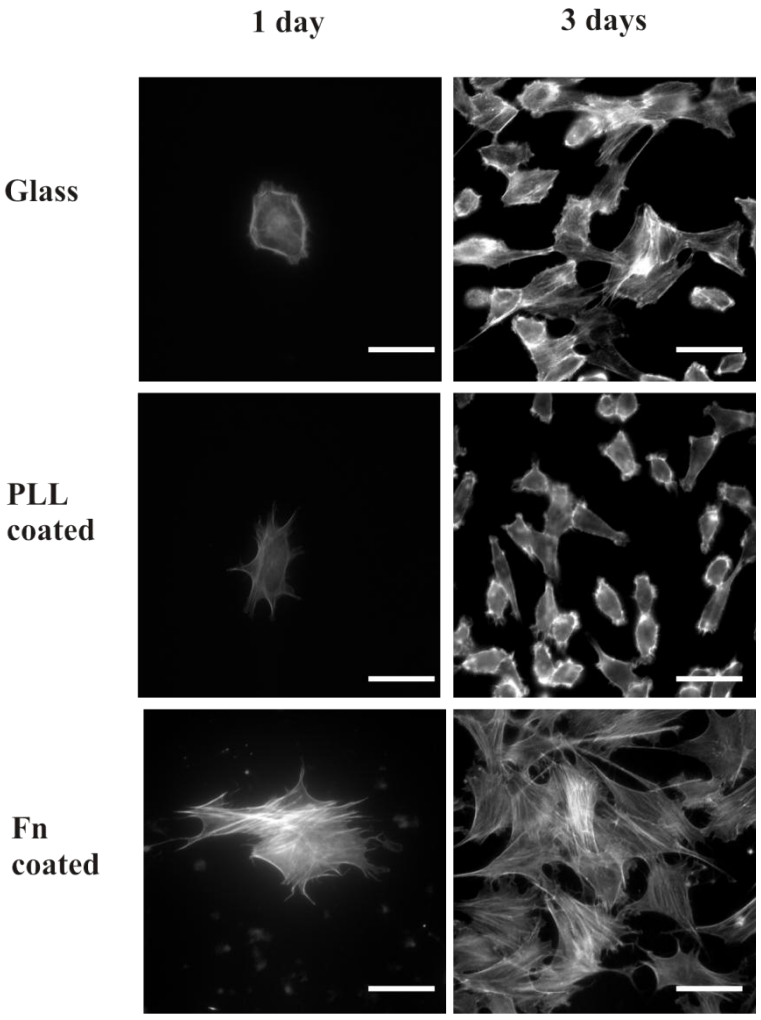

Figure 29: Fluorescence images of actin structures for cells cultured of 3T3 cells cultured on Fn, PLL and uncoated glass overnight and after 3 days. Scale = 50µm.

The disappearance of the differences in cell elasticity after 3 days culture probably suggests a scenario in which cells remodel their surrounding substrate and mask the engineered chemical cues. As shown in Figure 29 (left column), individual cells had already developed a spread morphology and a highly visible F-actin network after 1 day in culture (N.B. seeding density was optimized to maintain isolated cells for detecting effects that arose from the Fn and PLL coatings alone, rather than cell-cell interactions). Cells cultured on Fn coated substrates showed the highest intensity of filaments and highly organized networks, which were followed by cells cultured on uncoated control glass and those on PLL coated substrates. This difference in the F-actin structure and its intensity was in good agreement with the order of the elastic moduli as well as with the previous finding that the F-actin network determines the elastic properties of living cells (Rotsch and Radmacher 2000).

After 3 days culture, subconfluent cell layers had formed in all cases (Figure 29, right column). Many cells were connected with others in the near neighbourhood, which might have induced additional effects on cell elasticity. In addition, intensive F-actin networks were found in all cases without distinguishable variations. These qualitative observations and correlated quantitative elasticity measurements showed that physically absorbed chemical cues might influence cell mechanical properties in the short term (e.g. less than a day) but can be quickly overcome by the cells remodelling their local ECM. Previously, Lussi *et al.* have shown that chemical patterns in general have a limited lifetime, independent of the way they had been formed (Lussi, Falconnet et al. 2006).

To test this hypothesis, cell produced fibronectin (denoted as Cell-Fn) and Fn of bovine origin (denoted as bovine-Fn) were differentially labelled. Bovine Fn was present either on the Fn coated surfaces, or could have adsorbed to the surface from the FBS present in the culture serum. After 1 day in culture, cells on PLL coated and uncoated glass were fully covered with cell-Fn (Figure 30, cell-Fn column). In addition, scattered traces of cell-Fn were found in the surrounding areas. In contrast, cells cultured on Fn coated glass showed a central, dark patch with a limited amount of cell-Fn evident near the edges of the cell membrane (Figure 30A,

cell-Fn column). Interestingly, cell-shape-like well-organized cell-Fn matrix was found on the surface even after the cell(s) had migrated away (Figure 30A, white arrow in the cell-Fn column). Negligible bovine-Fn was found on PLL coated and uncoated glass, whereas substantial amounts of bovine-Fn was found on both the surface and the cells cultured on Fn-coated glass (Figure 30, bovine-Fn column).

The obvious difference in production of cell produced fibronectin after 1 day culture sheds light on the difference found in cell elasticity. Cells cultured on Fn-coated glass tend to remodel the bovine-Fn on the surface and add little of their own Fn, as suggested by the presence of bovine-Fn and the lack of cell-Fn on cells. It is worth noting that intensive and a well-organized cell-Fn matrix on the surface (Figure 30A, white arrow in the cell-Fn column) was only found for the cells cultured on Fn-coated glass after 1 day culture. Taken together, this means that the initial stage of the remodelling and integration process plays a key role in modulating cell cytoskeleton structure and results in the higher elasticity.

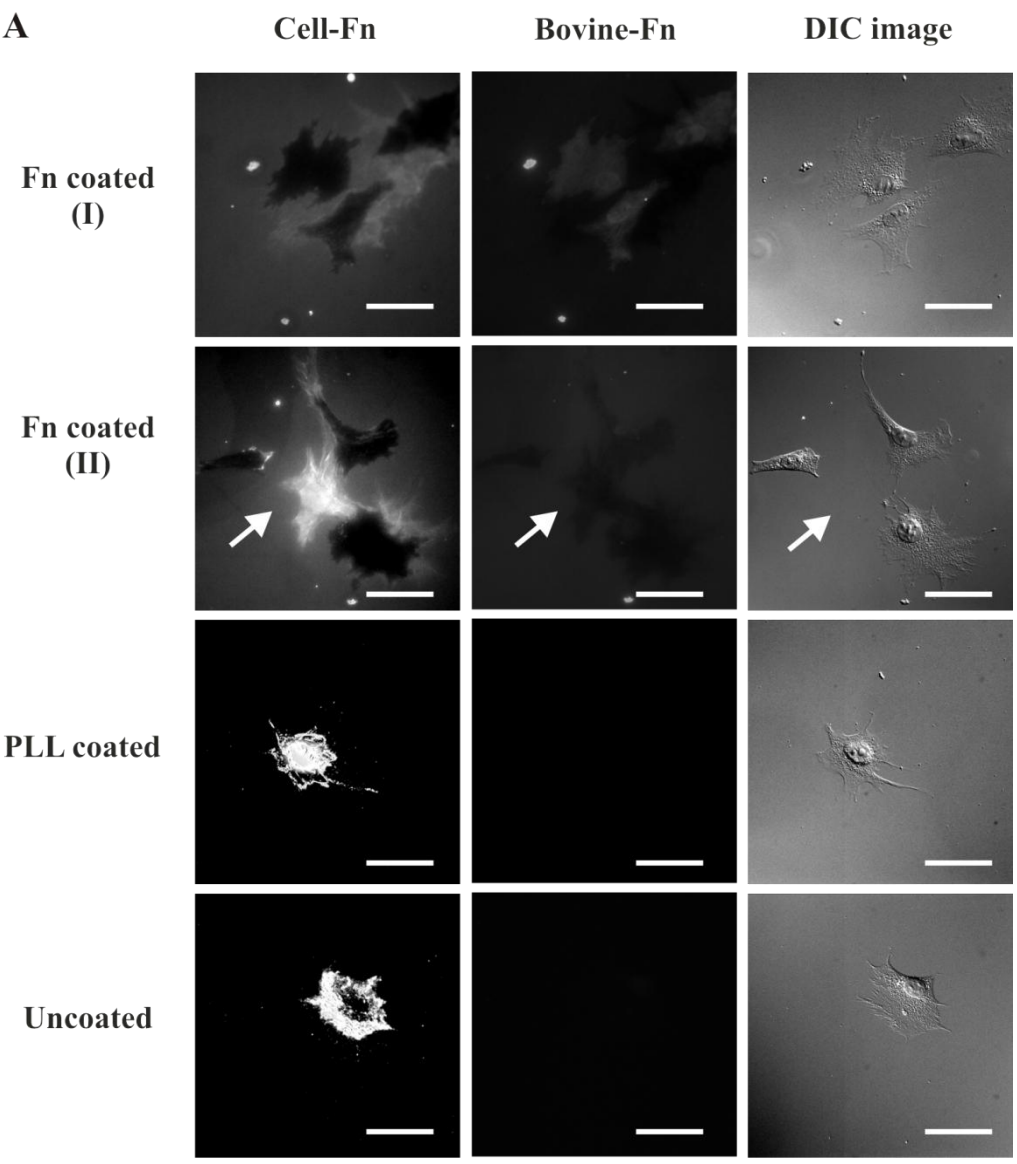
A
Cell-Fn
Bovine-Fn
DIC image
Fn coated (I)
Fn coated (II)
PLL coated
Uncoated

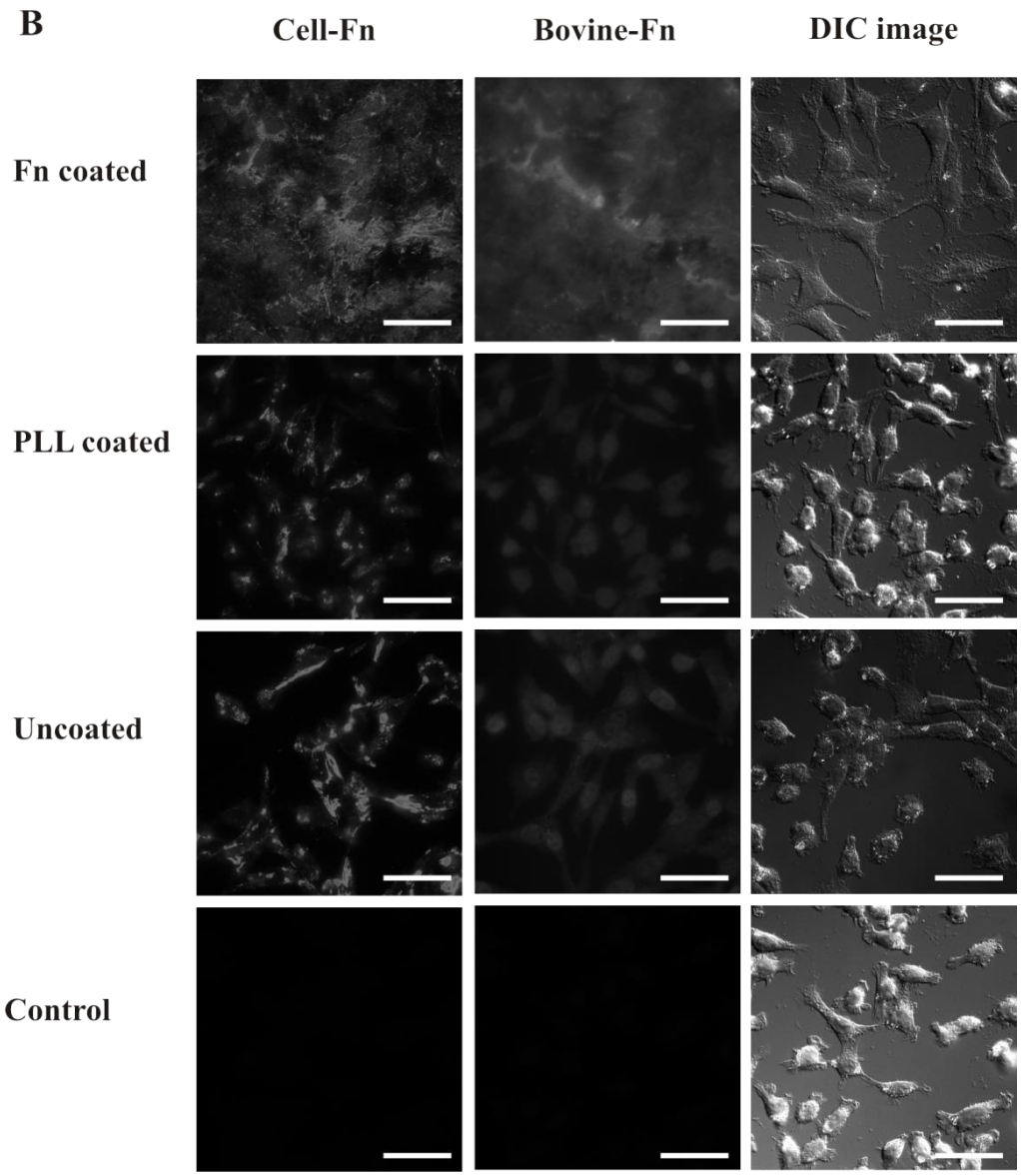

Figure 30: Immunofluorescence and DIC images of cell produced fibronectin (denoted as cell-Fn) and fibronectin from either Fn-coated surface or medium (denoted as bovine-Fn) on Fn, PLL and uncoated glass. The cell-Fn was detected by FITC labelling and the bovine-Fn by Cy5 labelling. (A) After 1 day culture. Two distinct phenomena were observed for cells cultured on Fn coated glass, which are presented in Fn-coated (I) and (II). The white arrow in the Fn-coated row indicates the cell-Fn left on the substrate after cell migration, since no cell is present in the DIC image. (B) After 3 days culture. Weak bovine-Fn was found on the three substrates. This is mainly due to unspecific binding of primary antibodies to cellular proteins, as shown by the control where only secondary antibodies were used and results in low background (the control row). Scale = 50 μm.

After 3 days culture, the significant differences observed after 1 day in culture disappeared (Figure 30B). Cell produced fibronectin matrix was found all over the cells and between cells in all cases. The phenomenon is in good agreement with the similar F-actin structure and elasticity values observed after 3 days in culture.

4.4.2 Does microtopographic structure affect cell elasticity both in the short and long term?

To address this question, similar indentation measurements were made on the cells cultured on flat (unstructured) PDMS and PDMS structured with microgrooves (dimension 12.5 μm period 1 μm deep) (Figure 31). To promote cell adhesion on PDMS and to provide a similar chemical environment to those discussed above, the PDMS substrates were coated with PLL. Much evidence has shown that cells adopt a fusiform shape and follow the micropattern (Clark, Connolly et al. 1990), which can be utilized to guide cell growth in applications such as neuron regeneration (Clark, Connolly et al. 1990; Sørensen, Alekseeva et al. 2007; Yu, Leipzig et al. 2008). However, so far little is known about how cellular mechanical properties are influenced by interactions between cells and topography and how this will evolve with time (Yim, Darling et al.).

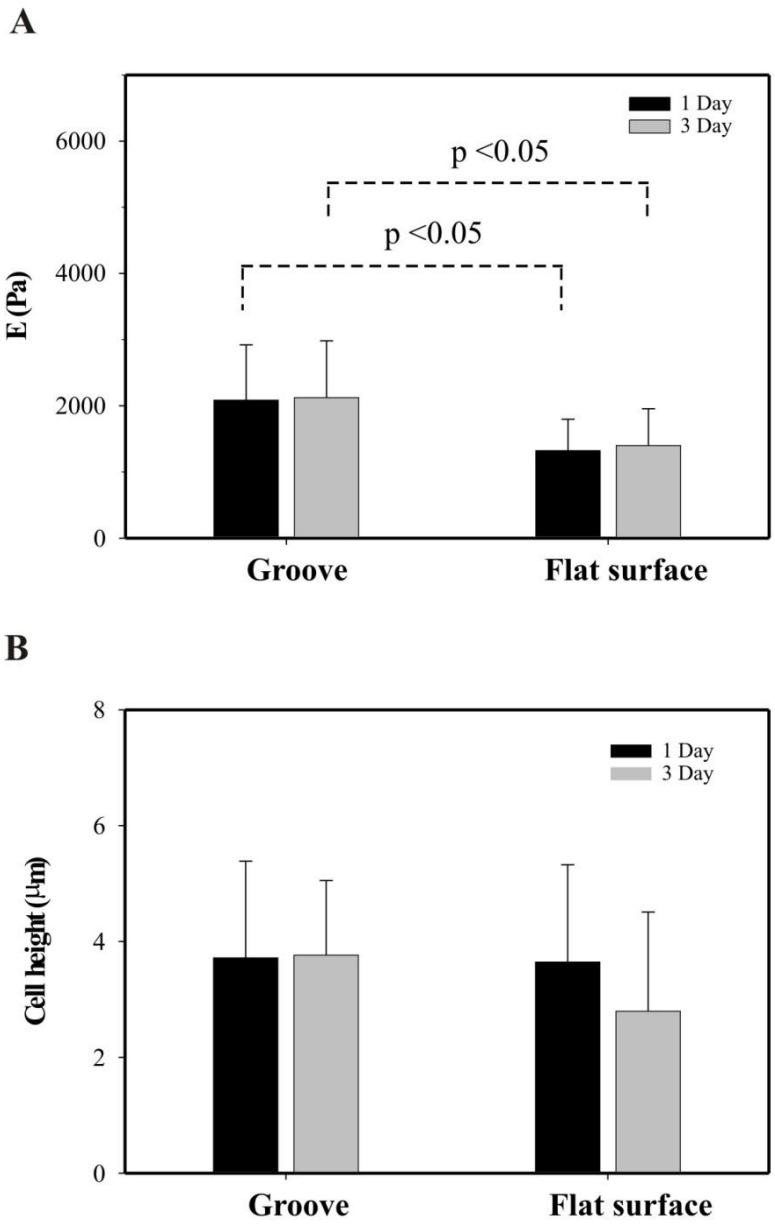

Figure 31: Influence of microtopography on cell elastic properties. A) Elastic modulus and B) cell height of 3T3 cells cultured on microgrooves and flat PDMS substrate respectively overnight (single cells) and after 3 days (sub-confluent cell layer). Cells cultured on grooves are statistically stiffer than those on the flat surface after overnight culture ($p<0.05$) and after 3 days culture ($p<0.05$). Error bars show 1 standard deviation from the mean value.

In contrast to the phenomenon observed in the study of chemical cues described above, cells cultured on microgrooves were significantly stiffer than those cultured on flat surfaces after 1 day culture ($p<0.05$) and this remained the same after 3 days culture ($p<0.05$), shown in Figure 31A. The average elastic modulus of cells cultured on grooves after 1 day culture reached 2.1 ± 0.8 kPa compared to 1.3 ± 0.5 kPa for those on the flat PDMS surface. Slight increases in the elastic modulus were observed in both cases after 3 days culture and, interestingly, the significant difference between these remained. It is worth noting that after 3 days culture the elastic modulus of cells on PLL coated flat PDMS (1.4 ± 0.6 kPa) is similar to those on PLL coated glass substrates (1.3±0.4 kPa). This suggests that the substrate underlying the PLL coat, PDMS versus glass, had only a negligible effect even though these are in principle very different materials (silicon-elastomer versus glass) with initially very different physicochemical surface properties. This result also underlines the robustness of the indentation and analysis protocol we have developed.

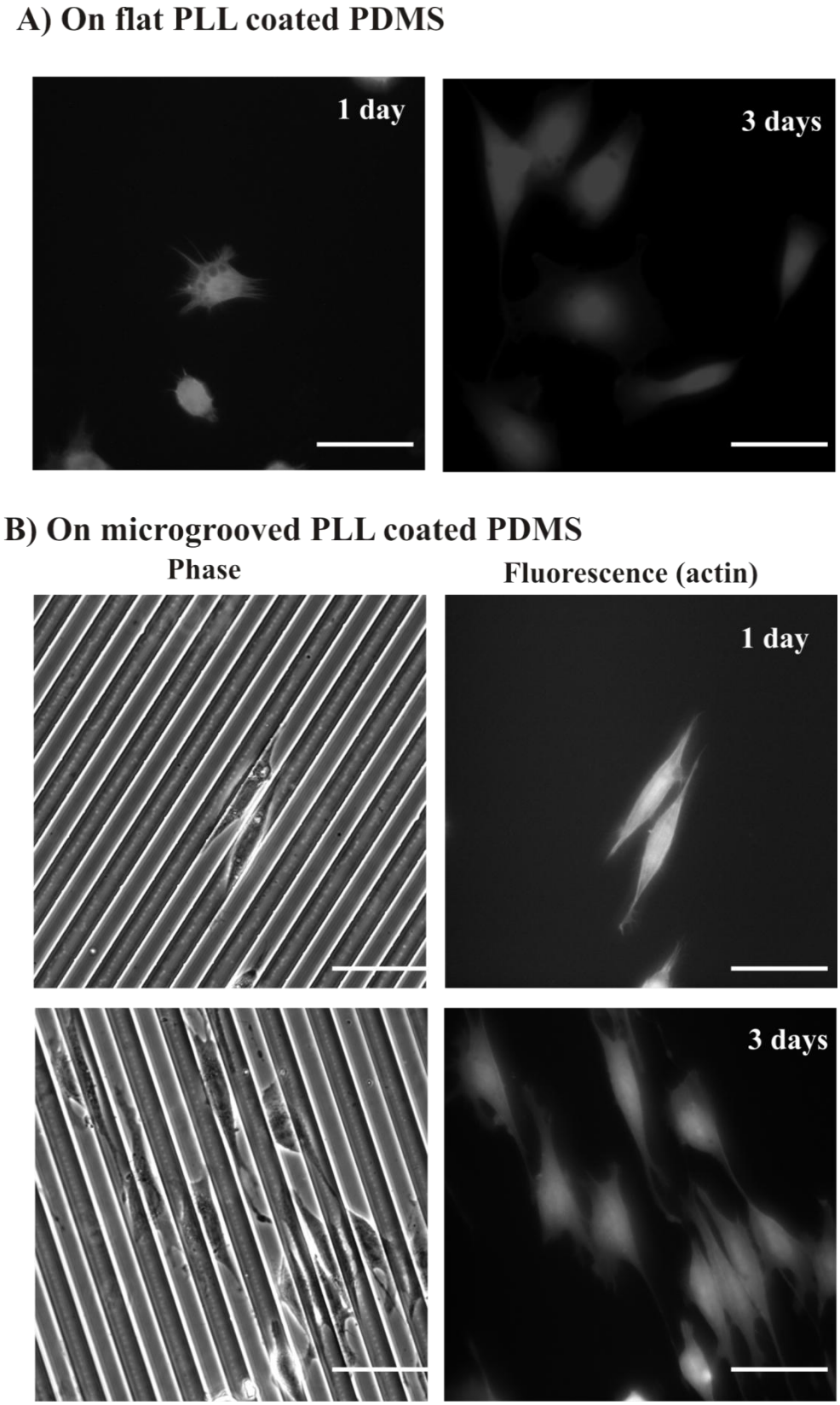

Figure 32: Optical and Fluorescence images of cells on microgrooved and flat PDMS substrates after different culture periods. (A) Fluorescence image (actin) of cells cultured on flat PDMS. (B) Phase contrast images (left) and fluorescence images of actin (right) of cells cultured on microgrooves. All scale bars are 50 μm.

No significant variations in cell height were observed (Figure 31B) suggesting that height variation might not account for the observed differences in stiffness. However, fluorescence images of cell cytoskeleton (F-actin) of the two populations showed that there were clear differences in intensity, which could be where the mechanical differences arise (Figure 32). After overnight culture, cells developed irregular shapes on the flat surface with a random F-actin network (Figure 32A). However, those on the microgrooves aligned themselves along the microgrooves. They adopted a spindle shape (Figure 32B) with the F-actin filaments following the underlying groove patterns. After 3 days of culture cell growth could be seen. Although cells became more spread over time on both types of substrates, they retained the fusiform/spindle shape on grooves or a "fried egg shape" on the flat substrate that they had adopted in the early stages of culture. This suggested that cells continuously sense the presence of the microgrooves. This is supported by studies where neurons were aligned by proxy of an aligned astrocyte monolayer (Sørensen, Alekseeva et al. 2007).

4.5 Conclusions

It is well established that the mechanical properties of living cells are linked to their shape, motility, and responses to biochemical and physical cues in their surroundings (Elson 1988; Fletcher and Mullins 2010). Mechanical characterization not only provides complementary information to that obtained by biochemical methods, but also has the potential to be a quantitative marker for cell growth and differentiation. Here the AFM is presented as a practical tool for evaluating quantitative differences in cellular elasticity induced by simple chemical modification to the substrate surface or topographical features.

Statistical differences in elasticity have been observed when 3T3 fibroblasts were cultured on Fn coated, PLL coated and uncoated control glass after 1 day culture, where cells on Fn-coated substrates presented the highest stiffness. This difference disappeared after a longer culture of 3 days. Immunofluorescence studies suggest that the remodelling of fibronectin coated on the substrates has played a significant role in the observed differences after 1 day culture. In contrast, significantly higher

elasticity values were recorded from cells grown on microgrooves, these values remained higher during the entire culture period. These variations found in elasticity correlated well with the immunofluorescence study of cytoskeleton structure.

Chapter five: The topographical influence on cellular elasticity

5.1 Abstract

The effects of topography on cell function and fate have been the focus of much research for many years. Simple geometries and arrangements of shapes such as parallel grooves and circular wells can induce behaviour in cells that goes far beyond morphological changes. However, the mechanisms by which cell's sense the surrounding topographical environment and alter behaviour accordingly is still largely unknown. We hypothesised that the arrangement of the cytoskeleton as dictated by topography transmits tension through the cytoplasm and influences gene transcription within the nucleus. Traditionally, this would be investigated using immunofluorescence microscopy and other common molecular biology techniques that involve cell fixation and lysis. However, in this study, atomic force microscopy (AFM) was exploited to investigate the evolving structural properties of live cells in response to their topographic environment, thus enabling an earlier more progressive understanding of the underlying mechanism.

Three topographies, namely grooves, pits and unstructured PDMS substrates were employed to induce the differentiation of MG63 osteoblast-like cells. Cellular elasticity values, an indication of the mechanical properties of the cytoskeleton, were quantified using AFM. Results showed that cells whose morphology was completely defined by pit geometry had a significantly softer elasticity (Young's modulus E= 0.862 kPa ± 0.28) than those where only a portion of the cell body was in contact with a pit and those either on grooves or on unstructured surfaces (E= 1.52-1.92 kPa) after 1 days culture. Further immunofluorescence study showed that activation of RUNX2, a transcription factor associated with osteoblast differentiation, was found in the nucleus of cells in pits only. However, no activation of RUNX2 was observed from cells in all conditions when the tension was inhibited using blebbistatin. The results strongly suggested that the pattern of tension acting on the nucleus affects gene transcription, this is in agreement with McBeath (McBeath, Pirone et al. 2004), Kilian (Kilian, Bugarija et al. 2010), Engler (Engler, Sen et al. 2006) and most recently McMurray (McMurray, Gadegaard et al. 2011).

5.2 Introduction

Within the body cells usually reside in extra cellular matrix (ECM) comprising of other cell types and proteins, such as collagen, elastin, glycoproteins and proteoglycans. The ECM provides cells with important structural support as well as chemical, biological and physical signals. These signals help determine cell fate and behaviours such as migration and differentiation and are vital to normal physiological function. In order to fully unravel these processes, it has become increasingly important to replicate *in vivo* conditions *in vitro*.

Micro and nanofabrication has become an effective method to create in vivo like microenvironments for cell studies (Richter, Reinhardt et al. 2010). Topographic and chemical patterns have been produced using conventional microfabrication methods, such as lithography and embossing (Charest, Eliason et al. 2006) and it has been demonstrated that topographic structures affect cell morphology as well as cell fate and function (Dalby, Gadegaard et al. 2007). This raises the possibility that gene transcription itself responds to topography alone.

However, it remains largely unknown how topography induces such a response. It is believed that mechanotransductive pathways are able to process topography induced cues (e.g. focal adhesion formations and cytoskeletal rearrangements) and in turn guide cell behaviour (Patel, Thakar et al. 2010). This points toward a complicated relationship between the cell, ECM and the microenvironment, independent of soluble chemical signals in the culture medium. Evidence for this can be found in the tendency of cells to change their elastic modulus in response to microtopography and substrate stiffness (Califano and Reinhart-King 2009; Steedman, Tao et al. 2010). In addition to the changes in elasticity, transcriptional changes and variations in protein expression are also evident using traditional molecular biological methods such as western blot analysis and immunostaining. However, this correlation between these global cytoskeletal changes and transcriptional changes remains unknown.

In this work, it is investigated how biophysical cues from the microenvironment could be influencing transcriptional changes within the nucleus. The hypothesis is that tension or patterns of tension induced by topography play a key role in

influencing cell cytoskeleton structure and function which might have the potential to induce signs of differentiation. We have previously shown that cellular elasticity as quantified by AFM indicates an early stage response of the cell to its environment (section 4.4 Results and Discussion). Utilizing the same approach we hope to shed light on the evolving physical properties of live cells as they conform to topographical features. These measurements are in conjunction with traditional molecular biological techniques such as immunofluorescence staining to reveal structures of interest. In particular, we focused our attention on the formation of phosphorylated myosin II structures within the cytoplasm of the cell. The actin-myosin relationship is a key mechanism of tension within the cell cytoskeleton and thus, when interacting with actin the myosin is in its active, phosphorylated, state. Therefore, staining for phospho-myosin is a way of visualizing the structure and orientation of tensile filaments within the cell. We also inhibited the function of myosin II within cells using blebbistatin. In this way, cells exposed to non-lethal concentrations of blebbistatin are unable to maintain the same levels of tension in their actin cortex as untreated cells and thus exhibit lower levels of elasticity (Martens and Radmacher 2008).

For this stage of the project we wished to employ a cell type in which differentiation could be identified as this was one of the key behavioural changes under investigation However, due to restricted access to mesenchymal stem cells – our first choice - we opted for MG63 osteoblast-like cells. This cell line has been transformed close to the mature osteoblast stage therefore still has some differentiation potential before it reaches maturity. Studies have previously shown this cell line to be capable of differentiation in response to surface roughness and composition (Martin, Schwartz et al. 1995; Lincks, Boyan et al. 1998) and specific growth factors (Bonewald, Kester et al. 1992) so it is our hypothesis that the cells have the potential to differentiate in response to topography alone. Culture conditions remain identical to those previously described in section 2.2 Cell Culture unless otherwise stated in the text.

In order to investigate the role tension plays in activating the differentiation machinery of a cell we stained for the phosphorylated RUNX2 transcription factor. RUNX2 is essential for the generation of healthy bone, it regulates the transcription

of several key genes and while not sufficient in itself to drive differentiation it is responsible for many important events in the process (Schroeder, Jensen et al. 2005). The presence of RUNX2 in the nuclei of MG63 cells is therefore a sign that aspects of differentiation signalling have been initiated. We looked for the appearance of the phosphorylated form of the transcription factor in the nuclei of MG63 cells cultured on microstructured PDMS substrates. Three topographies were tested; 12.5 μm wide, 1μm deep grooves, 40 μm diameter, 1μm deep pits and flat unstructured PDMS. Cells were cultured overnight on each topography and RUNX2 staining was carried out in parallel with AFM indentation measurements. These experiments were then repeated after overnight culture in blebbistatin infused media. Consistent with the hypothesis that tension within the cytoskeleton plays a role in activating the transcription machinery within a cell, we observed a reduction in cytoskeletal strength and failed to find any instances of activated RUNX2 within the nuclei of MG63 cells confined by the geometry of a pit.

5.3 Materials and Methods

Only those methods unique to this chapter are presented here. For more detail on general methods mentioned in this chapter please refer to Chapter two: Materials and methods.

5.3.1 Blebbistatin culture

Cells were seeded as before and placed in 37°C, 5% CO_2 incubator for ~45minutes. At this time, 100μl of blebbistatin solution, concentration 3.05 mM, was introduced to the culture media in the Petri dishes (2ml).

Cells were incubated overnight and AFM measurements were carried out the following day.

5.3.2 Phospho-myosin & phospho-runx2 detection

To image phospho-myosin and phospho-runx2 cells were cultured under the same conditions as for AFM measurements i.e. overnight on micro-engineered PDMS substrates. Cells were first fixed in 4% formaldehyde/PBS solution for 15min at 37°C then submerged in permeabilization buffer for 5 min at 4°C. After washing in 0.5% PBS/Tween 20 the cells were then blocked using 1%BSA/PBS solution for 5min at 37°C. After this cells were incubated with the selected primary antibody (p-runx2:

Abgent- AP3559a, p-myosin: Abcam-ab2480) in 1%BSA/PBS for 1 hour at 37°C, rhodamine-phalloidin was co-incubated with p-myosin stains to visualize filamentous actin. Cells were then washed for 3 x 5min in 0.5%PBS/Tween 20 before incubation with the biotin conjugated secondary antibody (Vector Labs) for 1 hour at 37°C and then washed again before final incubation with streptavidin-FITC (Vector Labs SA-5001) for 30min at 4°C. Cell were washed and stored in PBS at 4°C until imaged. Both transmission and fluorescent images of stained cells were taken using a Zeiss Axiovert inverted fluorescence microscope fitted with a cooled monochrome CCD digital camera (Andor iXon, Andor Technology). A filter set containing an exciter D475±40nm, a dichroic 495nm LP and an emitter E510nm LP were used for the FITC fluorescence detection. A filter set containing an exciter 500±25, a dichroic 525nm and an emitter 545nm were used for rhodamine fluorescence detection. All samples were imaged under the same acquisition conditions.

5.3.3 Phospho-runx2 activity analysis

Open source image analysis software 'ImageJ' was used to analyse contrast differences between the nuclei of cells and the surrounding cytoplasm. A standard circular sample area of 24units in diameter was drawn on each image and values for maximum, minimum and mean pixel values were recorded. This sampling area was positioned in three locations for each cell: 1; a region with no fluorescent features, 2; within the nuclear area of the cell in question and 3; a region of cytoplasm within the cell in question. After subtracting mean pixel background values of position 1 from those of the nucleus and cytoplasm, positions 2 and 3 respectively, the two were divided to give the difference in fluorescence intensity between the two locations (Equation 7). Differences greater than 1 indicated the nucleus was brighter that the surrounding cell, values less than 1 indicated the nucleus was darker.

$$\frac{N - B}{C - B}$$

Equation 7: N = mean pixel value of nucleus, C = mean pixel value of cytoplasm, B = mean pixel value of background.

Instances where the nucleus was found to be brighter than the surrounding cell were taken to indicate that phosphorylated transcription factor runx2 was active in the nucleus. The position of each cell ('in' pit, 'on' pit, groove, unstructured) was also recorded along with pixel intensity in order to build a picture of topography versus runx2 activity.

5.4 Results and discussion

5.4.1 Cellular elasticity on topography

AFM force-spectroscopy measurements were carried out on MG-63 cells on structured PDMS substrates at one and three day time points. As shown in Figure 33, following overnight (1 day) cultures, cells located in pits had a significantly lower elasticity (0.8621 ± 0.2836 kPa) than those on pits (1.8655 ± 0.5028 kPa), grooves (1.5188 ± 0.5933 kPa) or unstructured PDMS (1.9183 ± 0.5882 kPa). This difference was maintained until the three day time point (grey bars) when results show cells in pits still exhibiting a significantly softer elastic modulus (0.9012 ± 0.2656 kPa) than those on pits (1.6178 ± 0.3116 kPa), grooves (1.4317 ± 0.4875 kPa) or unstructured PDMS (1.9443 ± 0.6274 kPa). This highlights the ability of topography to maintain its influence over cells as opposed to the sometimes transient effect chemical patterns can have (McPhee, Dalby et al. 2010). It also shows that the 40µm Ø pits had a softening effect on the MG-63 cell cytoskeleton, decreasing elasticity by an average of 50% after 1 day and 45% after 3 days. Elasticity values obtained from cells on the remaining topographies are comparable to those from cells cultured on glass substrates and fall within the range of published data (Shin and Athanasiou 1999; Docheva, Padula et al. 2008).

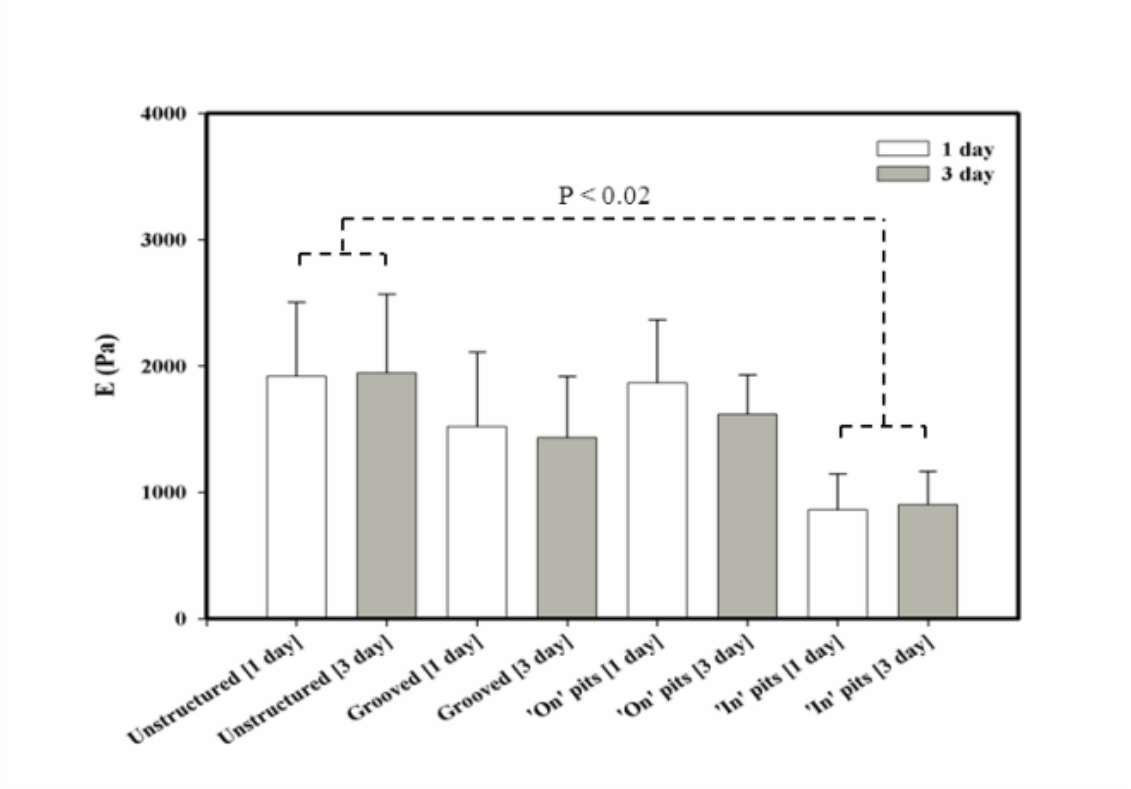

Figure 33: Shows elasticity values of MG63 cells after 1 & 3 days culture on unstructured, grooved and pitted PDMS substrates. Significant differences ($p < 0.02$) were found between the elasticity values of those cells fully confined by pits (In pits) and those on all other topographies. There were no significant differences found between cells on other topographies or between 1 & 3 day culture time points. Error bars show 1 standard deviation from the mean value.

5.4.2 Topography induced activation of differentiation

Immunofluorescent labelling of phospho-runx2, a marker for osteogenic differentiation (Schroeder, Jensen et al. 2005) was carried out on all cells after 1 day culture.

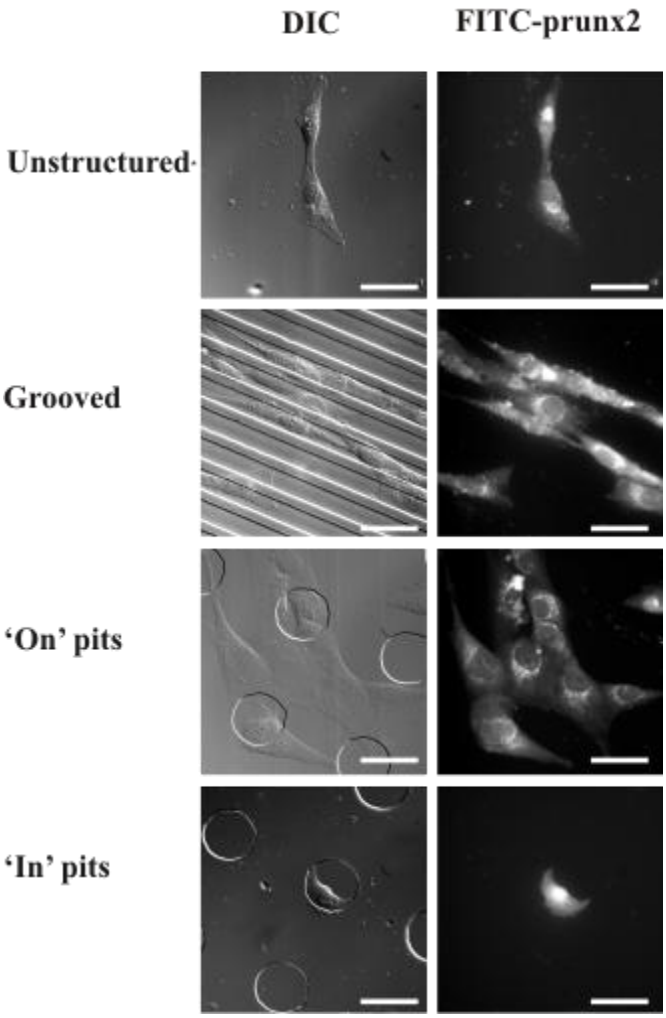

Figure 34: Immunofluorescence and DIC images of phosphorylated runx2 transcription factor on unstructured, grooved and pitted PDMS substrates after 1 day culture. The runx2 was detected using FITC. The images show an absence of fluorescence from the nuclei of all cells except those confined by pit geometry. Scale bar = 50μm.

Figure 34 shows activity of the runx2 transcription factor absent from the nuclei of cells on pits, unstructured and grooved substrates but present in most (78%) cells confined by pit geometry. Control staining experiments without the primary antibody showed normal levels of background fluorescence probably due to non-specific binding of the biotinylated secondary antibody. Statistical analysis of the images showed activity of the transcription factor present in 78% of cells confined

completely by pit geometry (IN pits), 15% of cells in contact with pits but not defined by (On pits) and 4% of cells on grooved and unstructured substrates (Table 1).

Table 1: Shows the mean pixel values of cell nuclei (N), cytoplasm (C) and background (B). Nuclear and cytoplasmic values (minus background) were divided to give the difference, <1 = nucleus is darker than surrounding cell, >1 = nucleus is brighter than surrounding cell.

Topography	N-B / C-B [<1]	N-B / C-B [>1]	Total cells	% active runx2
Flat	66	3	69	4
Grooves	52	2	54	4
On pits	35	6	41	15
IN pits	15	52	67	78
		Total cells	231	

5.4.3 Role of tension in cell differentiation

To investigate the role of tension in runx2 activation in the nuclei of cells in pits, blebbistatin was added to culture medium 45 minutes after seeding and left overnight. Blebbistatin is a small molecule which specifically inhibits the myosin head groups from binding to actin filaments – this has the effect of disabling the cytoskeleton of the cells and effectively removing tension (Limouze, Straight et al. 2004; Martens and Radmacher 2008). As Figure 35 shows, the previously observed difference in elasticity between cells 'in' and cells 'on' pits had disappeared. Both populations of cells had elasticity values comparable to those in pits (IN: 0.8895 kPa ± 0.5134, ON: 0.8289 kPa ± 0.4769). These results show that under normal culture conditions cells in pits are exhibiting levels of elasticity similar to those observed when the cytoskeleton is inhibited.

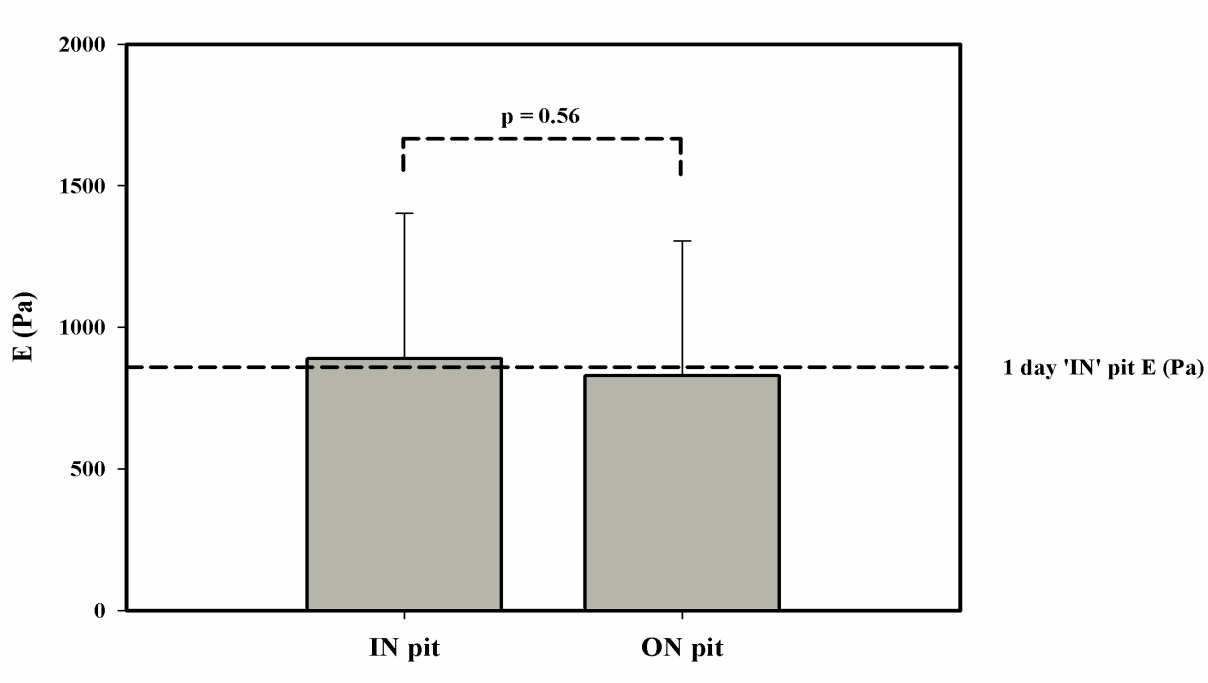

Figure 35: Shows the elasticity values recorded from cells confined by (IN) and in contact with (ON) pits after overnight culture with culture medium containing blebbistatin. The previous significant difference between the two groups has disappeared. Reference line shows elasticity values of cells defined by pits after 1 day culture without blebbistatin. Error bars show 1 standard deviation from the mean value.

5.4.4 Disruption of cytoskeletal tension

When runx2 staining was repeated on cells confined by pits cultured overnight with blebbistatin, no activity was observed in any cell nuclei (Figure 36). This lack of activation suggested that tension is required for activation of runx2.

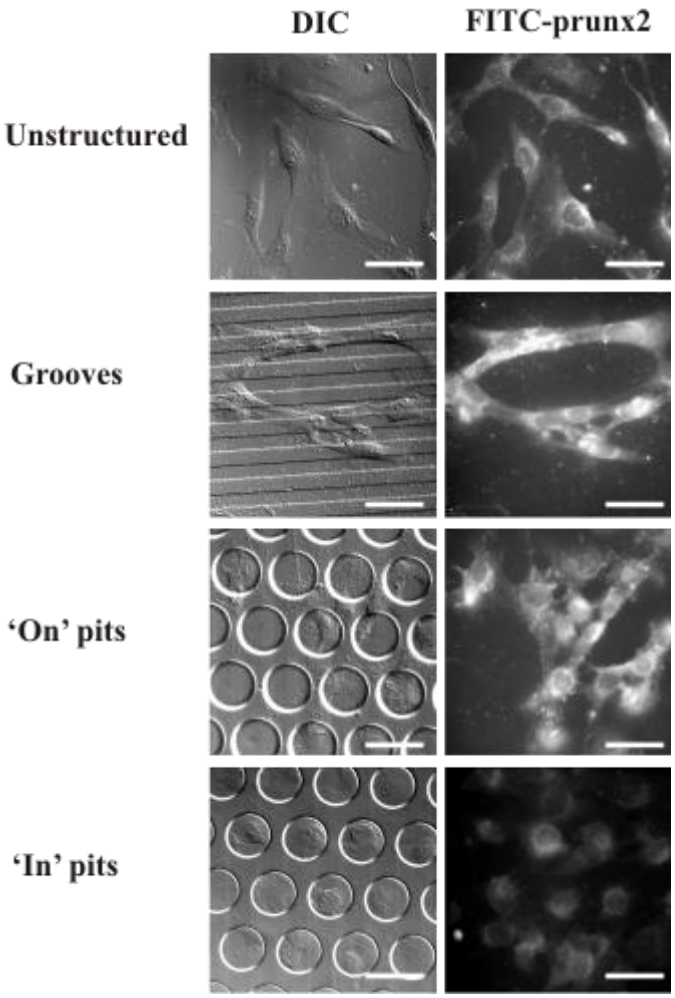

Figure 36: Immunofluorescence and DIC images of phospho-runx2 location in MG63 cells cultured overnight in the presence of blebbistatin. The lack of fluorescence in the nuclei of the cells indicates the absence of phosphorylated runx2. Scale bar = 50μm.

5.4.5 Location of tension within the cell

To further understand how tension plays a role in cell differentiation, immunostaining for the formation of phosphorylated myosin II structures within the cytoplasm of a cell was carried out on MG63 cells cultured overnight on all topographies (Figure 37). The actin-myosin relationship is a key mechanism of tension within a cell cytoskeleton and thus, when interacting with actin the myosin is in its active phosphorylated state. Therefore, staining for phospho-myosin is a way of visualizing the structure and orientation of tensile filaments within the cell.

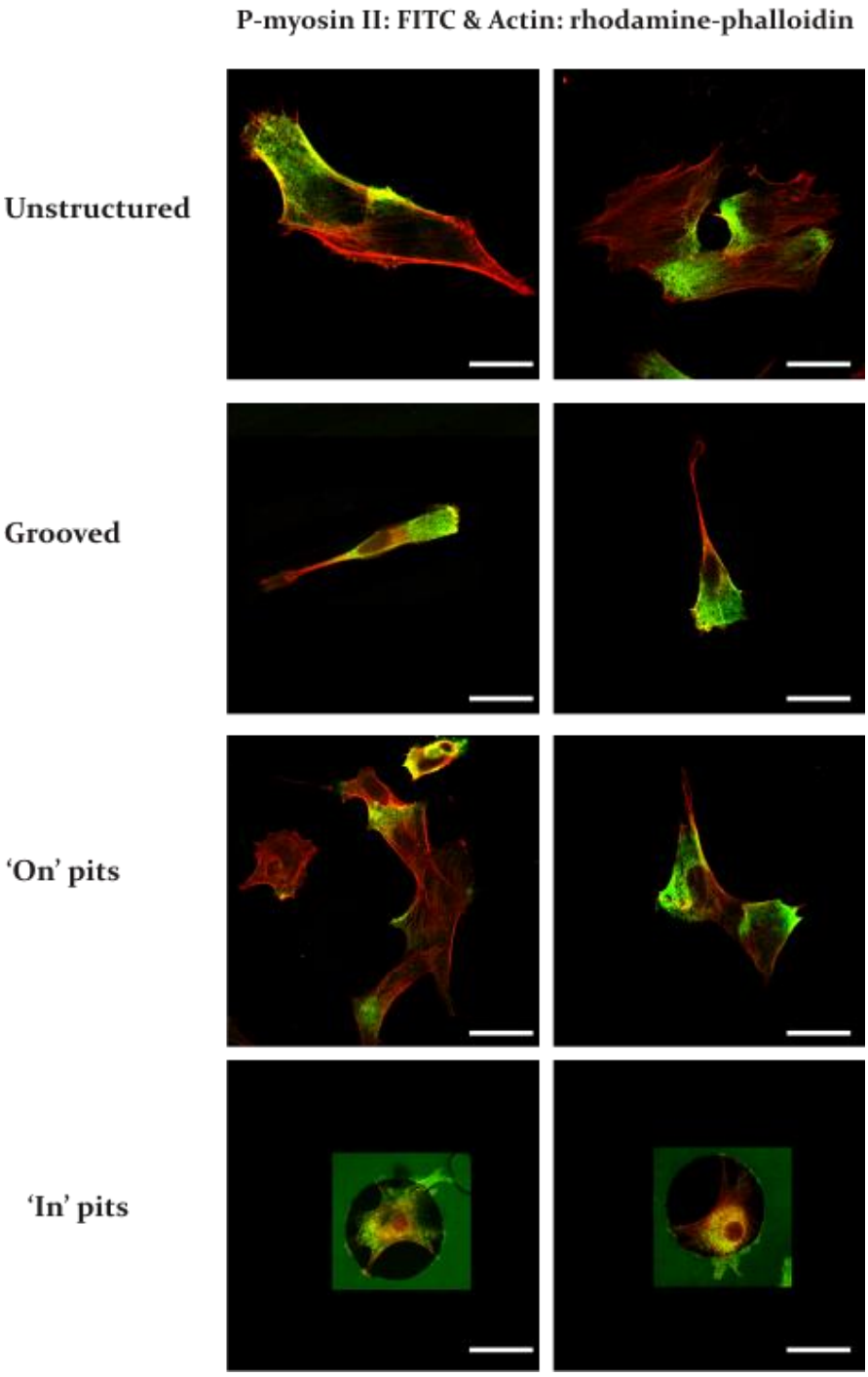

Figure 37: Immunofluorescence images showing phosphorylated myosin II (green) and filamentous actin (red) in MG63 cells cultured overnight on unstructured, grooved and pitted PDMS substrates. Co-localisation of the two proteins appears yellow. With the exception of cells 'in' pits, p-myosin appears to localise at one edge of a cell. Cells 'in' pits show a more general clustering of p-myosin around the nucleus and is noticeably absent from cell edges in the examples shown above. Scale bar = 40μm.

However, as is shown in Figure 37, phosphorylated myosin II structures do not present themselves as filaments, instead what we observed were granular clusters of phospho-myosin with no obvious directional motivation. This enabled us to look for differences in the location of the tensile regions within cells on the different topographies but not the direction of the tensile filaments.

Initial observations of stained cells show a tendency for those on flat or grooved surfaces to have co-localisation of phospho-myosin and actin in one location around the periphery of the cell. It was hypothesised that this would be the leading edge of the cell however no definitive investigations were carried out to confirm this. Examples of this co-localisation are also seen in cells designated as 'on pits' as can be seen in Figure 37, again we believe this to be the leading edge of these cells as they either move in to or away from a surface feature. This observation is in agreement with elasticity results shown in Figure 33 where it is shown that cells 'on' pits, grooves or unstructured surfaces show similar elasticity values.

Initial observation of cells designated as 'in' pits appears to show co-localisation not at a defined point on the cell periphery but in a general cloud formation around the nucleus (Figure 37: 'In pits'). We believe this apparent difference in the co-localisation of phospho-myosin and actin correlates with the reduced elasticity observed with the AFM (Figure 33) and could be a contributory factor to the differences in RUNX2 transcription seen in Figure 34 and Table 1.

Looking at the actin stress fibre orientation alone gives us some additional insight in to the possible role tension patterns could play. Clear differences exist between the structures present in cells that have managed to spread on the substrate and those confined by pit geometry. Few examples of long filamentous fibres were observed in cells confined by pits compared to those on grooves or unstructured PDMS; this is in agreement with elasticity data presented in Figure 33. Filamentous actin was observed around the cell edge under all conditions however it was not always possible to identify fibres directly orientated from here toward the nuclear region.

5.5 Discussion

The results observed in this work corroborate the hypothesis that cell morphology, passively influenced by topography, can induce gene transcription changes within a cell by means of tension, although we were unable to ascertain how the orientation of tensile filaments could be involved. Observations of filamentous actin orientation allowed us some insight in to the role of tensile filaments on transcription however not enough evidence was existed to draw a significant conclusion. Tension can be transmitted via various components of the cytoskeleton such as actin & microtubule filaments from the outer membrane and ECM to the nucleus. The forces acting upon the nuclear membrane could induce positional transformations on the chromatin in the nucleus, in turn influencing the likelihood of particular genes being transcribed (Maniotis, Bojanowski et al. 1997; Maniotis, Chen et al. 1997; Dalby, Biggs et al. 2007; Dalby, Gadegaard et al. 2007). That cell morphology, function and viability can all be influenced by microtopography of suitable scales is well known and many examples exist in the literature, (Clark, Connolly et al. 1990; Chen, Mrksich et al. 1997; Chen, Mrksich et al. 1998; Lam, Clem et al. 2008), but it is clear that this is just the first phase of a more complicated series of steps leading to eventual fate or phenotype changes in cells.

It is known that cell elasticity is a function of the strength and structure of the cytoskeleton and in particular the actin network – which provides cells with a strong scaffolding against which force can be applied in order to manipulate cell morphology and produce movement (Laevsky and Knecht 2003). When topography is employed to alter cell morphology, the cytoskeletal architecture is also modified, resulting in elasticity changes (Figure 33).

The MG-63 osteoblast-like cells used in this study are a transformed cell line that can be stimulated to exhibit behaviour of mature osteoblasts. Typically, this stimulation takes the form of secreted hormones (Kraus, Deschner et al. 2011) or chemical cues (Kawano, Ariyoshi et al. 2011), but here we showed that topography alone can potentially play the same role. Interestingly, when these cells were exposed to micron-scale topographical features in the form of pits it induced a softening of the cell's overall mechanical stiffness. This result is in contrast to that detailed in section 4.4.2 'Does microtopographic structure affect cell elasticity both

in the short term and long term?' where it was shown that 3T3 cells exhibit a stiffening of their cytoskeleton in response to grooved topographical features. This contrast in response to topography, we hypothesis, could be attributed to several key differences between the experiments. Firstly, it is possible that these two cell lines (MG63 & 3T3) respond differently to topography due to each having a cell type specific proteome, thus enabling them to react according to type when faced with environmental cues (Clark, Connolly et al. 1990; Lewandowska, Pergament et al. 1992; Stevens and George 2005). It is also possible that the difference in response is due to the difference in topographical feature; pits vs. grooves. This chapter discusses the possibility that the location of focal adhesions throughout the cell is involved in gene transcription patterns and therefore cell behaviour; it therefore follows that topographical variations could result in different focal adhesion positioning and therefore induce various responses from cells (Boyan, Hummert et al. 1996).

Little evidence exists in the literature suggesting topography can induce such a response in MG-63 cells, owing partly to them being a transformed cell line and therefore less common in differentiation experiments. However A. Mata *et al* observed such behaviour with human mesenchymal stem cells (hMSCs),(Alvaro Mata 2009). Increased osteogenic differentiation was recorded when culturing hMSCs in 40µm holes constructed from randomly orientated nano fibres (Alvaro Mata 2009). While hMSCs and MG-63 cells are significantly different, it is thought that topography offers a constant stimulus that transcends cell state and continues to induce osteoblastic differentiation in cells at all stages of the lineage. 12.5µm grooves were chosen as the comparison topography because they are significantly different from the pits and therefore more likely to induce a recordable difference. They are also well characterised and have been used in this field of research since the 1960's (Curtis and Varde 1964). They are also simple to fabricate(Curtis and Wilkinson 1997) and have been shown to induce differentiation along a completely different lineage to the MG63 cells in other cell types (Dalby, Riehle et al. 2003). Evidence for this is seen in Figure 34 where activity of the osteogenic transcription factor RUNX2 is seen to be significantly increased in cells confined by pit geometry. This is in contrast to those cells cultured on grooved PDMS and those on

unstructured flat PDMS. We hypothesise that the constant contact with curved edges is producing a specific pattern of focal adhesions which are interpreted by cell mechanosensitive receptors and translated in to chromatin changes, resulting in transcription changes. The cells on other topographies are not exposed to the same patterns and so do not adhere in the same way. Evidence for this comes from those cells on pits but not fully confined by them, aka 'on' pit cells as shown in Figure 34. Here, although the cell can be seen spreading over the structure its morphology appears to remain unaffected. It is unsurprising then, that the elasticity values of these cells are similar to those found in cells cultured on unstructured PDMS (Figure 33).

Evidence supporting the hypothesis that tension is essential to the activation of differentiation pathways is seen in Figure 35 and Figure 36. Figure 35 shows that in the presence of blebbistatin the Young's modulus of cells can be drastically softened. In the case of the cells in contact with pits we see a drop from 1.8655 ± 0.5028 kPa to 0.8289 ± 0.4769 kPa however for cells confined by pits there is little change (0.8621 ± 0.2836 kPa to 0.8895 ± 0.5134 kPa respectively) indicating that pit geometry encourages soft cytoskeletons. Figure 36 shows that although Young's modulus values had been reduced to similar levels as those observed for cells confined by pits, there was no evidence of activated RUNX2 in the nuclei of any cells regardless of their location 'in' a pit or 'on' a pit. This result highlighted the need to further investigate the tension within the cell cytoskeleton. In order to do this we stained for phosphorylated myosin II hoping to visualize where it comes in to contact with actin filaments of the cell (Figure 37). This enabled us to locate areas of increased tension within cells on various topographies and attempt to identify similarities between groups. It was thought that these differing tension profiles created by the topographical features would increase our knowledge of the intervening steps between morphological change and transcriptional changes. Although we were unable to resolve the filamentous structure of the phosphorylated myosin II – actin network despite numerous and thorough repeats of the experiment, we were able to correlate differences in the co-localisation of phospho-myosin and actin with elasticity values and phospho-RUNX2 levels. Due to this result we have been able to implicate patterns of tension in directing cell fate and

function. It is also well documented that substrate stiffness contributes greatly to cell differentiation. Engler *et al (Engler, Sen et al. 2006)* demonstrated that stiff substrates will induce differentiation down the osteoblastic lineage while soft substrates promote neurogenic differentiation. We hypothesise that PDMS mixed at a 10:1 ration of polymer to primer results in a substrate too stiff to be manipulated by cells and thus could be considered as a possible promoter of osteogenic differentiation.

5.6 Conclusions

The work presented in this chapter has shown that topography alone can contribute to the activation of cell differentiation pathways and that tension plays a vital role in the decision to alter behaviour. We have shown the AFM to be a useful instrument for gathering structural information during the early stages of change and that the elasticity values recorded can help us understand how morphological influences can affect the cell cytoskeleton. We have shown that specific geometries can have differing effects on cell behaviour and hinted at the possibility of curved edges being key to osteogenic differentiation. We have also demonstrated the potential for MG63 cells to be used in future differentiation studies where the procurement of stem cells is not an option.

Investigations in to the apparent differences in patterns of tension observed in Figure 37 are on-going as increasing numbers of cells required to make a confident assessment of the results. To compliment this it is our future aim to co-stain MG63 cells on topographies with phospho-myosin and phospho-runx2 antibodies as this would allow us to observe directly any relationship between the two that at the moment remains as correlation.

Chapter 6: Conclusions and future work

6.1 Abstract

This chapter will discuss the main conclusions that can be drawn from the work described here; evaluating how the aims and objectives of the thesis have been dealt with and the next steps that could be taken to further the investigations.

6.2 Discussion and conclusions

The phenomenon of cellular response to the microenvironment has many contributing factors. It encompasses aspects of molecular and cellular biology, biophysics and biochemistry. As such, approaches aimed at better understanding the fundamentals within the area have to address each aspect of the relationship one at a time. In the work presented here, a systematic approach was adopted to investigate the possibility of using elasticity as an early stage indicator of cellular responses to the microenvironment.

Beginning with simple chemical modifications to glass substrates using common adhesive molecules, I utilized the AFM to extract elasticity differences between populations of single cells. Repeated elasticity measurements performed at a later time points indicated that the initial effects of chemical modifications can be transient and overcome by the local secretion of extracellular matrix by the cells themselves. This observation prompted the use of microfabricated topography in cell elasticity studies. Beginning with simple grooved structures moulded in PDMS, cell elasticity was measured at two time points similar to the previous chemical modification experiment. It was found that topography was able to maintain an influence over cellular elasticity for at least the duration of the experiment.

These observations encouraged further investigation in to topography and its potential influences over cellular elasticity. In light of the findings from a recent paper by Alvaro Mata (Alvaro Mata 2009) it was decided that the topography to be investigated would be circular pits. The reason for this was the discovery that cells cultured within the confines of the pit showed increased levels of osteogenic marker proteins. Our aim was culture MG63 osteoblast-like cells in microfabricated pits in an investigation in to the relationship between cell morphology and function.

As well as using the AFM to gather elasticity data from individual cells under various conditions, the results were complimented at each stage by routine immunostaining techniques and fluorescence microscopy. This provided us with a convincing argument for the topographical influence over cell function as it was shown in section 5.4.2: Topography induced activation of differentiation; that the initial differences in elasticity measured using the AFM could be backed-up with established molecular biological methods.

The combination of an engineered ECM, immunofluorescence staining and AFM has led to an improved understanding of how cells respond to the microenvironment. The theory introduced in chapter 5 that patterns or levels of tension present within the cytoskeleton of the cell can influence transcription within the nucleus is not new. It was the aim of this chapter to go some way to filling in missing pieces of the relationship; from force sensing focal adhesions bridging the gap between the cytoplasm and the surrounding environment to the transport of mechanical signals through the cytoskeleton to the nuclear membrane. We observed the localisation of tension within cells by staining for phosphorylated myosin II. This allowed us to relate cellular elasticity values and observed transcriptional changes to tension within the cell.

Unfortunately it was not possible to gather sufficient cell numbers as part of the phospho-myosin experiment (Figure 37). Several attempts were made however the experiment only worked on a precious few occasions. All avenues were explored to try and achieve clear images of regions of tension within the cell however none proved successful. It is my hope that should the work of this chapter continue in the near future this experiment continue to be further investigated. However, the data gathered from the cells imaged to this date appear to show that further investigation is warranted. From the examples shown in Figure 37 we can observe a clear difference in the co-localisation of phospho-myosin and actin in cells confined by pits compared to those unconfined by pits or on grooved / unstructured surfaces. In conclusion, we have demonstrated the merits of using the AFM as a versatile tool for gathering multiple forms of data from live cells. Focussing on its performance as a nanoscale indenter, we have highlighted its ability to carry out precise elasticity measurements under physiologically relevant conditions and on a variety of

biological samples with high spatial resolution. The optimisation of the method described in Chapter 3 emphasises the importance of indentation speed, force and depth and the need to tailor aspects of the protocol to the specific needs of the experiment at hand, for example; indenting on non-adherent cell lines in section 5.4.2: Topography induced activation of differentiation. The ability to complement 3D topographical information with high resolution elasticity maps will aid in the elucidation of the mechanotransduction pathway investigated here as well as many more fields of interest. The option gather this data without prior treatment of the sample such as fixing, coating and the like offers an incentive to biologists in particular concerned with the possible effects of these processes on the systems and structures under investigation.

6.2.1 Wider applications

In addition to the work pertaining to the overall aims of the project the AFM technique has been applied to a variety of wider applications as a result of numerous collaborations with groups both within the University of Glasgow and further afield.

One such application involved systematic force spectroscopy measurements on soft polyacrylamide gels in collaboration with Dr Panwong Kuntanawat from the Centre for Cell Engineering, University of Glasgow. Here, the AFM was utilized to ascertain height profiles of the gels and look for regions of varying stiffness. Polymer gels are used frequently in tissue engineering research and 3D culture scaffolds. Substrate stiffness can have significant effects on cellular processes (Janmey, Winer et al. 2009; Nemir and West 2010) and so characterisation of gel stiffness can provide researchers with useful data on which to build subsequent experiments. It can also help provide explanations for unusual or interesting cellular behaviour.

6.2.2 Limitations

There are limitations to take in to consideration however, beginning with the relationship between tip geometry and elasticity results. As can be seen in Figure 25, tip geometry can have a significant effect on the values returned by the measurement even if all other experimental conditions are kept constant. It is therefore imperative that when comparing elasticity values from the literature or from previous experiments that this be taken in to consideration. This is one explanation offered for the wide range of values published for elasticity of various cell types. In the work presented here, spherical indenters were chosen to increase the indentation footprint of the tip on the cell based on the understanding that a more representative elasticity value would be returned.

Analysing the force-distance curves produced by the AFM introduces another limiting aspect to the method, the mathematical models used to fit the measurement curves. As reported in the literature and discussed in section 1.7: Cell elasticity quantification by AFM, no model perfectly fits the physical parameters of indentation measurements. It was not the aim of this work to develop and test new models or explore the limitations of each and so the decision was taken to use the Hertz model throughout. The Hertz model comes with its own set of limitations, detailed in section 1.7, however the advantage of this model is that the limitations are well understood and so we are in a position to combat the affect they have on the data. Through an understanding of the model we have been able to change aspects of the experimental method, such as indentation depth, to produce curves that fit the model well and produce reliable results. This is an area that could benefit from further investigation by physicists keen to produce a model suited to the parameters of AFM indentation measurements.

6.3 Future work

Aspects of this work showed promise and scope for further investigation, specifically the exploitation of microfabrication technology to recreate aspects of the physical environment experienced by cells *in vivo*. Due to the scale of features present at this level of biology it takes great control and precision to fabricate features relevant to cells. Knowledge of what to incorporate, in terms of feature size and shape, can only be gathered from an in depth understanding of the extracellular matrix and experience in cell culture on various topographies. As mentioned previously, much work has been done on the effects of substrate elasticity on cell behaviour and it would be of great interest to incorporate this in to topographical variations. As such, the PDMS used in this study is not soft enough to be manipulated by cells however materials such as matrigel and collagen gels can be moulded in a similar way so as to provide the same topographical features but with a Young's modulus able to be contorted by the cells.

It would have been an advantage, had time allowed, to further investigate the effects documented in Chapter 5 using different cell types. Although MG63 cells are suitable to this kind of investigation, much could be learned from the behaviour of less terminally differentiated cells such as mesenchymal stem cells or indeed primary cells. Should the phospho-myosin experiment ever yield encouraging results it would seem obvious to attempt to recreate the phenomenon with different cell types. It would also be of interest to look at other characterisations of intracellular tension, perhaps calculating it by cell volume or height. This would give us a more comprehensive understanding of the distribution and level of tension present within cells which could compliment phospho-myosin and actin staining results.

References

A-Hassan, E., W. F. Heinz, et al. (1998). "Relative Microelastic Mapping of Living Cells by Atomic Force Microscopy." Biophys. J. **74**(3): 1564-1578.

A-Hassan, E., W. F. Heinz, et al. (1998). "Relative microelastic mapping of living cells by atomic force microscopy." Biophysical Journal **74**(3): 1564-1578.

A Mantovani J. G, A. A. D. P., A Warmack R. J, A Ferrell T. L, A Ford J. R, A Manos R. E, A Thompson J. R, A Reddick B. B, A Jacobson K. B (1990). "Scanning tunnelling microscopy of tobacco mosaic virus on evaporated and sputter-coatted palladium/gold substrates." Journal of microscopy **158**(8): 109-116.

A Rosa-Zeiser, E. W., S Hild, O Marti (1997). "The simultaneous measurement of elastic, electrostatic and adhesive properties by scanning force microscopy: pulsed-force mode operation. ." Measurement Science and Technology **8**(11).

A. Ashkin, J. M. D., J. E. Bjorkholm, and Steven Chu (1986). "Observation of a single-beam gradient force optical trap for dielectric particles." Opt. Lett. **11**: 288-290.

Allison, D. P., N. P. Mortensen, et al. (2010). "Atomic force microscopy of biological samples." Wiley Interdisciplinary Reviews: Nanomedicine and Nanobiotechnology **2**(6): 618-634.

Altschuler, S. J. and L. F. Wu (2010). "Cellular Heterogeneity: Do Differences Make a Difference?" Cell **141**(4): 559-563.

Alvaro Mata, L. H., Ramille Capito, Conrado Aparicio, Karl Henrikson, Samuel Stupp. (2009). "Micropatterning of bioactive self-assembling gels." Soft Matter **5**(6): 1228-1236.

Ando, T., T. Uchihashi, et al. (2008). "High-speed AFM and nano-visualization of biomolecular processes." Pflügers Archiv European Journal of Physiology **456**(1): 211-225.

Artmann, G. M., K. L. Sung, et al. (1997). "Micropipette aspiration of human erythrocytes induces echinocytes via membrane phospholipid translocation." Biophysical Journal **72**(3): 1434-1441.

Ashkin, A. (1970). "Acceleration and Trapping of Particles by Radiation Pressure." Physical Review Letters **24**(4): 156.

Ashkin, A. and J. Dziedzic (1987). "Optical trapping and manipulation of viruses and bacteria." Science **235**(4795): 1517-1520.

Bausch, A. R., F. Ziemann, et al. (1998). "Local Measurements of Viscoelastic Parameters of Adherent Cell Surfaces by Magnetic Bead Microrheometry." Biophys. J. **75**(4): 2038-2049.

Berdyyeva, T. K., C. D. Woodworth, et al. (2005). "Human epithelial cells increase their rigidity with ageing in vitro: direct measurements." Physics in Medicine and Biology **50**(1): 81-92.

Binnig, G., C. F. Quate, et al. (1986). "Atomic Force Microscope." Physical Review Letters **56**(9): 930.

Binnig, G. and H. Rohrer (1983). "Scanning tunneling microscopy." Surface Science **126**(1-3): 236-244.

Blanchard, C. R. (1996). "Atomic Force Microscopy." The Chemical Educator **1**(5): 1-8.

Bonewald, L. F., M. B. Kester, et al. (1992). "Effects of combining transforming growth factor beta and 1,25-dihydroxyvitamin D3 on differentiation of a human osteosarcoma (MG-63)." Journal of Biological Chemistry **267**(13): 8943-8949.

Boyan, B. D., T. W. Hummert, et al. (1996). "Role of material surfaces in regulating bone and cartilage cell response." Biomaterials **17**(2): 137-146.

Braet, F., C. Rotsch, et al. (1998). "Comparison of fixed and living liver endothelial cells by atomic force microscopy." Applied Physics A: Materials Science & Processing **66**(0): S575-S578.

Burridge, K. and M. ChrzanowskaWodnicka (1996). "Focal adhesions, contractility, and signaling." Annual Review of Cell and Developmental Biology **12**: 463-518.

Burridge, K., K. Fath, et al. (1988). "Focal Adhesions: Transmembrane Junctions Between the Extracellular Matrix and the Cytoskeleton." Annual Review of Cell Biology **4**(1): 487-525.

Butt, H. J., B. Cappella, et al. (2005). "Force measurements with the atomic force microscope: Technique, interpretation and applications." Surface Science Reports **59**(1-6): 1-152.

C.B. Prater, P. G. M., K.L. Kjoller, M.G. Heaton (2004). "TappingMode Imaging and Applications and Technology." Veeco Instruments.

Caille, N., O. Thoumine, et al. (2002). "Contribution of the nucleus to the mechanical properties of endothelial cells." Journal of Biomechanics **35**(2): 177-187.

Califano, J. P. and C. A. Reinhart-King (2009). The effects of substrate elasticity on endothelial cell network formation and traction force generation. Engineering in Medicine and Biology Society, 2009. EMBC 2009. Annual International Conference of the IEEE.

Celeste M. Nelson, M. J. B. (2006). "Of Extracellular Matrix, Scaffolds, and Signaling: Tissue Architecture Regulates Development, Homeostasis, and Cancer." Annual Review of Cell and Developmental Biology **22**: 287-309.

Chan E, U. M. (1997). "Relastionship between stiffness, internal cell pressure and shape of outer hair cells isolated from the guinea-pig hearing organ. ." Acta Physiol Scand **4**(161): 533-539.

Charest, J. L., M. T. Eliason, et al. (2006). "Combined microscale mechanical topography and chemical patterns on polymer cell culture substrates." Biomaterials **27**(11): 2487-2494.

Charras, G. T. and M. A. Horton (2002). "Single Cell Mechanotransduction and Its Modulation Analyzed by Atomic Force Microscope Indentation." Biophys. J. **82**(6): 2970-2981.

Charras, G. T., P. P. Lehenkari, et al. (2001). "Atomic force microscopy can be used to mechanically stimulate osteoblasts and evaluate cellular strain distributions." Ultramicroscopy **86**(1-2): 85-95.

Chen, C. S., J. L. Alonso, et al. (2003). "Cell shape provides global control of focal adhesion assembly." Biochemical and Biophysical Research Communications **307**(2): 355-361.

Chen, C. S., M. Mrksich, et al. (1997). "Geometric Control of Cell Life and Death." Science **276**(5317): 1425-1428.

Chen, C. S., M. Mrksich, et al. (1998). "Micropatterned Surfaces for Control of Cell Shape, Position, and Function." Biotechnology Progress **14**(3): 356-363.

Chen, W. T. (1971). "Computation of stresses and displacements in a layered elastic medium." International Journal of Engineering Science **9**(9): 775-800.

Chen, W. T. and P. A. Engel (1972). "Impact and contact stress analysis in multilayer media." International Journal of Solids and Structures **8**(11): 1257-1281.

Clark, P., P. Connolly, et al. (1990). "Topographical control of cell behaviour: II. Multiple grooved substrata." Development **108**(4): 635-644.

Clark, P., P. Connolly, et al. (1990). "Topographical control of cell behavior .2. multiple grooved substrate " Development **108**(4): 635-644.

Constant A. J. Putman, K. O. V. d. W., Bart G. De Grooth, Niek F. Van Hulst, Jan Greve (1994). "Tapping mode atomic force microscopy in liquid." Applied Physics Letters **64**(16).

Costa, K. D. and F. C. P. Yin (1999). "Analysis of indentation: Implications for measuring mechanical properties with atomic force microscopy." Journal of Biomechanical Engineering-Transactions of the Asme **121**(5): 462-471.

Cross, S. E., Y. S. Jin, et al. (2007). "Nanomechanical analysis of cells from cancer patients." Nature Nanotechnology **2**(12): 780-783.

Curtis, A. and C. Wilkinson (1997). "Topographical control of cells." Biomaterials **18**(24): 1573-1583.
Curtis, A. S. and M. Varde (1964). "CONTROL OF CELL BEHAVIOR: TOPOLOGICAL FACTORS." Journal of the National Cancer Institute **33**: 15-26.
Curtis, A. S. G. and M. Varde (1964). "Control of Cell Behavior: Topological Factors." Journal of the National Cancer Institute **33**(1): 15-26.
Curtis, A. S. G. and C. D. W. Wilkinson (1998). "Reactions of cells to topography." Journal of Biomaterials Science, Polymer Edition **9**: 1313-1329.
Dalby, M. J. (2005). "Topographically induced direct cell mechanotransduction." Medical Engineering & Physics **27**(9): 730-742.
Dalby, M. J., M. J. P. Biggs, et al. (2007). "Nanotopographical stimulation of mechanotransduction and changes in interphase centromere positioning." Journal of Cellular Biochemistry **100**(2): 326-338.
Dalby, M. J., N. Gadegaard, et al. (2007). "Nanomechanotransduction and Interphase Nuclear Organization influence on genomic control." Journal of Cellular Biochemistry **102**(5): 1234-1244.
Dalby, M. J., N. Gadegaard, et al. (2007). "The control of human mesenchymal cell differentiation using nanoscale symmetry and disorder." Nat Mater **6**(12): 997-1003.
Dalby, M. J., M. O. Riehle, et al. (2003). "Nucleus alignment and cell signaling in fibroblasts: response to a micro-grooved topography." Experimental Cell Research **284**(2): 272-280.
Darling, E. M., M. Topel, et al. (2008). "Viscoelastic properties of human mesenchymally-derived stem cells and primary osteoblasts, chondrocytes, and adipocytes." Journal of Biomechanics **41**(2): 454-464.
Darling, E. M., S. Zauscher, et al. (2007). "A Thin-Layer Model for Viscoelastic, Stress-Relaxation Testing of Cells Using Atomic Force Microscopy: Do Cell Properties Reflect Metastatic Potential?" Biophysical Journal **92**(5): 1784-1791.
Derganc, J., B. Bo~i, et al. (2000). "Stability Analysis of Micropipette Aspiration of Neutrophils." Biophysical Journal **79**(1): 153-162.
Dimitriadis, E. K., F. Horkay, et al. (2002). "Determination of Elastic Moduli of Thin Layers of Soft Material Using the Atomic Force Microscope." Biophysical Journal **82**(5): 2798-2810.
Discher, D., C. Dong, et al. (2009). "Biomechanics: Cell Research and Applications for the Next Decade." Annals of Biomedical Engineering **37**(5): 847-859.
Docheva, D., D. Padula, et al. (2008). "Researching into the cellular shape, volume and elasticity of mesenchymal stem cells, osteoblasts and osteosarcoma cells by atomic force microscopy." Journal of Cellular and Molecular Medicine **12**(2): 537-552.
Dufrêne, Y. F. (2002). "Atomic Force Microscopy, a Powerful Tool in Microbiology." Journal of Bacteriology **184**(19): 5205-5213.
Dufrene, Y. F., E. Evans, et al. (2011). "Five challenges to bringing single-molecule force spectroscopy into living cells." Nat Meth **8**(2): 123-127.
Dulinska, I., M. Targosz, et al. (2006). "Stiffness of normal and pathological erythrocytes studied by means of atomic force microscopy." Journal of Biochemical and Biophysical Methods **66**(1-3): 1-11.
Elson, E. L. (1988). "Cellular Mechanics as an Indicator of Cytoskeletal Structure and Function." Annual Review of Biophysics and Biophysical Chemistry **17**(1): 397-430.
Engler, A. J., C. Carag-Krieger, et al. (2008). "Embryonic cardiomyocytes beat best on a matrix with heart-like elasticity: scar-like rigidity inhibits beating." Journal of Cell Science **121**(22): 3794-3802.
Engler, A. J., S. Sen, et al. (2006). "Matrix elasticity directs stem cell lineage specification." Cell **126**(4): 677-689.
Erickson, H. P., N. Carrell, et al. (1981). "Fibronectin molecule visualized in electron microscopy: a long, thin, flexible strand." The Journal of Cell Biology **91**(3): 673-678.

Ezzell, R. M., W. H. Goldmann, et al. (1997). "Vinculin Promotes Cell Spreading by Mechanically Coupling Integrins to the Cytoskeleton." Experimental Cell Research **231**(1): 14-26.

Fabry, B., G. N. Maksym, et al. (2001). "Signal transduction in smooth muscle - Selected contribution: Time course and heterogeneity of contractile responses in cultured human airway smooth muscle cells." Journal of Applied Physiology **91**(2): 986-994.

Faria, E. C., N. Ma, et al. (2008). "Measurement of elastic properties of prostate cancer cells using AFM." Analyst **133**(11): 1498-1500.

Faulstich, H., H. Trischmann, et al. (1983). "Preparation of Tetramethylrhodaminyl-Phalloidin and Uptake of the Toxin into Short-Term Cultured-Hepatocytes by Endocytosis." Experimental Cell Research **144**(1): 73-82.

Feneberg, W., M. Aepfelbacher, et al. (2004). "Microviscoelasticity of the Apical Cell Surface of Human Umbilical Vein Endothelial Cells (HUVEC) within Confluent Monolayers." Biophys. J. **87**(2): 1338-1350.

Fletcher, D. A. and R. D. Mullins (2010). "Cell mechanics and the cytoskeleton." Nature **463**(7280): 485-492.

Florian Rehfeldt, A. J. E., Adam Eckhardt, Fariyal Ahmed, Dennis Discher (2007). "Cell responses to the mechanochemical microenvironment - implications for regenerative medicine and drug delivery." Advanced Drug Delivery Reviews **59**(13): 1329-1339.

Folch, A. and M. Toner (2000). "Microengineering of cellular interactions." Annual Review of Biomedical Engineering **2**: 227-+.

French, S. A., J. A. Fulkerson, et al. (2000). "Increasing Weight-Bearing Physical Activity and Calcium Intake for Bone Mass Growth in Children and Adolescents: A Review of Intervention Trials." Preventive Medicine **31**(6): 722-731.

Gadegaard, N., S. Thoms, et al. (2003). "Arrays of nano-dots for cellular engineering." Microelectronic Engineering **67–68**(0): 162-168.

Galajda, P. (2002). "Rotors produced and driven in laser tweezers with reversed direction of rotation." Appl. Phys. Lett. **80**(24): 4653.

Geiger, B., A. Bershadsky, et al. (2001). "Transmembrane crosstalk between the extracellular matrix and the cytoskeleton." Nat Rev Mol Cell Biol **2**(11): 793-805.

Geiger, B., J. P. Spatz, et al. (2009). "Environmental sensing through focal adhesions." Nat Rev Mol Cell Biol **10**(1): 21-33.

Gernot Friedbacher, H. F. (1999). "Classification of Scanning Probe Microscopies." International Union of Pure and Applied Chemistry **71**(7): 1337-1357.

Gimbrone, M. A., N. Resnick, et al. (1997). "Hemodynamics, Endothelial Gene Expression, and Atherogenesisa." Annals of the New York Academy of Sciences **811**(1): 1-11.

González-Cruz, R. D., V. C. Fonseca, et al. (2012). "Cellular mechanical properties reflect the differentiation potential of adipose-derived mesenchymal stem cells." Proceedings of the National Academy of Sciences.

Guck, J., S. Schinkinger, et al. (2005). "Optical deformability as an inherent cell marker for testing malignant transformation and metastatic competence." Biophysical Journal **88**(5): 3689-3698.

Guilak, F., D. M. Cohen, et al. (2009). "Control of Stem Cell Fate by Physical Interactions with the Extracellular Matrix." Cell Stem Cell **5**(1): 17-26.

Guilak, F., J. R. Tedrow, et al. (2000). "Viscoelastic Properties of the Cell Nucleus." Biochemical and Biophysical Research Communications **269**(3): 781-786.

Guo, L. J. (2007). "Nanoimprint Lithography: Methods and Material Requirements." Advanced Materials.

Gusnard, D. and R. H. Kirschner (1977). "Cell and organelle shrinkage during preparation for scanning electron microscopy: effects of fixation, dehydration and critical point drying." Journal of microscopy **110**(1): 51-57.

Haga, H., S. Sasaki, et al. (2000). "Elasticity mapping of living fibroblasts by AFM and immunofluorescence observation of the cytoskeleton." Ultramicroscopy **82**(1-4): 253-258.

Hansma, P. K., B. Drake, et al. (1989). "The scanning ion-conductance microscope." Science **243**(4891): 641-643.

Ho, H. and P. West (1996). "Optimizing AC-mode atomic force microscope imaging." Scanning **18**(5): 339-343.

Hochmuth, R. M. (2000). "Micropipette aspiration of living cells." Journal of Biomechanics **33**(1): 15-22.

Houchmandzadeh, B. and S. Dimitrov (1999). "Elasticity Measurements Show the Existence of Thin Rigid Cores Inside Mitotic Chromosomes." The Journal of Cell Biology **145**(2): 215-223.

Huang, H., R. D. Kamm, et al. (2004). "Cell mechanics and mechanotransduction: pathways, probes, and physiology." American Journal of Physiology - Cell Physiology **287**(1): C1-C11.

Humphries, J. D., A. Byron, et al. (2006). "Integrin ligands at a glance." Journal of Cell Science **119**(19): 3901-3903.

Icard-Arcizet, D., O. Cardoso, et al. (2008). "Cell Stiffening in Response to External Stress is Correlated to Actin Recruitment." Biophys. J. **94**(7): 2906-2913.

Ingber, D. E., L. Dike, et al. (1994). Celluar tensegrity - exploring how mechanical changes in the cytoskeleton regulate cell - growth, migration, and tissue pattern during morphogenesis International Review of Cytology - a Survey of Cell Biology, Vol 150. San Diego, Academic Press Inc. **150:** 173-224.

Innovations, W. F. (2001). Pulsed Force Mode Applications: Race Car Tires. Pulsed Force Mode Applications, WITec Wissenschaftliche Instruments und Technologie.

Janmey, P. A. (1998). "The cytoskeleton and cell signaling: Component localization and mechanical coupling." Physiological Reviews **78**(3): 763-781.

Janmey, P. A. and C. A. McCulloch (2007). "Cell mechanics: Integrating cell responses to mechanical stimuli." Annual Review of Biomedical Engineering **9**: 1-34.

Janmey, P. A., J. P. Winer, et al. (2009). "The hard life of soft cells." Cell Motility and the Cytoskeleton **66**(8): 597-605.

Jaschke, H. J. B. a. M. (1995). "Calculation of thermal noise in atomic force microscopy." Nanotechnology **6**(1).

K. L. Johnson, K. K., A. D. Roberts (1971). "Surface Energy and the Contact of Elastic Solids." Proceedings of the Royal Society of London. Series A, Mathematical and Physical Sciences **324**(1558): 301-313.

Karl A. Piez, A. H. R., Ed. (1984). Extracellular Matrix Biochemistry, Elsevier.

Kawano, M., W. Ariyoshi, et al. (2011). "Mechanism involved in enhancement of osteoblast differentiation by hyaluronic acid." Biochemical and Biophysical Research Communications **405**(4): 575-580.

Kilian, K. A., B. Bugarija, et al. (2010). "Geometric cues for directing the differentiation of mesenchymal stem cells." Proceedings of the National Academy of Sciences **107**(11): 4872-4877.

Kim, J., M. Shen, et al. (2012). "Stabilizing Nanometer Scale Tip-to-Substrate Gaps in Scanning Electrochemical Microscopy Using an Isothermal Chamber for Thermal Drift Suppression." Analytical Chemistry **84**(8): 3489-3492.

Kodera, N., D. Yamamoto, et al. (2010). "Video imaging of walking myosin V by high-speed atomic force microscopy." Nature **468**(7320): 72-76.

Kollmannsberger, P. and B. Fabry (2007). "High-force magnetic tweezers with force feedback for biological applications." Review of Scientific Instruments **78**(11): 114301-114306.

Korchev, Y. E., M. Raval, et al. (2000). "Hybrid Scanning Ion Conductance and Scanning Near-Field Optical Microscopy for the Study of Living Cells." Biophys. J. **78**(5): 2675-2679.

Kramer, R. H., X. D. Shen, et al. (2005). "Tumor cell invasion and survival in head and neck cancer." Cancer and Metastasis Reviews **24**(1): 35-45.

Kraus, D., J. Deschner, et al. (2011). "Human β-defensins differently affect proliferation, differentiation, and mineralization of osteoblast-like MG63 cells." Journal of Cellular Physiology: n/a-n/a.

Kris Noel Dahl, S. M. K., Katherine L Wilson and Dennis E Discher (2004). "The nuclear envelope lamina network has elasticity and compressibility limit suggestive of a molecular shock absorber " Journal of Cell Science **117**: 4779-4786.

Kuhn, J. R. and T. D. Pollard (2005). "Real-Time Measurements of Actin Filament Polymerization by Total Internal Reflection Fluorescence Microscopy." Biophysical Journal **88**(2): 1387-1402.

Kumar, S. and V. Weaver (2009). "Mechanics, malignancy, and metastasis: The force journey of a tumor cell." Cancer and Metastasis Reviews **28**(1): 113-127.

Kuznetsova, T. G., M. N. Starodubtseva, et al. (2007). "Atomic force microscopy probing of cell elasticity." Micron **38**(8): 824-833.

Laevsky, G. and D. A. Knecht (2003). "Cross-linking of actin filaments by myosin II is a major contributor to cortical integrity and cell motility in restrictive environments." Journal of Cell Science **116**(18): 3761-3770.

Lam, M. T., W. C. Clem, et al. (2008). "Reversible on-demand cell alignment using reconfigurable microtopography." Biomaterials **29**(11): 1705-1712.

Le Grimellec, C., E. Lesniewska, et al. (1998). "Imaging of the Surface of Living Cells by Low-Force Contact-Mode Atomic Force Microscopy." Biophysical Journal **75**(2): 695-703.

Lee YJ, P. D., Park S (2011). "Local Rheology of Human Neutrophils Investigated Uding Atomic Force Microscopy." International Journal of Biological Sciences **1**(7): 102-111.

Lewandowska, K., E. Pergament, et al. (1992). "Cell-Type-Specific adhesion mechanisms mediated by fibronectin adsorbed to chemically derivatized substrata." Journal of Biomedical Materials Research **26**(10): 1343-1363.

Li, Q. S., G. Y. H. Lee, et al. (2008). "AFM indentation study of breast cancer cells." Biochemical and Biophysical Research Communications **374**(4): 609-613.

Lieber, S. C., N. Aubry, et al. (2004). "Aging increases stiffness of cardiac myocytes measured by atomic force microscopy nanoindentation." American Journal of Physiology-Heart and Circulatory Physiology **287**(2): H645-H651.

Limouze, J., A. Straight, et al. (2004). "Specificity of blebbistatin, an inhibitor of myosin II." Journal of Muscle Research and Cell Motility **25**(4): 337-341.

Lin, B. J. (1975). "Deep UV lithography." Journal of Vacuum Science and Technology **12**(6): 1317-1320.

Lin, D. C., E. K. Dmitriadis, et al. (2007). "Robust strategies for automated AFM force curve Analysis-II: Adhesion-influenced indentation of soft, elastic materials." Journal of Biomechanical Engineering-Transactions of the Asme **129**(6): 904-912.

Lincks, J., B. D. Boyan, et al. (1998). "Response of MG63 osteoblast-like cells to titanium and titanium alloy is dependent on surface roughness and composition." Biomaterials **19**(23): 2219-2232.

Lindsay SM, T. T., Nagahara L, Knipping U, Rill, RL (1989). "Images of the DNA double helix in water." Science **244**: 1063-1064.

Luca Cardamone, A. L., Vincent Torre, Rajesh Shahapure, Antioio DeSimone (2011). "Cytoskeletal action networks in motile cells are critically self-organized ystems synchronized by mechanical interactions." Proceedings of the National Academy of Sciences **34**(108): 13978-13983.

Lussi, J. W., D. Falconnet, et al. (2006). "Pattern stability under cell culture conditions - A comparative study of patterning methods based on PLL-g-PEG background passivation." Biomaterials **27**(12): 2534-2541.

M. Loferer-KroBbacher, J. K. a. R. P. (1998). "Determination of Bacterial Cell Dry Mass by Transmission Electron Microscopy and Densitometric Image Analysis." Applied Environmental Microbiology **2**(64).

Macintyre, D. S. and S. Thoms (2006). "Nanometre scale overlay and stitch metrology using an optical microscope." Microelectronic Engineering **83**(4–9): 1051-1054.

Mahaffy, R. E. (2000). "Scanning Probe-Based Frequency-Dependent Microrheology of Polymer Gels

and Biological Cells." Physical Review Letters **85**(4).

Mahaffy, R. E., S. Park, et al. (2004). "Quantitative Analysis of the Viscoelastic Properties of Thin Regions of Fibroblasts Using Atomic Force Microscopy." Biophysical Journal **86**(3): 1777-1793.

Maniotis, A. J., K. Bojanowski, et al. (1997). "Mechanical continuity and reversible chromosome disassembly within intact genomes removed from living cells." Journal of Cellular Biochemistry **65**(1): 114-130.

Maniotis, A. J., C. S. Chen, et al. (1997). "Demonstration of mechanical connections between integrins, cytoskeletal filaments, and nucleoplasm that stabilize nuclearâ€‰structure." Proceedings of the National Academy of Sciences of the United States of America **94**(3): 849-854.

Maniotis, A. J., K. Valyi-Nagy, et al. (2005). "Chromatin Organization Measured by AluI Restriction Enzyme Changes with Malignancy and Is Regulated by the Extracellular Matrix and the Cytoskeleton." The American Journal of Pathology **166**(4): 1187-1203.

Marenzana, M., N. Wilson-Jones, et al. (2006). "The origins and regulation of tissue tension: Identification of collagen tension-fixation process in vitro." Experimental Cell Research **312**(4): 423-433.

Margetson, J. (1970). "The indentation of elastic and viscoelastic strips by rigid or elastic cylinders." Zeitschrift für Angewandte Mathematik und Physik (ZAMP) **21**(6): 1040-1052.

Marquez, J. P., E. L. Elson, et al. (2010). "Whole cell mechanics of contractile fibroblasts: relations between effective cellular and extracellular matrix moduli." Philosophical Transactions of the Royal Society A: Mathematical, Physical and Engineering Sciences **368**(1912): 635-654.

Martens, J. and M. Radmacher (2008). "Softening of the actin cytoskeleton by inhibition of myosin II." Pflügers Archiv European Journal of Physiology **456**(1): 95-100.

Martin, J. Y., Z. Schwartz, et al. (1995). "Effect of titanium surface roughness on proliferation, differentiation, and protein synthesis of human osteoblast-like cells (MG63)." Journal of Biomedical Materials Research **29**(3): 389-401.

Mathur, A. B., A. M. Collinsworth, et al. (2001). "Endothelial, cardiac muscle and skeletal muscle exhibit different viscous and elastic properties as determined by atomic force microscopy." Journal of Biomechanics **34**(12): 1545-1553.

McBeath, R., D. M. Pirone, et al. (2004). "Cell Shape, Cytoskeletal Tension, and RhoA Regulate Stem Cell Lineage Commitment." Developmental Cell **6**(4): 483-495.

McCann, M. M. (2004). Nanoindentation of Gold Single Crystals. Materials Science and Engineering. Blacksburg, Virginia Virginia Polytechnic Institure and State University. **Doctor of Philosophy**

McMurray, R. J., N. Gadegaard, et al. (2011). "Nanoscale surfaces for the long-term maintenance of mesenchymal stem cell phenotype and multipotency." Nat Mater **10**(8): 637-644.

McPhee, G., M. Dalby, et al. (2010). "Can common adhesion molecules and microtopography affect cellular elasticity? A combined atomic force microscopy and optical study." Medical and Biological Engineering and Computing: 1-11.
Mitchison, J. M. and M. M. Swann (1954). "The Mechanical Properties of the Cell Surface: I. The Cell Elastimeter." J Exp Biol **31**(3): 443-460.
Moffitt, J. R., Y. R. Chemla, et al. (2008). "Recent Advances in Optical Tweezers." Annual Review of Biochemistry **77**(1): 205-228.
Moffitt, J. R., Y. R. Chemla, et al. (2008). "Recent advances in optical tweezers." Annual Review of Biochemistry **77**: 205-228.
Mueller, M. J. and K. S. Maluf (2002). "Tissue Adaptation to Physical Stress: A Proposed "Physical Stress Theory" to Guide Physical Therapist Practice, Education, and Research." Physical Therapy **82**(4): 383-403.
Munter, S., J. Enninga, et al. (2006). "Actin polymerisation at the cytoplasmic face of eukaryotic nuclei." BMC Cell Biology **7**(1): 23.
Neil Barclay, A. (1999). "Concluding remarks and the challenge from the immune system." Faraday Discussions **111**: 345-350.
Nemir, S. and J. West (2010). "Synthetic Materials in the Study of Cell Response to Substrate Rigidity." Annals of Biomedical Engineering **38**(1): 2-20.
Neumann, T. (2011). Determining the elastic modulus of biological samples using atomic force microscopy. JPK Application Reports. Berlin, JPK Instruments**:** 9.
Okabe, Y., M. Furugori, et al. (2000). "Chemical force microscopy of microcontact-printed self-assembled monolayers by pulsed-force-mode atomic force microscopy." Ultramicroscopy **82**(1–4): 203-212.
Owen, J. D., P. J. Ruest, et al. (1999). "Induced Focal Adhesion Kinase (FAK) Expression in FAK-Null Cells Enhances Cell Spreading and Migration Requiring Both Auto- and Activation Loop Phosphorylation Sites and Inhibits Adhesion-Dependent Tyrosine Phosphorylation of Pyk2." Mol. Cell. Biol. **19**(7): 4806-4818.
Owen, T. A., M. Aronow, et al. (1990). "Progressive development of the rat osteoblast phenotype in vitro: Reciprocal relationships in expression of genes associated with osteoblast proliferation and differentiation during formation of the bone extracellular matrix." Journal of Cellular Physiology **143**(3): 420-430.
Pajerowski, J. D., K. N. Dahl, et al. (2007). "Physical plasticity of the nucleus in stem cell differentiation." Proceedings of the National Academy of Sciences of the United States of America **104**(40): 15619-15624.
Park, S., D. Koch, et al. (2005, December 1, 2005). "Cell Motility and Local Viscoelasticity of Fibroblasts." Biophys. J. Retrieved 6, 89, from http://www.biophysj.org/cgi/content/abstract/89/6/4330.
Parker, K. K., A. L. Brock, et al. (2002). "Directional control of lamellipodia extension by constraining cell shape and orienting cell tractional forces." Faseb Journal **16**(10): 10.
Paszek, M. J., N. Zahir, et al. (2005). "Tensional homeostasis and the malignant phenotype." Cancer Cell **8**(3): 241-254.
Patel, A., R. Thakar, et al. (2010). "Biophysical mechanisms of single-cell interactions with microtopographical cues." Biomedical Microdevices **12**(2): 287-296.
Pellettieri, J. and A. S. Alvarado (2007). "Cell Turnover and Adult Tissue Homeostasis: From Humans to Planarians." Annual Review of Genetics **41**(1): 83-105.
Peter Eaton, P. W. (2010). Atomic Force Microscopy, Oxford University Press.
Popov, G. I. (1962). "The contact problem of the theory of elasticity for the case of a circular area of contact." Journal of Applied Mathematics and Mechanics **26**(1): 207-225.
Putman, C. A. J. C. A. J. (1994). "Tapping mode atomic force microscopy in liquid." Applied Physics Letters **64**: 2454-2456.
Rand, R. P. and A. C. Burton (1964). "Mechanical Properties of the Red Cell Membrane: I. Membrane Stiffness and Intracellular Pressure." Biophys. J. **4**(2): 115-135.

Revenko, I., F. Sommer, et al. (1994). "Atomic force microscopy study of the collagen fibre structure." Biology of the Cell **80**(1): 67-69.
Richter, C., M. Reinhardt, et al. (2010). "Spatially controlled cell adhesion on three-dimensional substrates." Biomedical Microdevices **12**(5): 787-795.
Rosenbluth, M. J., W. A. Lam, et al. (2006). "Force microscopy of nonadherent cells: A comparison of leukemia cell deformability." Biophysical Journal **90**(8): 2994-3003.
Rotsch, C., K. Jacobson, et al. (1999). "Dimensional and mechanical dynamics of active and stable edges in motile fibroblasts investigated by using atomic force microscopy." Proceedings of the National Academy of Sciences **96**(3): 921-926.
Rotsch, C. and M. Radmacher (2000). "Drug-induced changes of cytoskeletal structure and mechanics in fibroblasts: An atomic force microscopy study." Biophysical Journal **78**(1): 520-535.
Sader, J. E. (2003). "Susceptibility of atomic force microscope cantilevers to lateral forces." Review of Scientific Instruments **74**(4).
Sam Walcott, S. X. S. (2010). "A mechanical model of actin stress fiber formation and substrate elasticity sensing in adherent cells." Proceedings of the National Academy of Sciences **17**(107): 7757-7762.
Sánchez, D., U. Anand, et al. (2007). "Localized and non-contact mechanical stimulation of dorsal root ganglion sensory neurons using scanning ion conductance microscopy." Journal of Neuroscience Methods **159**(1): 26-34.
Sanchez, D., N. Johnson, et al. (2008). "Noncontact Measurement of the Local Mechanical Properties of Living Cells Using Pressure Applied via a Pipette." Biophys. J. **95**(6): 3017-3027.
Schift, H. (2008). "Nanoimprint lithography: An old story in modern times? A review." J. Vac. Sci. Technol. B **26**(2): 458.
Schroeder, T. M., E. D. Jensen, et al. (2005). "Runx2: A master organizer of gene transcription in developing and maturing osteoblasts." Birth Defects Research Part C: Embryo Today: Reviews **75**(3): 213-225.
Schulze, C., K. Müller, et al. (2009). "Compaction of cell shape occurs before decrease of elasticity in CHO-K1 cells treated with actin cytoskeleton disrupting drug cytochalasin D." Cell Motility and the Cytoskeleton **66**(4): 193-201.
Seo, Y. and W. Jhe (2008). "Atomic force microscopy and spectroscopy." Reports on Progress in Physics **71**(1): 016101.
Shaw, J. E., R. F. Epand, et al. (2006). "Correlated Fluorescence-Atomic Force Microscopy of Membrane Domains: Structure of Fluorescence Probes Determines Lipid Localization." Biophysical Journal **90**(6): 2170-2178.
Shemesh, T., A. B. Verkhovsky, et al. (2009). "Role of Focal Adhesions and Mechanical Stresses in the Formation and Progression of the Lamellum Interface." Biophysical Journal **97**(5): 1254-1264.
Shigeru Amemiya, A. J. B., Fu-Ren F Fan, Michael V Mirkin, Patrick R Unwin (2008). "Scanning Electrochemical Micoscopy." Annual Review of Analytical Chemistry **1**: 95-131.
Shin, D. and K. Athanasiou (1999). "Cytoindentation for obtaining cell biomechanical properties." Journal of Orthopaedic Research **17**(6): 880-890.
Simon, A., T. Cohen-Bouhacina, et al. (2003). "Characterization of dynamic cellular adhesion of osteoblasts using atomic force microscopy." Cytometry Part A **54A**(1): 36-47.
Sit, P. S., A. A. Spector, et al. (1997). "Micropipette aspiration on the outer hair cell lateral wall." Biophysical Journal **72**(6): 2812-2819.
Smith, B. A., B. Tolloczko, et al. (2005). "Probing the viscoelastic behavior of cultured airway smooth muscle cells with atomic force microscopy: Stiffening induced by contractile agonist." Biophysical Journal **88**(4): 2994-3007.

Sørensen, A., T. Alekseeva, et al. (2007). "Long-term neurite orientation on astrocyte monolayers aligned by microtopography." Biomaterials **28**(36): 5498-5508.
Spencer, V., R. Xu, et al. (2010). "Gene Expression in the Third Dimension: The ECM-nucleus Connection." Journal of Mammary Gland Biology and Neoplasia **15**(1): 65-71.
Steedman, M., S. Tao, et al. (2010). "Enhanced differentiation of retinal progenitor cells using microfabricated topographical cues." Biomedical Microdevices **12**(3): 363-369.
Stevens, M. M. and J. H. George (2005). "Exploring and Engineering the Cell Surface Interface." Science **310**(5751): 1135-1138.
Sulchek, T., G. G. Yaralioglu, et al. (2002). "Characterization and optimization of scan speed for tapping-mode atomic force microscopy." Review of Scientific Instruments **73**(8): 2928-2936.
Takai, E., K. D. Costa, et al. (2005). "Osteoblast elastic modulus measured by atomic force microscopy is substrate dependent." Annals of Biomedical Engineering **33**(7): 963-971.
Tan, J. L., J. Tien, et al. (2003). "Cells lying on a bed of microneedles: An approach to isolate mechanical force." Proceedings of the National Academy of Sciences **100**(4): 1484-1489.
Tang, H., H. Yao, et al. (2007). "NIR Raman spectroscopic investigation of single mitochondria trapped by optical tweezers." Opt. Express **15**(20): 12708-12716.
Tao, N. J., S. M. Lindsay, et al. (1992). "Measuring the microelastic properties of biological - material." Biophysical Journal **63**(4): 1165-1169.
Thoms, S. and D. S. Macintyre (2007). "Tilt-corrected stitching for electron beam lithography." Microelectronic Engineering **84**(5–8): 793-796.
Tu, Y.-O. G., D.C. (1964). "The contact problem of a plate pressed between two spheres." Journal of Applied Mechanics **31**(4).
van Poll, D., B. Parekkadan, et al. (2008). "Mesenchymal Stem Cell Therapy for Protection and Repair of Injured Vital Organs." Cellular and Molecular Bioengineering **1**(1): 42-50.
VanLandingham, M. R. (2003). "Review of Instrumented Indentation." Journal of research of the National Institure of Standards and Technology **108**(4): 249-265.
Victor J. Morris, A. R. K., A. Patrick Gunning (2010). Atomic Force Microscopy for Biologists, Imperial College Press.
Vieu, C., F. Carcenac, et al. (2000). "Electron beam lithography: resolution limits and applications." Applied Surface Science **164**(1-4): 111-117.
Vinckier, A. and G. Semenza (1998). "Measuring elasticity of biological materials by atomic force microscopy." FEBS Letters **430**(1–2): 12-16.
Vistica, D. T., D. Scudiero, et al. (1990). "New Carbon Dioxide-Independent Basal Growth Medium for Culture of Diverse Tumor and Nontumor Cells of Human and Nonhuman Origin." Journal of the National Cancer Institute **82**(12): 1055-1061.
W. Richard Bowen, N. H., Ed. (2009). Atomic Force Microscopy in Process Engineering, Elsevier.
Wagh, A. A., E. Roan, et al. (2008). "Localized elasticity measured in epithelial cells migrating at a wound edge using atomic force microscopy." American Journal of Physiology - Lung Cellular and Molecular Physiology **295**(1): L54-L60.
Wang, M. D., H. Yin, et al. (1997). "Stretching DNA with optical tweezers." Biophysical Journal **72**(3): 1335-1346.
Wang, N. and D. Stamenović (2000). "Contribution of intermediate filaments to cell stiffness, stiffening, and growth." American Journal of Physiology - Cell Physiology **279**(1): C188-C194.
Wang, N., I. M. Tolic-Norrelykke, et al. (2002). "Cell prestress. I. Stiffness and prestress are closely associated in adherent contractile cells." American Journal of Physiology-Cell Physiology **282**(3): C606-C616.

Watt, F. M., M. D. Kubler, et al. (1993). "Regulation of keratinocyte terminal differentiation by integrin-extracellular matrix interactions." Journal of Cell Science **106**(1): 175-182.
Watt, J. C. A. a. F. M. (1993). "Regulation of development and differentiation by the extracellular matrix. ." The Company of Biologists (117): 1183-1198.
Wayne M. Becker, J. B. R., Martin F. Poenie (1996). The World of the Cell, The Benjamin/Cummings Publishing Company.
Whitesides, G. M., E. Ostuni, et al. (2001). "SOFT LITHOGRAPHY IN BIOLOGY AND BIOCHEMISTRY." Annual Review of Biomedical Engineering **3**(1): 335-373.
Wong, W. W., T. Y. Tsai, et al. (2007). "Single-cell zeroth-order protein degradation enhances the robustness of synthetic oscillator." Mol Syst Biol **3**.
Wozniak, M. J., N. Kawazoe, et al. (2009). "Monitoring of mechanical properties of serially passaged bovine articular chondrocytes by atomic force microscopy." Micron **40**(8): 870-875.
Xinyu Liu, J. S., Zong Zong, Kai-Tak Wan, Yu Sun (2012). "Elastic and Viscoelastic Characterization of Mouse Oocytes Using Micropipette Indentation." Annals of Biomedical Engineering.
Xu, R., A. Boudreau, et al. (2009). "Tissue architecture and function: dynamic reciprocity via extra- and intra-cellular matrices." Cancer and Metastasis Reviews **28**(1): 167-176.
Yim, E. K. F., E. M. Darling, et al. "Nanotopography-induced changes in focal adhesions, cytoskeletal organization, and mechanical properties of human mesenchymal stem cells." Biomaterials **31**(6): 1299-1306.
Yizhi Meng, Y.-X. Q., Elaine DiMasi, Xiaolan Ba, Miriam Rafailovich, Nadine Pernodet (2009). "Biomineralization of a Self-Assembled Extracellular Matrix for Bone Tissue Engineering." Tissue Engineering **15**(2).
Yokokawa, M., S. H. Yoshimura, et al. (2006). "Fast-scanning atomic force microscopy reveals the molecular mechanism of DNA cleavage by ApaI endonuclease." IEE Proceedings - Nanobiotechnology **153**(4): 60-66.
Yu, L. M. Y., N. D. Leipzig, et al. (2008). "Promoting neuron adhesion and growth." Materials Today **11**(5): 36-43.
Zahn, J. T., I. Louban, et al. (2011). "Age-Dependent Changes in Microscale Stiffness and Mechanoresponses of Cells." Small **7**(10): 1480-1487.
Zhao, T., Y. Li, et al. (2009). "How Focal Adhesion Size Depends on Integrin Affinity." Langmuir **25**(3): 1540-1546.